

https://dspace.org/

Support Design for Wide Stoping Heights Resulting from Footwall Lifting of Previously Mined Merensky Panels

Tati, Buntu Bantu

2024

University of the Witwatersrand, Johannesburg

https://hdl.handle.net/10539/45907

Tati, Buntu Bantu. (2024). Support Design for Wide Stoping Heights Resulting from Footwall Lifting of Previously Mined Merensky Panels [Master`s dissertation, University of the Witwatersrand, Johannesburg]. WIReDSpace.

Downloaded from a DSpace repository. https://dspace.org/

School of Mining Engineering

UNIVERSITY OF THE
WITWATERSRAND,
JOHANNESBURG

SUPPORT DESIGN FOR WIDE STOPING HEIGHTS RESULTING FROM FOOTWALL LIFTING OF PREVIOUSLY MINED MERENSKY PANELS

Buntu Bantu Tati

0705847X

I declare that this research report is my own unaided work. It is being submitted for the degree of Master of Science at the University of the Witwatersrand, Johannesburg. It has not been submitted before for any degree or examination to any other university.

Johannesburg, 2024

DECLARATION

I have familiarised myself with the University of the Witwatersrand Student Academic Misconduct Policy (SAMP). I hereby declare that the work I am submitting for assessment is my original work. I affirm that I have not plagiarised, misrepresented, or colluded with any other person or source. I have properly acknowledged, cited, and referenced all the sources that I have used in my work. I also declare that I have used artificial intelligence (AI) tools only as a means of guidance. The ideas and arguments presented in my work are my original thoughts and interpretations. I acknowledge that any academic misconduct, such as plagiarism or collusion will result in serious consequences. These consequences may include a reduced grade, a fail mark, or disciplinary action according to the SAMP. The School of Mining Engineering has my consent to investigate any potential academic misconduct in my work. This investigation may include the use of similarity and AI detection software to check the originality of my work. I undertake to abide by the decision of any such investigation.



_____

(Signature of Candidate)

29 of March 2024

(Day) (month) (year)

.

"While I know myself as a creation of God, I am also obligated to realize and remember that everyone else and everything else is also God's creation."

Maya Angelou

ABSTRACT

This research report is based on project work conducted at Impala Platinum Mine No. 20 Shaft. The purpose of the project was to provide suitable support and an extraction sequence to mine a mineralized zone in the footwall of previously mined Merensky Reef stopes. An estimated 1.4 kt of ore was available at an average grade of 1.75 g/t (68 000 ounces) at this shaft. A geotechnical investigation was done to gain an understanding of the footwall Pegmatoid mineralization as well as the structural characteristics of the rockmass. A footwall lifting method needed to be developed that incorporated a support system that was based on sound design principles. A tendon and cement pack support system was determined through both a deterministic and a probabilistic key block approach. The support design was limited to local pane support and did not include pillar behaviour. Cable anchors were the selected replacement units for timber elongates removed by the footwall extraction method. A cable anchor length greater than the anticipated fall-out height of 1.77 m was required. The analysis showed that the support length had a much smaller effect on rock fall-out results than the support spacing. Cable anchors spaced 1.5 m x 2.0 m with a length of 2.5 m were determined to be the optimal support configuration for stability. Despite this finding, only 3.5 m long cable anchors were readily available at the No 20 Shaft and were subsequently used in the trial. The *Trench and Retreat Mining Method* was used in the trial over three months. During this period, a proof of concept was developed for the support and extraction method. Various recommendations are provided in this report to enhance the methods and better optimise extraction in the long term.

ACKNOWLEDGMENTS

First and foremost, I must acknowledge the Almighty God, my Lord and Saviour in Jesus Christ who is my guide and nourishes my mind, body, and spirit. Completing my research would not be possible without the heavenly divine intervention that was bestowed upon me.

Senior mine management:

I would also like to thank the Impala Platinum senior management team who entrusted me to carry out this research project. The technical and operational support that was provided can never be overlooked and stands as a testimony to the resilience and trustworthiness of the Impala Platinum leadership.

Colleagues and peers:

I would like to also acknowledge my colleagues and peers who challenged my thought processes, concepts and ideas. The roles fulfilled by all the various disciplines were instrumental in integrating components of the research to produce a meaningful project for Impala operation.

Supervisor:

A special message of appreciation goes to my supervisor Professor Bryan Watson for his guidance, patience, and willingness to impart his knowledge throughout my studies. I am incredibly grateful for your assistance during this period of high academic pressure.

Wife and family:

The continued love and support of my family goes without saying. The time sacrificed to complete this research report has impacted our time as a Family. It is a journey I would not be able to walk and complete without your love and support.

TABLE OF CONTENTS

DECLARATION i

ABSTRACT iii

ACKNOWLEDGMENTS iv

TABLE OF CONTENTS v

LIST OF FIGURES viii

LIST OF TABLES xiii

LIST OF EQUATIONS xiv

LIST OF ABBREVIATIONS AND SYMBOLS xv

1 INTRODUCTION 1

1.1 Research Background and Context 1

1.2 Problem Statement 4

1.3 Justification for Research 5

1.4 Research Objectives 6

1.5 Research Methods 6

1.6 Sources of Data 8

1.7 Research Validation 9

1.8 Structure of the Research Report 9

2 LITERATURE REVIEW 12

2.1 Introduction 12

2.2 Key Concepts, Theories and Studies 12

2.3 Key Debates and Controversies 50

2.4 Chapter Summary 54

3 RESEARCH MODEL 55
3.1 Introduction 55
3.2 Data Validation Process 56
3.3 Chapter Summary 56
4 DATA FOR THE STUDY 57
4.1 Introduction 57
4.2 Pegmatoid thickness analysis 57
4.3 Grade Resource Estimation 64
4.4 Geotechnical Structural Mapping 66
4.5 Chapter Summary 75
5 RESEARCH AND FINDINGS 77
5.1 Support Design Philosophy Deterministic Approach 77
5.2 Geotechnical Data Analysis 93
5.3 J-Block Analysis (Key block): Probabilistic Approach 97
5.4 Footwall mining methodology and mining sequence 103
5.5 Monitoring and Control 109
5.6 Alternative trench and retreat footwall mining methodology (support installation, drilling and cleaning sequence) 110
5.7 Stability Monitoring: 115
5.8 Chapter Summary 118
6 ANALYSIS OF RESEARCH FINDINGS 120
7 CONCLUSIONS AND RECOMMENDATIONS 127
7.1 Introduction 127
7.2 Summary of Conclusions 127
7.3 Research Contributions 129
7.4 Research Limitations 129

7.5 Recommendations for Future Research Work 129

8 References 130

APPENDIX A. FOOTWALL MINING BLOCK & GRADE RESOURCE ESTIMATION 141

APPENDIX C: 2A SHAFT- INSTOPE BOLTING HIGH STOPING WIDTH SUPPORT STANDARD – VERSION 1 144

APPENDIX D: 2A SHAFT- INSTOPE BOLTING HIGH STOPING WIDTH SUPPORT STANDARD – VERSION 2 145

APPENDIX E: DMR INSTRUCTION 146

APPENDIX F. GEOTECHNICAL LOGGING 148

APPENDIX G. FALL OF GROUND DATABASE 151

APPENDIX H. J-BLOCK RUN HAZARD RESULTS 152

LIST OF FIGURES

Figure 1-1: Plan of Impala Platinum lease area. 1
Figure 1-2: Diagram illustrating H-reef grade distribution profile 2
Figure 1-3: Delineation of 20# A-Reef and H-Reef zones (left) and zones of mined-out panels identified for footwall mining (right) 4
Figure 2-1: Key support characteristics 18
Figure 2-2: Flow chart indicating the principal design steps for support design methodology 20
Figure 2-3: Graph for adjusting the load-deformation curves for different deformation rates 24
Figure 2-4: Idealized creep curve showing staring versus time and the three major creep stages 25
Figure 2-5: Rockfall failure modes 27
Figure 2-6: Definition of dip (β) and dip direction (α)) 29
Figure 2-7: Joint spacing along a scanline 30
Figure 2-8: Patton's (1966) saw-tooth experiment (left) & bilinear shear strength model (right) 33
Figure 2-9: Area mapping 37
Figure 2-10: Photogrammetric mapping 37
Figure 2-11: Straight scanline mapping 39
Figure 2-12: An illustration of joint orientation bias in a scan line survey 41
Figure 2-13: Terzaghi geometric weighting factor, W compensate for orientation bias 42
Figure 2-14: Double-cut mining layout and support 44
Figure 2-15: Layout (top) and section diagram (bottom) of footwall ribs for stoping of footwall bands 46
Figure 2-16: Photograph of 6.0 m high stope (top) and PHASE2 model layout for 20.0 m wide x 6.0 m high stope (bottom) 47

Figure 2-17: Copy of stope plan for 20.0 m wide panel with 6.0 m x 15.0 m planned grid pillars 48
Figure 2-18: Causes of fatalities in the South African mining industry from 1999 to 2021 51
Figure 2-19: FOG-related reportable injuries and fatal accidents 51
Figure 2-20: Impala Platinum FOG Statistics and Rock Engineering Safety Initiatives Implemented - 2004 to 2023 52
Figure 2-21: MOSH permanent-workface-areal-mesh-adoption-process 53
Figure 3-1: Research design process flow 55
Figure 4-1: Photograph indicating the visual difference between Pegmatoid and footwall formations 58
Figure 4-2: GPR scan results showing Pegmatoid thickness along 20 21 014A PAN 2N ASG trial site 59
Figure 4-3: GPR scan results showing Pegmatoid thickness along 20 21 014A PAN 1EC and 1ED Back area. 60
Figure 4-4: Photographs showing various steps in the borehole camera assessments 62
Figure 4-5: Photographs indicating images observed inside the various inspection holes 63
Figure 4-6: Diagram showing drilled inspection holes used to determine Pegmatoid thickness 64
Figure 4-7: Sample cutting in the Merensky Pegmatoid footwall 65
Figure 4-8: Merensky H -reef grade distribution results from cut samples 66
Figure 4-9: Copy of the mine plan showing scanlines, geology and Q-ratings and planned footwall extraction. 68
Figure 4-10: Photographs indicating the structural mapping done using an iPhone compared to a magnetic compass using the scanline technique 69
Figure 4-11: Example of the structural data mapping sheet 73

Figure 5-1: 95% Cumulative fallout height for stoping filtered for the back area, face area and ASG 78
Figure 5-2: Laboratory compression tests conducted on 1.5 m long timber elongates. 80
Figure 5-3: Load deformation graph for 1.5 m long timber 80
Figure 5-4: Graph for adjusting the load-deformation curves for different deformation rates 81
Figure 5-5: Timber elongate tributary area 82
Figure 5-6: Timber elongate tributary area 82
Figure 5-7: Photographs indicating laboratory UTS tests conducted on 4.5 m long 18 mm diameter cable steel samples at the Groundwork testing facility 83
Figure 5-8: Test No.1 - Load deformation graph for 4.5 m long 18 mm diameter cable steel 84
Figure 5-9: Test No.2 - Load deformation graph for 4.5 m long 18 mm diameter cable steel 84
Figure 5-10: Test No. 3 - Load deformation graph for 4.5 m long 18 mm diameter cable steel 85
Figure 5-11: Test No. 4 - Load deformation graph for 4.5 m long 18 mm diameter cable steel 85
Figure 5-12: Dura-Pak press-test and load-deformation curve 87
Figure 5-13: Photographs of Dura-Paks arresting the propagation of large-scale collapses 89
Figure 5-14: Support Scenario 1 - Layout configuration for CAs installed during the drilling shift (CAs at 1.5 m x 2.0 m pattern) 90
Figure 5-15: Support Scenario 2 - Layout configuration for CAs installed during the drilling shift (CAs at 2.0 m x 2.0 m pattern) 91
Figure 5-16: Dip stereo-net spatial plot of joints grouped into joint sets with Terzaghi weighted analysis 94
Figure 5-17: Graph showing the key block size distribution 97

Figure 5-18: 28 m panel excavation outline with 50 m back length..... 99
Figure 5-19: Installation angle for CAs along the panel back area..... 101
Figure 5-20: Support Scenario 1 – 34 ton – CA in 1.5 m dip x 2.0 m strike, Dura-Paks 3.0 m x 12 m apart. 102
Figure 5-21: Support Scenario 2 – 34 ton CA in 2.0 m strike x 2.0 m dip, Dura-Paks 3.0 m x 12 m apart 103
Figure 5-22: Diagram indicating the drilling direction of footwall mining shot-holes..... 105
Figure 5-23: Cable anchor pre-support work and footwall drilling to establish the trench..... 106
Figure 5-24: Blasted footwall after cleaning and next portion of cable anchor pre-supporting and footwall drilling. 107
Figure 5-25: Dura-Pak breaker line installed at 12 m intervals, footwall drilling to leapfrog ahead of Dura-Pak breaker line. 107
Figure 5-26: Photographs showing cable anchors pre-installed and footwall drilling. 108
Figure 5-27: Trench creation and retreating mining sequence in the alternative footwall mining method..... 111
Figure 5-28: FOG stick monitoring devices installations and RDO's leapfrogging the retreating face to create a new trench.. 112
Figure 5-29: Section view diagram showing the alternative drill and blast design from an established free-breaking face..... 113
Figure 5-30: Diagram indicating top view and side view of alternative blast design 114
Figure 5-31: Alternative trench and retreat method being implemented. 114
Figure 5-32: Diagram indicating FOG stick installation positions in 20 21 014A PAN 1ED 116
Figure 5-33: Photographs of FOG stick installation in 20 21 014A PAN 1ED Production output 117

Figure 6-1: Graphical comparison of the number of failed tendons for various CA lengths and spacings..... 122
Figure 6-2: Graphical comparison of successful tendons for various cable anchor lengths and spacings..... 124
Figure 6-3: Graphical comparison of short tendons for various cable anchor lengths and spacings 124
Figure 6-4: Graphical comparison of failed tendons for various cable anchor lengths and spacings. 125

LIST OF TABLES

Table 1-1: No 20 Shaft Geological Succession Merensky H-reef to Footwall 1B. 3
Table 2-1: ESR values for various excavation categories 15
Table 4-1: Relative in situ rock densities for rock-type units around the Merensky Reef horizon 58
Table 4-2 Summary of Borehole Camera Assessment 64
Table 4-3: Summary information of the Traverse Scan-Lines taken in the project trial site. 74
Table 5-1: Summary of UTS test conducted on four 18 mm diameter cable steel samples. 86
Table 5-2: Static Yield Loads for various Dura-Pak sizes 87
Table 5-3: SR and FOS for various tributary area zones (SS1 - 2 m x 2 m cable anchor pattern) based on the 95% FOH. 92
Table 5-4: SR and FOS for various tributary area zones (SS2 - 1.5 m x 2 m cable anchor pattern) based on the Barton et al (1980) formula. 92
Table 5-5: Joint set 1 statistical data summary 95
Table 5-6: Joint set 2 statistical data summary 95
Table 5-7: Joint set 3 statistical data summary 96
Table 5-8: Joint set 4 statistical data summary 96
Table 5-9: Summary of FOG stick installation position & readings 116
Table 5-10: Footwall mining 3-month production output 118
Table 6-1: Statistical outputs results for the carious support scenario simulations. 121
Table 6-2: Tendon performance results, ... 123

LIST OF EQUATIONS

Equation 2-1: Demand Support Resistance 13
Equation 2-2: Estimated fallout height 14
Equation 2-3: Demand Support Resistance 17
Equation 2-4: Demand Support Resistance 19
Equation 2-5: Timber elongate load adjustment 23
Equation 2-6: Timber force correction factor 23
Equation 2-7: Joint spacing (d) 30
Equation 2-8: Coulomb failure criterion 31
Equation 2-9: Bilinear shear strength 32
Equation 2-10: Barton-Bandis shear strength model 33
Equation 2-11: JRC scale influence 35
Equation 2-12: JCS scale influence 35
Equation 2-13: JCS scale influence 35
Equation 2-14: Bias compensation factor 41
Equation 4-1: Pegmatoid thickness calculation 63
Equation 4-2: Total Pegmatoid thickness 63
Equation 4-3: True joint spacing 70
Equation 5-1: Barton anticipated fallout height 78
Equation 5-2: SR required to support the demand 79
Equation 5-3: Underground timber strength adjustment 81
Equation 5-4: FOH supported by timber elongate 82

LIST OF ABBREVIATIONS AND SYMBOLS

Abbreviation	Description
PGM	Platinum Group Metals
6E	Six elements
20#	No. 20 Shaft
OEM	Original Equipment Manufacturer
FOG	Fall of ground
ROM	Run of mine
FOS	Factor of safety
DIPS	Data Interpretation Package using Stereographic projection
MHSC	Mine Health and Safety Council
DMRE	Department of Mineral Resources and Energy
MOSH	Mining Industry Occupational Safety & Health
EEMS	Early Entry Examination and Making Safe
TARP	Trigger Action Response Plan
GPR	Ground penetrating radar
RD	Relative density
SSP	Subsurface profiler
GCD	Ground control district
UCS	Uniaxial compressive strength
Jr	Joint roughness
Ja	Joint alteration
COP	Code of Practice
ASG	Advance strike gully
FOH	Fall out height
TAT	Tributary area theory
TA	Tributary area
CA	Cable anchor
UTS	Uniaxial tensile strength
SS1	Support Scenario 1
SS2	Support Scenario 2
RDO	Rock drill operator

Symbol	Description	Units
φ	Joint friction angle	^{0}
λti	true joint spacing	m
αi	dip angle of the joint	^{0}
αs	plunge	^{0}
g	Gravitational Acceleration	m/s^2
ρ	Density	kg/m^3
β	Dip	^{0}
α	Dip direction	^{0}
Θ	angle between the scanline and the mean orientation of the joint set	^{0}

1 INTRODUCTION

1.1 Research Background and Context

Impala 20 shaft is one of nine operational shafts in the Rustenburg region forming part of the Impala Mining Group (Implats). It lies on the Western lobe of the Bushveld Complex (Figure 1-1). The shaft is located approximately 80 km North-West of Rustenburg in the North-West province. The shaft began mining the Merensky Reef in 2008 and ramped up production to a steady state by 2019. The shaft currently produces an average of 135 kt of PGM ore per month at an average grade of 4.01 g/t. Mining activities are taking place at a depth range of between 700 m and 1050 m below the surface.

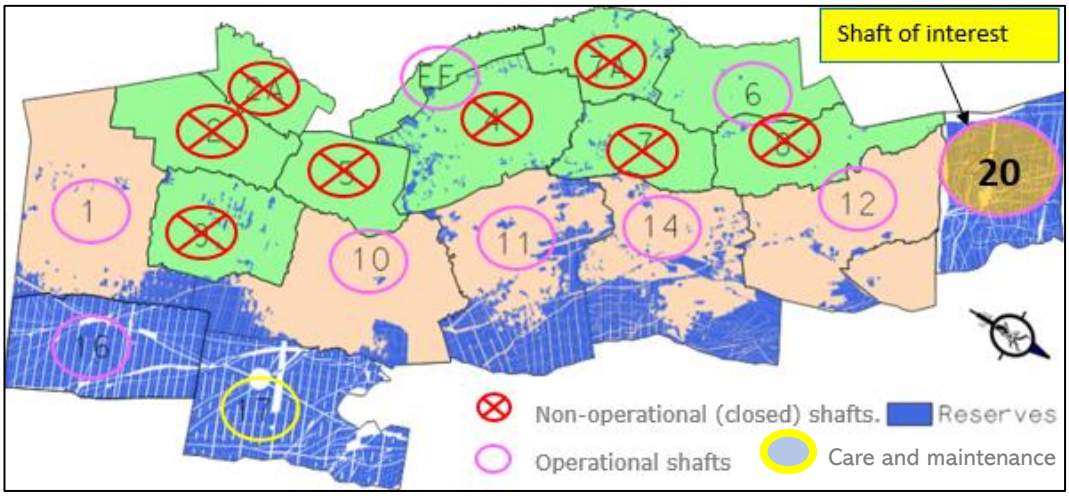


Figure 1-1: Plan of Impala Platinum lease area (Carollo, L, 2023).

Impala Platinum 20 shaft currently mines the Merensky Reef orebody that consists of 2 reef types (A reef and H-reef). Of the two reef types, the H-reef is known to have a wider mineralized zone. The mineralized zone consists of a Pyroxenite hangingwall, Chromitite layer, and Pegmatoid footwall of varying thickness from 0.5 m – 3.5 m (Mabogo, 2021). The focus of extraction has been targeted at mining the economic channel width that provides the highest average grade as shown in Figure 1-2. Panels were therefore mined at an average stoping width of 1.35 m for economic and practical mining reasons (Fouche, 2019).

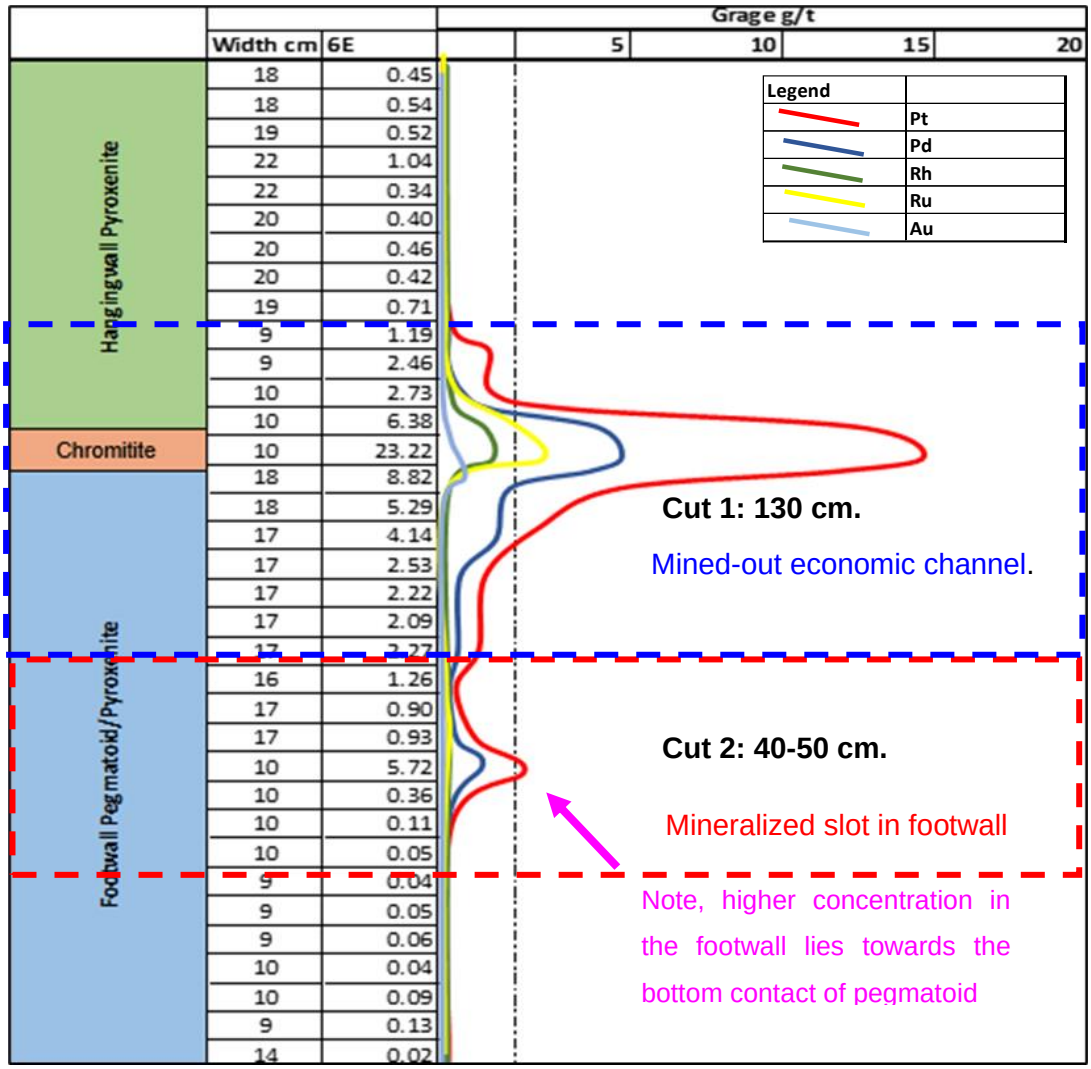
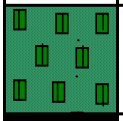
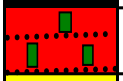


Figure 1-2: Diagram illustrating H-reef grade distribution profile (Mabogo, 2021)

The lithology of the rock mass on the No. 20 shaft consists of alternating layers of Chromitite, Pyroxenite, Norite and several types of Anorthosite layers. These layers dip towards the northeast at an average of nine degrees (Carollo, L, 2023). Of interest to the research is the lithology around the mineralized Merensky zone. At No. 20 shaft, there are two common reef types known as the A-reef and H-reef. The A-reef consists of a Pyroxenite hangingwall separated by a thin Chromitite layer with Footwall 1 “A” (FW 1 “A”) below. That is, for A-reef, there is no Pegmatoid below the Chromitite layer. The H-reef consists of a Pyroxenite hangingwall separated by a thin Chromitite layer with a Pegmatoid footwall (Mabogo, 2021) indicated in the geological succession of the Merensky Reef in Table 1-1.

Table 1-1: No 20 Shaft Geological Succession Merensky H-reef to Footwall 1B (Impala Platinum Limited, 2006).

Geological Column	Thickness (m)	Unit	Rock Type	Description
	0.77 to 10.57	Merensky	Pyroxenite	Light brown to brown, medium to granular
	5mm to 2cm	Merensky 'H'	Chromitite	Metallic grey stringer
	0 to 3.30	Merensky	Pegmatoid	Brownish grey, course grained Scattered sulphides and chromite stingers
	0.2 to 8.7	FW 1 'A'	Mottled Anorthosite	Brownish grey to milky white, medium grained. Mottled and Spotted Anorthosite
	1.9 to 9.3	FW 1 'B'	Spotted Anorthosite	

Various attempts were made by mine management in the past to mine a wider cut (high stoping width panels) to maximize the extraction of the channel width. However, these attempts have not been successful due to several factors including:

- A low confidence level in the distribution of the mineral content throughout the H-reef channel width (insufficient sampling and drilling information);
- Support design changes and risks associated with buckling of timber elongates in high-stoping width panels; and
- Difficulty in cleaning due to high accumulation of ore resulting in longer mining cycles, affecting crew efficiencies and production output.

The Sampling and Geology departments have increased their geological confidence level, through drilling and sampling of the H-reef confirming mineral value in the Pegmatoid package. PGM (Platinum Group Metals) content value of six elements (6E) locked in the footwall of mined-out panels is estimated to be in the order of 1.75 g/m^2. A total of 43 blocks in the H-reef zone have been identified as containing the mineralized Pegmatoid package (Figure 1-3). The stopes in

these blocks were mined out between March 2012 and August 2022 and have been standing for approximately 2-10 years**.** Production pressures, congestions in raiselines, ounce targets, and operational flexibility requirements have prompted an investigation on how to mine out the remaining PGM ounces left in the footwall.

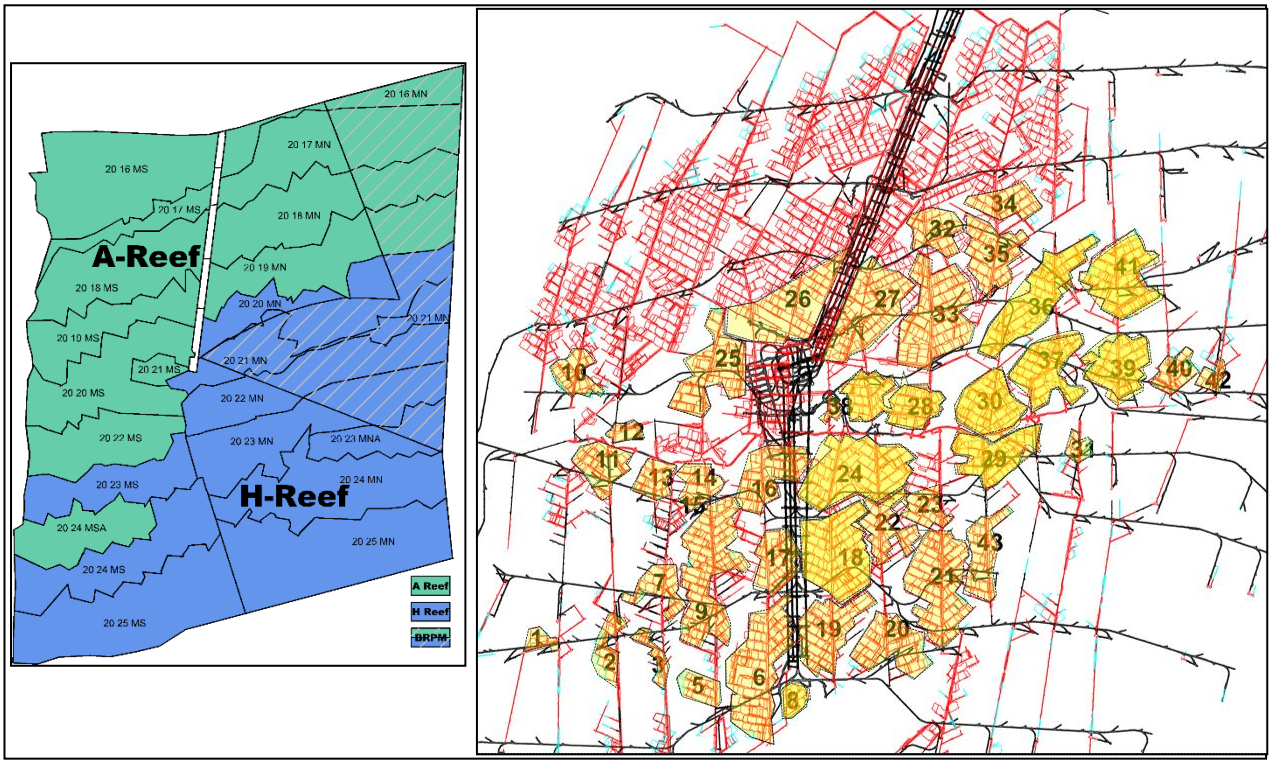


Figure 1-3: Delineation of 20# A-Reef and H-Reef zones (left) and zones of mined-out panels identified for footwall mining (right) (Mabogo, 2022)

1.2 Problem Statement

The research project entailed the removal of timber elongate support and replacing the units with long cable anchors. The removal of timber elongates that were supporting the back area was expected to impact stability and would affect the safety of underground employees. It was therefore important that a safe extraction methodology be developed together with correct support requirements.

The areas envisaged for footwall mining extraction were situated in a shallow mining environment between 800 m to 1000 m below the surface. The rock mass was characterized by joint-bound key blocks. The mining of the footwall was

planned for mined-out panels where the availability of services could be affected due to:

- Cable theft;
- Stripping of service columns;
- Deterioration of ground and support conditions (corrosion of steel tendons);
- Flooding; and
- Sealing off activities in raiselines.

A significant amount of re-equipping and rehabilitation of access ways to these blocks was therefore expected. A key concern in the project was the risk of Falls Of Ground (FOGs) associated with key blocks currently held up by timber elongates. A practical compromise had to be reached in terms of the area that can be exposed at a time before support is installed.

1.3 Justification for Research

The justification for the research was to investigate means to maximise safe extraction of the Merensky Reef. This would potentially provide additional ounces to the production profile. Such a trial project was expected to have a minor increase in overall mining costs as the infrastructure to mine the areas was still predominantly in place. A limited amount of re-equipping and establishing was required.

There are 1.4 kt of *insitu* ore which translates to 68 000 ounces at an average grade of 1.75 g/t that stands to be extracted in the footwall of these identified wide H-reef zones shown in Appendix A (Mabogo, 2021). This is valued at ZAR 1.58 billion based on a ZAR 23 000 per oz basket price. Based on the 42 blocks identified in Figure 1-3, the total estimated cost for this extraction is estimated to be ZAR 1.45 billion where (Mooketsi, 2023):

- ZAR 31 million is estimated for the rehabilitation of access ways and stopes;
- ZAR R990 million is estimated to be the mining cost based on the contractors' mining rate;

- ZAR 315 million support cost; and
- ZAR 82 million explosive costs.

1.4 Research Objectives

The main objective of the research project was to determine a suitable mining and support methodology to optimally extract a mineralized zone in the immediate footwall of mined-out panels safely and economically. Since conventional drill and blast methods were planned it was necessary to ensure that no FOGs occurred in the working area and that there was an escape route should an unexpected event occur.

1.5 Research Methods

The trial project was conducted by a mining contractor at a suitable underground trial site shown in Appendix B. Information was gathered from the trial site during the implementation of the method and was used to compile the findings of the research project that took cognisance of:

- Ground conditions (rock mass rating) and key block analysis;
- Performance and capacity of the newly installed cable anchor replacement support;
- Allowable area to be mined in given shift, safe spans between blasted out support and remaining support; and
- An integrated practical mining cycle.

The research followed industry-accepted methods for the designing of underground support systems as described in the literature review in Chapter 2. Various sets of data were gathered from the underground trial sites through observations and measurements. Data for the research project was gathered from the following assessments:

- Internal Impala Footwall Mining Risk Assessment with all relevant stakeholders, including the Mining department, Safety department, Geology department, Rock Engineering department and union structures;
- Data gathering in the trial site that covered validation of the footwall mineralization and thickness, joint structural mapping, grade sampling valuations, and selection of support elements.
- A key block analysis using J-Block to simulate, validate, and enhance the support design testing the impact of variations in support spacing and length.
- Evaluating on a conceptual and practical level, through an underground trial the implementation of the support design and extraction method over 3 months by a stoping crew comparing productivity, stability, and safety achieved.

The project was run parallel with normal Run Of Mine (ROM) stoping operations that included:

- Entry examination and making safe;
- Support installation;
- Rock face drilling;
- Charging-up; and
- Cleaning.

A resolute technical instructor was used to provide daily underground support to the mining team. The mine's rock engineering personnel was familiarised with the technical aspects of the technique and provided technical assistance to the mining team. Continuous monitoring and regular audits were conducted by the author and the mine's rock engineering personnel.

1.5.1 Qualitative research

There were no qualitative research methods used during the project.

1.5.2 Quantitative research

The research used quantitative methods that made use of numerical values that were objective-based. This included the following:

- Analysis of GRP scan outputs and Borehole camera observations to determine Pegmatoid thickness in the footwall;
- Analysis of grade outputs from sampled data;
- Support design calculations providing numerical outputs of Factor Of Safety (FOS) values;
- Statistical analysis of geotechnical data collected used in the Rocscience software; Data Interpretation Package using Stereographic projection “DIPS” and J-Block software;
- Analysis of output results from J-Block software;
- Analysis of graphs from statistical outputs from J-Block software;
- Measuring and assessing the stability of the support design executed by visually assessing the FOG stick monitoring device; and;
- Measuring results of the production output during the trial.

1.6 Sources of Data

The data for the research project was obtained from the following sources:

- Underground measurements and observations
    - Borehole camera observations;
    - GPR scans;
    - Underground joint mapping; and
    - Closure monitoring device
- Internal departmental information from:
    - Rock Engineering department;
    - Geology and Sampling departments; and
    - Surveying department
- Public data from literature sources.

- Public data from industry bodies:
    - Mine Health and Safety Council – MHSC;
    - Department of Mineral Resources and Energy – DMRE; and
    - Minerals Council South Africa).

1.7 Research Validation

Validity in the research was obtained through numerical modelling. Subsequently, a trial site was instrumented and visually monitored.

1.8 Structure of the Research Report

This research project consists of seven Chapters. Chapter 1 is the introduction and covers the background of the research topic. The problem statement, the justification for the research, and the research objectives are also specified in this chapter. The research methodologies followed in this study and the sources of the information are explained.

Chapter 2 of the research project is broad and covers a literature review based on various topics covered during the research project. This included a deterministic stope support design philosophy where the elements affecting support design were discussed with emphasis on shallow mining conditions. The function of various tendon-based support elements as well as timber-based support were each discussed. An enhancement to the deterministic support design approach through a probabilistic key block analysis approach is introduced into the literature review. Joint characterization and joint data collection methods that are essential in the key-block analysis are covered as well as the errors associated with joint mapping. The wide reef mining concept was briefly described and the known cases of multi-cut mining in stopes were discussed. Various monitoring techniques and instrumentation used in stopes were also briefly discussed. The effects of blasting on stopes stability were also briefly described. Reference is then drawn to historical statistical fall of ground data in a South African context with relations drawn to innovations in support design.

Chapter 3 of the research report details the structure in the form of a project process model. The various stages in the project process are briefly described.

Chapter 4 of the research report details the data-gathering processes that were followed. It details the data-gathering done in the project site including Pegmatoid thickness estimations, grade and sampling estimations as well as geotechnical data from structure mapping. The support elements used in the trial as well as the rationale for their selection are covered.

Chapter 5 begins with the deterministic support design approach where various fall-out heights are discussed, and support requirements defined. The external testing programmes from original-equipment-manufacturers (OEM) suppliers on the support elements used in the trial and support design were discussed. These test results formed the support specifications and were used as a basis to determine the strength requirements of the support design. A deterministic evaluation was then done where various Factor of Safety (FOS) values were determined.

The chapter then moves into unpacking the geotechnical data collected that was analysed through the DIPS software program to arrange and organize the data into a format required in J-Block. The probabilistic key-block analysis that was conducted using the J-Block programme was described and the steps for constructing the J-Block model were explained.

This chapter then covers the methodology of the footwall mining project integrated with the designed support system. It explains the methodology in steps and qualitatively provides findings on the implementation. The concept, processes, challenges, and solutions to teething issues encountered are discussed. The chapter lastly summarises production outputs obtained during the project execution phase of the project as well as results from the monitoring instrumentation installed at the trial site.

Chapter 6 of the research report is the analysis section that discusses the output results that were obtained from the J-Block program. Two support system design scenarios that utilize the same support elements with different lengths and

spacings were evaluated and the results were analysed through the use of tables and graphs.

Chapter 7 of the research report provides the concluding elements of the project. It also suggests steps to be taken forward to build on the existing body of knowledge.

2 LITERATURE REVIEW

2.1 Introduction

The literature review covers a wide variety of topics discussed in the research project with particular emphasis on shallow stoping conditions. Various aspects of tendon-specific support design including key block probabilistic analyses. Various joint data collection and mapping techniques are covered with an explanation of the various biases (errors) encountered in joint mapping. The concept of wide reef mining is explained and known cases of multi-cut mining are briefly discussed. Monitoring and instrumentation principles as well as rock breaking (blasting) issues affecting stability and support design in stopes are briefly covered.

2.2 Key Concepts, Theories and Studies

2.2.1 Stope Support Design Philosophy

Stope support design traditionally follows a deterministic method where support resistance and energy absorption criteria form the basis of the design (Jager & Ryder, 1999). In a shallow mining environment, the risk of dynamic rockburst conditions is low, therefore energy absorption criteria are not considered. The support system designed must address the most significant risk for given geotechnical conditions (Stacey, 2008). The key elements of the support design process that must be considered are listed below (Ryder & Jager, 2002):

- Support *demand*
    - Fall out height;
    - Rock mass characteristics;
    - Loading/Closure rates; and
    - Field stress state.
- Support *capacity*
    - Support characteristics; and
    - Support spacing and tributary areas.

2.2.2 Static Support Resistance Demand

The Support Resistance (SR) demand is the deadweight of a potential rockfall that can fall out from the hangingwall, which is expressed in Equation 2-1 as:

$$SR_{Demand} = \rho \times g \times t \qquad \text{Equation 2-1}$$

where: ρ - density, g - gravitational force and t – thickness of potential rockfall

Fall out height:

Fall out height (FOH) is a critical rock mass parameter in support design that marks the height of the potentially unstable rock mass in the hangingwall. FOH is used to determine the support resistance a proposed support system would have to meet. The weight of potentially unstable rock in the hanging wall is determined based on the rock density, potential FOH and force of gravitational acceleration expressed as the SR demand in the design.

FOH historically was determined by rock engineers from observations of previous falls of ground that took place where support was installed and, in some instances, unsupported areas between the face and permanent support. In the 1990s, Roberts (1995) made use of a comprehensive database of all fall-of-ground-related fatalities in the gold mines. A cumulative fall-out height of 95% of all fall-out heights was determined for and later updated by Daehnke, et al (1998) for the criterion to include more fatality data (Daehnke, et al., 2001).

Nowadays the FOH database includes non-fatality related falls of ground determined from back analysis of previous falls of ground in each Ground Control District (GCD) or Geotechnical area (Daehnke, et al., 2001). Jager and Ryder (1999) suggest that a database should consist of at least 100 rockfall data points, or the analysis may be biased to underestimation.

Empirical design methods can be used when there is insufficient rockfall data. Barton et al (1980) suggested a method of estimating tendon length based on the

span of excavation and the Excavation Support Ratio (ESR). The ESR is a value allocated for each excavation type based on the purpose of the individual excavation, and its anticipated life expectancy. The approach is based on the back analysis of numerous case studies from low-stress civil engineering and tunnelling applications. Over time these empirical design methods have found their place in shallow mines (platinum, diamond, and base metals) that operate at depths where in-situ stress and stress change are small in comparison to the rock strength (Ryder & Jager, 2002). Equation 2-2 is used for calculating appropriate tendon and/or anchor lengths given as (Barton, et al., 1980.)

$$L = \frac{2+0.15\times B}{ESR} \qquad \text{Equation 2-2}$$

Where: B Excavation width

L Anticipated fallout height

ESR Excavation Support Ratio

The ESR value is dependent on the intended use of the excavation and the degree of security demand required on the support system. (Barton, et al., 1974) suggested the following ESR values shown in Table 2-1:

Table 2-1: ESR values for various excavation categories (Barton, et al., 1974)

Excavation category		ESR
A	Temporary openings	3 - 5
B	Permanent mine openings, water tunnels for hydro power (excluding high pressure penstocks), pilot tunnels, drifts and headings for large excavations	1.6
C	Storage rooms, water treatment plants, minor road and railway tunnels, surge chambers, access tunnels	1.3
D	Power stations, major road and railway tunnels, civil defence chambers, portal intersections	1.0
E	Underground nuclear power stations, railway stations, sports and public facilities, factories	0.8

Rock mass characteristics

The behaviour and deformation of the rock mass are largely influenced by the mining-induced stress and geological discontinuities (joints, beddings, faults, dykes and shears) (Daehnke, et al., 1998). The presence of geological discontinuities in the hangingwall had a significant influence on the potential FOG conditions that may exist in a stope. These conditions are largely influenced by the orientation, spacing and interface properties of discontinuities (geological structures) (Daehnke, et al., 2001).

Daekhnke, et al (1998) suggests that the thicker falls of ground are normally associated with geological structures. The more densely spaced discontinuities are, the more closely spaced support units need to be to achieve the required support interaction to stabilize the span between support units. The frictional properties (as represented by the friction angle) of discontinuities, affect the probability of blocks falling out and must be considered in the support design (Daehnke, et al., 2001).

Roberts, et al (2002) described hangingwall conditions in shallow Platinum mines to be different to that of deep-level Gold mines in that mining-induced stress

fractures are less common. Jointing, hangingwall bedding, and geological features are the significant contributors to hangingwall instability in shallow Platinum mines. The hangingwall is characterised as blocky consisting of multiple blocks separated by discontinuities.

In the Merensky reef horizon, the first horizontal parting layer is 8 m – 30 m above the reef across the Impala operation and often creates a very thick stable hangingwall beam. Joint persistence is not significant enough to make the hangingwall beam unstable. The spacing of joints, however, is significantly more intense than the stress fracturing ranging between 0.5 m – 2.0 m. Instability problems in the hangingwall however arise in the vicinity of potholes, and structures like domes and faults (Roberts, et al., 2002).

Closure/loading rates

Closure rates play an important role when selecting stope support units for Quasi-static loading conditions. Timber elongates range in a stope panel are required to do support work within their yield range throughout the elongate's working life. When the timber elongates deform beyond the yield range, unpredictable failure and buckling can occur. In shallow mines where closure rates are low, elongates don't need to have a large yield range. In a low-closure environment, timber elongates must be pre-stressed to prevent units from being blasted out (Daehnke, et al., 2001).

Stress state (mining depth)

The rock mass at a depth below the surface, before any mining disturbances occur is known as the virgin or primitive stress state. Stoping involves the removal of the large volume of rock which changes the stress state in the rock mass influencing the stability of the excavation (Jager & Ryder, 1999).

At shallow depths, two out of the three principal stresses may be tensile promoting the release of blocks in a discontinuous hangingwall. Conversely, in deeper mines, the hangingwall experiences larger compressive forces that act to clamp and stabilize the hangingwall, however, stress fracturing and the release of strain

energy impact stability. The depth of mining and field stress therefore have a significant influence on rockmass behaviour, stability and support requirements (Jager & Ryder, 1999).

At shallow depths, where the hangingwall is in a state of tension, blocks formed by unfavourably orientated discontinuities are unstable and rely on support to keep the blocks in place. Where parting planes are sub-parallel to the hangingwall, bed separation may arise if the cohesive strength of the parting is overcome by the tensile stresses where large collapses can occur. The use of stiff active support units is required in these mining environments (Jager & Ryder, 1999).

2.2.3 Support Resistance Capacity

The SR capacity of the support system is evaluated against the SR demand rockfall criterion. SR capacity is the load-carrying ability the support system provides in the tributary area (A_T) installed. It is expressed as the force (F) provided by the support element/s per unit area (m^2) shown in Equation 2-3 (Stacey, 2008).

$$SR_{capacity} = \frac{F}{A_T} \qquad \text{Equation 2-3}$$

where: F - support unit load (kN), A_T - tributary area (m^2)

Support systems are designed for various areas/zones of excavations in the reef horizon that are categorized mainly as (Jager & Ryder, 1999):

- Face area / Working area;
- Back area; and
- Gullies.

The capacity of the support system in each zone must be considered. The capacity must be evaluated against the demand to ensure adequate stability is achieved for the zone i.e. $SR_{capacity} > SR_{Demand}$.

Support Characteristics

Support units may be classified as passive or active. Active refers to the units being pre-tensioned immediately applying forces directly to resist rock mass deformation. Passive support refers to support units that rely on rock mass deformation to become active. Key support characteristics are summarised in Figure 2-1 and listed below as follows (Jager & Ryder, 1999):

- Initial stiffness;
- Yield load (peak strength);
- Yieldability; and
- Energy absorption capacity;

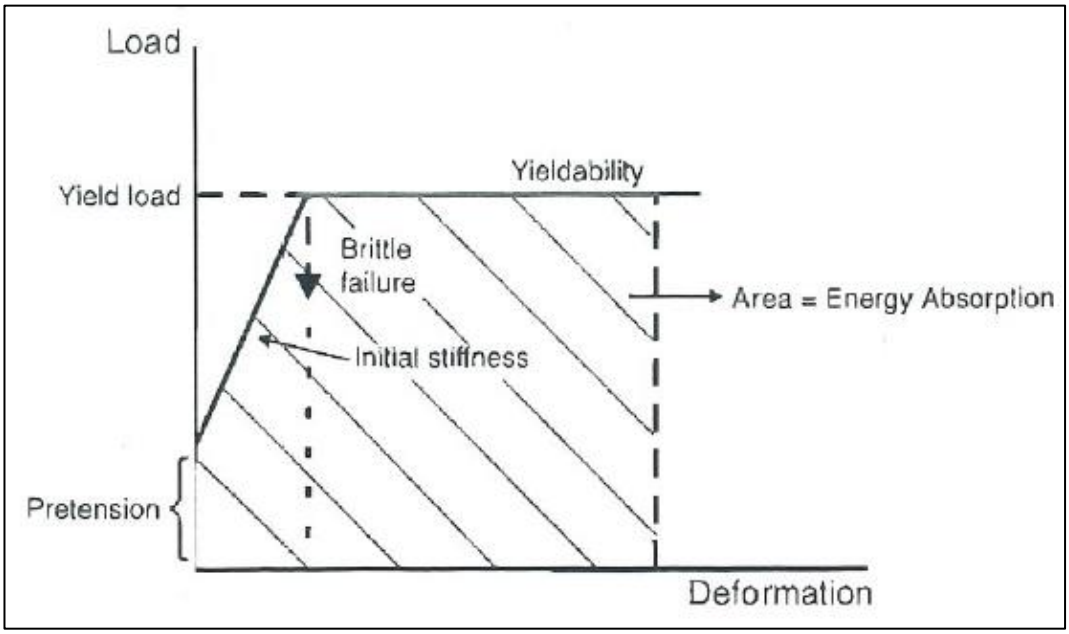


Figure 2-1: Key support characteristics (Jager & Ryder, 1999)

When several different types of support work in a combined team, they form a support system. The contribution from each unit adds to the overall support system characteristics.

Tributary area

A tributary area (TA) concept is applied during the support design where the number of support elements in a pre-defined zone (area) of the stope is known. The area in this pre-defined zone is dependent on the face layout (Daehnke, et al., 2001). The area in the plane of the reef is divided between a fixed number of support elements that are assumed to carry the weight of the rock that is based on the 'fall-out height'. The maximum tributary area (A_T) that can be supported by a single support unit for rockfall conditions is expressed in Equation 2-4.

$$A_T = \frac{F}{\rho \times g \times t} \qquad \text{Equation 2-4}$$

where:
F – Force supplied by support unit load (kN),
A_T - tributary area (m^2)
ρ - density,
g - gravitational force
t – thickness of potential rockfall

Factor of safety

When the capacity exceeds demand, stability is expected. The ratio between the SR and the rockfall criterion is said to provide the FOS expressed by dividing the capacity by the demand. It is recommended that the demand should not exceed 68% of the support capacity (FOS=1.5) as the accepted normal practice in South African mines (Stacey, 2001).

Daehnke, et al (2001) suggested that the principal design steps to be followed when designing stope support suited for a specific geotechnical area are indicated in the flow chart in Figure 2-2.

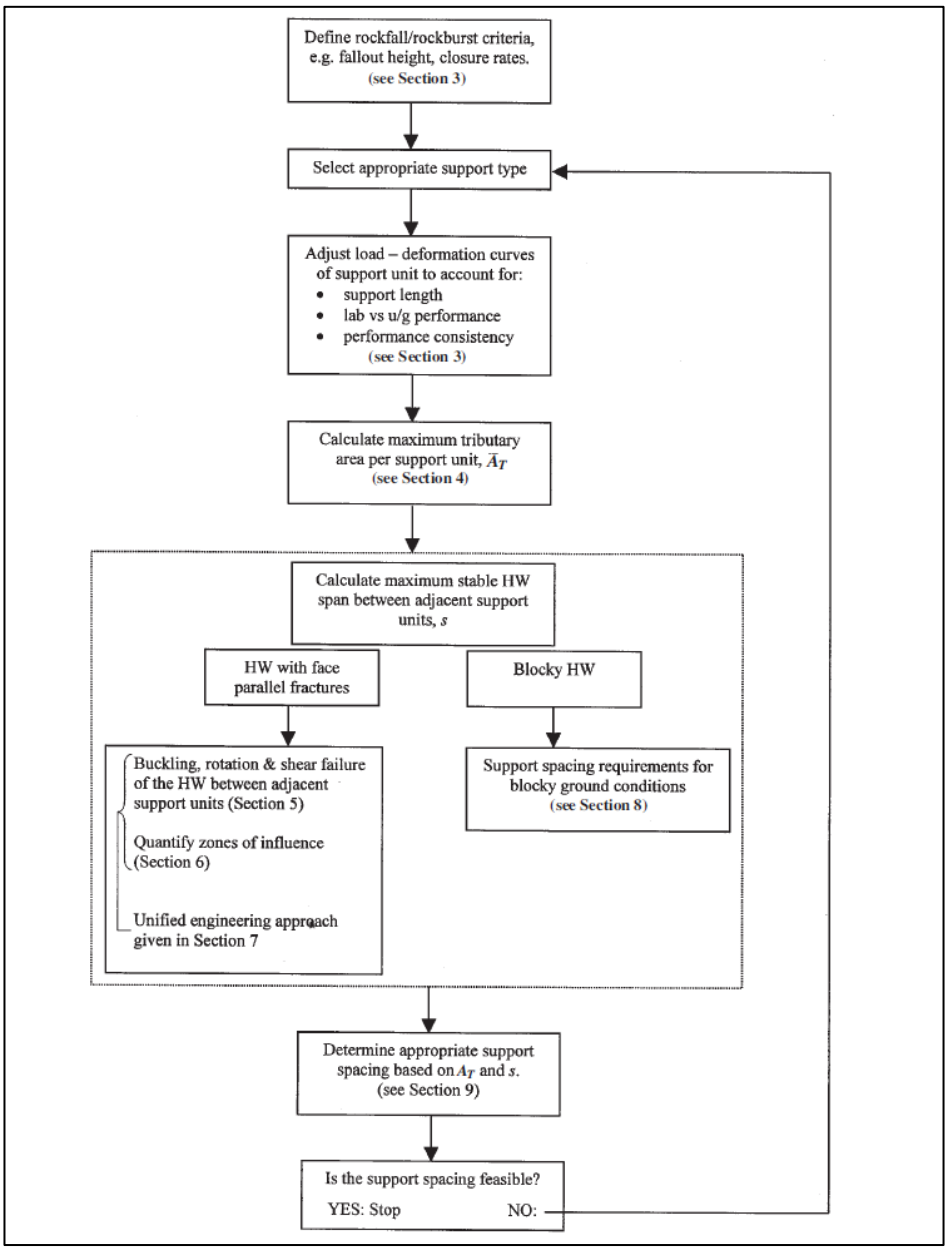


Figure 2-2: Flow chart indicating the principal design steps for support design methodology (Daehnke, et al., 2001)

2.2.4 Tendon support philosophy

Potential instability in rock mass surrounding excavations is when there is noticeable displacement between intact rock blocks. These unstable rock blocks ultimately may fall out following a rotation of the block or when their adjacent blocks no longer provide sufficient confinement to keep the blocks in place. The main function of tendons therefore is to reduce relative displacement between blocks

and reduce the probability of blocks falling out (Roberts, et al., 2002). This can be done through two main applications. Roberts, et al (2002) describe these two main applications for tendons in rock masses as:

- "Suspension" – which involves the anchoring of a fractured or loose unstable block /beam into a more competent stable rock mass. This is common for bedded rock masses where hangingwall creates a defined beam. Pre-tensioned mechanical end anchor bolts or cable anchors are suitable for this function.
- "Reinforcement" - where the integrity of the rock mass is increased by binding a discontinuous assemblage of blocks together to make the hangingwall self-supporting. Reinforcement is a more complex concept and works when the discontinuity pattern, rock mass failure mode, and bolt pattern are complimentary (Roberts, et al., 2002). Most tabular excavations aim to maintain the integrity of the hangingwall where the tendon support's role tends to be beam building rather than arc formation.

Length requirements of tendon stope support

Stacey (2001) suggests that the tendon length of support should be 200 mm greater than the FOH or above the parting plane. However, in practice, bond lengths between 250 mm and 300 mm are commonly used in support design. This effectively suspends the unstable block/beam to a more competent rock mass. Tendons should be drilled as vertically as possible to maximise the length of the tendon. In the absence of elongates, when tendons are not long enough, back-breaks can occur along a parting plane above the tendon anchor point. Tendons provide subtle signs of failure that are not as evident as elongates. The loud cracking noise and bending action of failing elongates provide an easy-to-identify warning sign of an imminent collapse. It is therefore important that the correct length must be selected (Stacey, 2001).

Tendon support has several advantages over other permanent supports used in conventional hard rock stopes. These include (Daehnke, et al., 1998):

- Clamping of hangingwall partings;
- Not obstructing the face area to enable other activities to be done safely such as drilling the face and cleaning broken rock; and
- Tendons can be installed as close as the temporary support on the face reducing unsupported span after the blast and creating a safer area for the re-entry crews.

2.2.5 Cable Anchors

A variety of tendon types are available to be used in stopes. Mechanically end anchored bolts and split sets were the common types in narrow reef stoping however other tendon support types such as cable anchors discussed below have become increasingly more common nowadays (Mining Qualification Authority, 2006).

Cable anchors (CAs) consist of a high-strength steel cable that is fitted with an expansion shell at the end and a washer plate with a barrel plate in the front. These units are pre-tensioned (active) and often used with cementitious grout for long-term support purposes. The support unit has good yielding capabilities and performs well under seismic rock mass conditions. The benefit of these units is the extended length (3 m - 15 m) that they can support compared to other support tensions. Therefore, they are commonly used in large excavations (Potvin & Hadjigeorgiou, 2020).

2.2.6 Timber support design philosophy

The strength of timber is dependent on the loading rate. At higher loading rates, the strength of timber-based support increases (Ryder & Jager, 2002). This was demonstrated by Roberts et al (1987) who conducted a series of laboratory tests on support units where they assessed various parameters that included temperature, humidity, timber quality and loading rate. Roberts et al (1987) and Daehnke et al (1998) ultimately demonstrated that the load-deformation behaviour of support units installed underground can be significantly downrated in comparison to load-deformation curves obtained from laboratory testing. Underground testing done by (Piper & Malan, 2013) found the derating methods done by Roberts et al (1987) to be somewhat conservative but suitable in the absence of other alternatives.

To account for this, Roberts (1995) suggested a correction factor shown in Equation 2-5 be used to adjust for the force/load of timber elongates where:

$$F_{u/g} = F_{lab}\left\{m\ log\ \frac{V_{u/g}}{V_{lab}}\right\} + 1 \qquad \text{Equation 2-5}$$

Where:	$F_{u/g}$	Timber load downrated for underground loading
	F_{lab}	Timber load generated in laboratory conditions
	V_{lab}	Laboratory test velocity (typically 10 – 30 mm/min)
	$V_{u/g}$	Underground loading/closure rate (5 – 30 mm/day)
	m = 0.123	Empirically determined correction factor m

The timber load adjustment Equation 2-5 can be re-written as Equation 2-6 where:

$$F_{u/g} = k\ F_{lab} \qquad \text{Equation 2-6}$$

Where:	k	Correction factor
	F_{lab}	Timber load generated in laboratory conditions
	V_{lab}	Laboratory test velocity (typically 10 – 30 mm/min)
	$V_{u/g}$	Underground loading/closure rate (5 – 30 mm/day)

Figure 2-3 shows a graphical representation of the force correction factors for different velocities for timber elongates and for timber and cementitious packs.

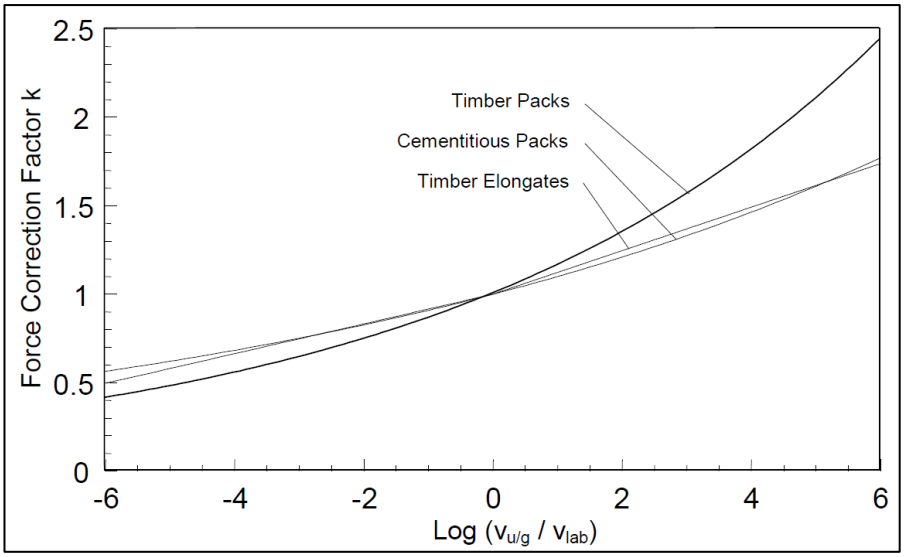


Figure 2-3: Graph for adjusting the load-deformation curves for different deformation rates (Ryder & Jager, 2002)

2.2.7 Time dependent deterioration (Creep)

Glamheden & Höekmark (2010) defines creep as "…*the time-dependent deformation of rock under a load that is less than the short-term strength of the rock. Creep strain can seldom be recovered fully when loads are removed, thus it is largely plastic deformation*." (Glamheden & Hökmark, 2010)

When mining is static, the effects of creep behaviour can be observed in underground excavations where the surrounding rock mass is relatively weak and subjected to a constant elevated state of stress. There is a time-dependent non-violent dispassion of strain energy where closure and convergence (squeezing) mechanisms are visible. The initiation, development, and propagation of stress-related fractures (cracks) in intact rock can lead to the creation of unstable rock mass conditions (Ryder & Jager, 2002). In shallower Platinum mines, creep is less common, however can manifest along pre-existing discontinuities where the extent of discontinuities grow intersecting other planes forming loose wedge blocks over time (Napier & Malan, 2012). Creep behaviour in many literature sources is

expressed as a strain-time function subdivided into three phases shown in Figure 2-4 where:

- I is the primary or transient creep stage;
- II is the secondary or steady creep state and;
- III is the tertiary or accelerating creep stage (occurs before sample failure).

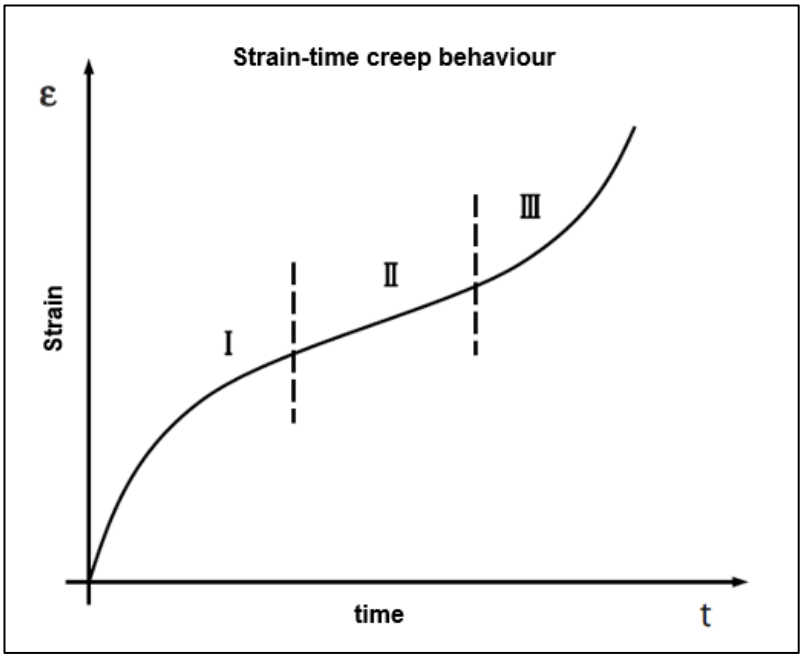


Figure 2-4: Idealized creep curve showing staring versus time and the three major creep stages (Glamheden & Hökmark, 2010)

The rate and extent of creep deformation for intact rock and discontinuities at each stage of the creep curve can vary from hours, days, months, to years. This variation is dependent on factors that include *(Glamheden & Hökmark, 2010)*:

- Crystalline structure & existing micro fractures
- Humidity/Moisture
- Temperature
- Joint frequency and orientation;
- Normal and shear stress components along joint planes;
- Joint roughness;

- Joint infill and;
- Groundwater.

2.2.8 Key Block Analysis (Probabilistic Method)

An enhancement to the stope support design process is the inclusion of key block analysis. J-Block is a commercially available program that makes use of key block analysis (Kotze, 2012). It generates statical distributions of potential key blocks of varying size in a mined area consisting of a defined support system (Kotze, 2012). The program simulates possible falls of grounds in the mined-out area and assesses various failure modes under the influence of gravity (Kotze, 2012).

Unlike the deterministic (support capacity and demand) approach described above, this approach considers variation in joint structures that form key blocks. It also considers the variation of support installation due to human error. Various zones in the stopes are categorized and exposure levels are defined. Each block formed in each zone is tested against the support in the area. The test assesses whether a FOG occurs due to failure of the support, failure between the support, or failure by rotation as shown in Figure 2-5 (Joughin, et al., 2012).

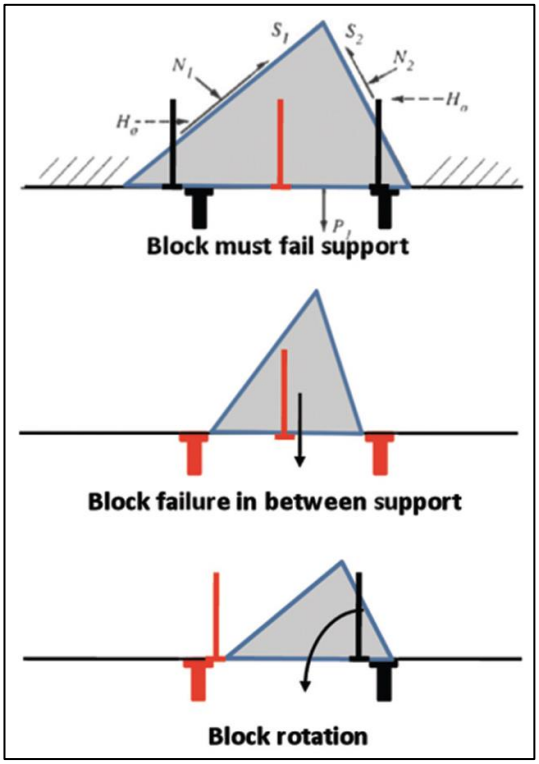


Figure 2-5: Rockfall failure modes (Joughin, et al., 2012)

Comparison between deterministic tributary area approach versus key block probabilistic approach

The traditional deterministic approach that looks at the cumulative 95% of fallouts and tributary areas assumes one specific failure mode. That is, failure occurs when the load exceeds the load-carrying capability of support units. Whereas failure can occur between support units or in rotation as shown in Figure 2-7. A key block analysis using J-Block on the other hand can enhance a design by considering all three failure modes. These two approaches are different but ultimately provide two sets of perspectives on the same problem. It is therefore suggested that they should be used in unison as opposed to two mutually exclusive approaches.

2.2.9 Data Collection and Characterization of Discontinuities

Discontinuities refer to joints, fractures, faults and other geological structures. The literature study will commonly refer to joints for simplicity; however, all discontinuities are considered during joint data collection and characterization.

The accuracy of joint data collected is of vital importance as these joint surveys are used to statistically describe rock masses for rock engineering support design purposes. This has been emphasised by various authors such as Call and Nicholas (1978), Beacher (1983), Dershowitz and Einstein (1988), as well as Barton (1995). Key block analysis methods make use of the statistical distribution of the joint properties to assess stability. Priest and Samaniego (1983), Priest (1985) and Goodman and Shi (1984) consider the following joint properties important to collect during joint surveys:

- Joint orientation;
- Joint spacing;
- Joint length; and
- Shear strength properties.

(Gumede & Stacey, 2007) discuss the collection of these joint properties in South African context from underground gold mines.

Joint orientation

Orientation relates to the dip and dip direction of the joint relative to a reference point. Figure 2-6 defines the dip and dip direction on an inclined joint plane model. The dip (β) of the joint is the angle between a horizontal line drawn perpendicular to the strike of the joint plane. The direction (α) is the angle measured clockwise taken from true North to a line drawn perpendicular to the strike of the joint. Joints are noted to be planar in geometry and when aligned in sub-parallel groups are called joint sets (Priest & Samaniego, 1983). Orientation data is commonly recorded in the format of dip (two digits)/dip direction (three digits).

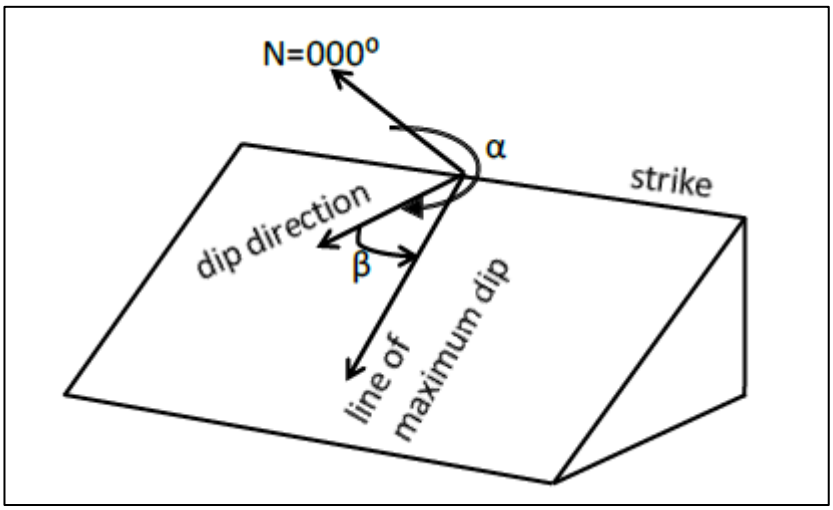


Figure 2-6: Definition of dip (β) and dip direction (α) (Joughin, et al., 2011)

Stereographical projections can be used to visually present captured joint orientation data where sub-parallel joints can be grouped in sets. Joints that do not fall within a set group are random. All the joints that form part of the dataset are given equal weighting for characteristic properties. The joint data must therefore be as comprehensive as possible where mean, maximum, minimum, and standard deviation values for the joint set properties are known (Joughin, et al., 2011).

Joint spacing

Joint spacing is the perpendicular distance between two adjacent sub-parallel joints in the same set (Figure 2-7). The maximum and minimum spacing between joints in a set is required when conducting a key block stability analysis in J-Block. The spacing of the joints influences the sizes and shapes of the blocks formed in the rock mass. It is suggested that the length of the area sample be greater than 10 times the estimated spacing for reliable joint mapping (ISRM Commission on Standardization of Laboratory and Field Tests, 1978). The distance between joints can be simplified into a 2D solution indicated in Figure 2-7 and Equation 2-7.

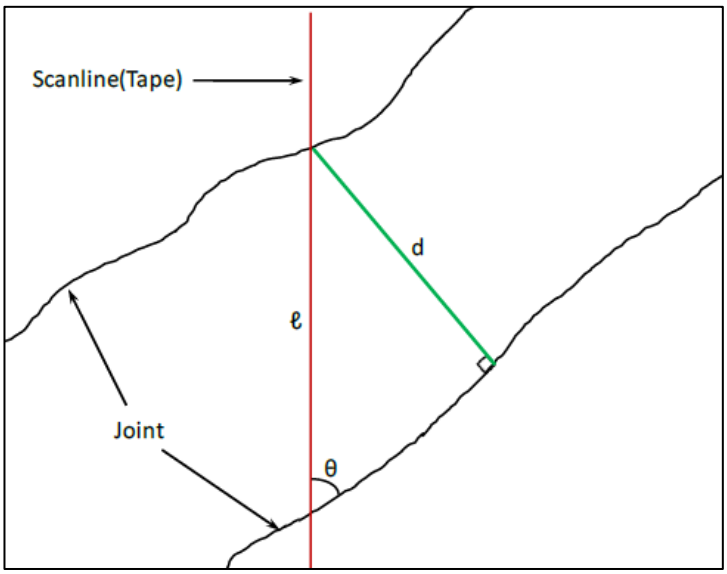


Figure 2-7: Joint spacing along a scanline (Joughin, et al., 2011)

$$d = \ell \sin \theta$$ Equation 2-7:

Where: ℓ is the distance between successive joints of the same set along the scanline

d Is the true spacing distance

θ Is the angle between the scanline and the mean orientation of the joint set.

Joint length (trace)

Joint length also known as traces in this context is the measurable distance between the ends of a joint often marked by the intersection of other joints or the excavation wall rock. These trace lines are measured in straight lines that show the persistence of the joint or the length a joint extends. Joint trace lengths are

estimates as they are often difficult to measure accurately since the entire joint surface cannot be easily seen (Gumede, 2006).

Joint shear strength

Joint shear strength has a significant influence on rock mass behaviour particularly when assessing key block stability. Joint shear strength is a measure of the resistance that a joint surface must resist sliding on its opposite plane. Material infill that can be found between the joint surfaces also affects the joint strength in aiding the sliding motion between joint planes (Joughin, et al., 2011). Several models have been developed to determine joint shear strength such as the Coulomb model (1776), Bilinear shear strength model (Roberds and Einstein (1978), Barton-Bandis model (1990), Barton (1976), Barton et al, (1985), Bandis et al (1983) and Barton (2002) model. These models are discussed in more detail below.

Coulomb model

The Coulomb (1776) failure criterion, for joint shear strength depends on two components expressed in Equation 2-6. These two components are a constant in the joint cohesion (C_j) and the normal stress-dependent frictional component (σ_n tan φ). The weakness in this failure criterion is that it assumes the relationship between the two components is linear which tends to overestimate the joint shear strength at high normal stress. (Joughin, et al., 2011).

$$\tau = C_j + \sigma_n \tan \varphi \qquad \text{Equation 2-8:}$$

Where:

τ	Joint shear strength
C_j	Joint cohesion
σ_n	effective normal stress
φ	internal friction angle of the joint

Bilinear shear strength model

Patton (1966) developed the Bilinear shear strength model to address the weakness associated with the Coulomb model. The model assumes a non-linear shear-normal stress relation that was demonstrated through a toothed saw joint plane experiment shown in Figure 2-8. At low normal stresses, shear failure is driven by sliding of the joint surfaces whereas at higher normal stress, shear failure is driven by a breaking-off of the asperities of the joint plane. This later condition presents a weakness in this model where the breaking-off of asperities is seen to relate more closely with intact material failure rather than shear joint failure (Joughin, et al., 2011). Patton (1966) concluded that the change in the gradient of the failure envelope represents a change in the failure mechanism. The Bilinear shear strength model is expressed in Equation 2-7 as follows:

$$\tau = \mathrm{C}_j + \sigma_n \tan \varphi_b + i \qquad \text{Equation 2-9}$$

Where:

τ	Joint shear strength
C_j	Joint cohesion
σ_n	effective normal stress
φ_b	basic friction angle of a smooth joint surface
i	The roughness angle of the saw-toothed face

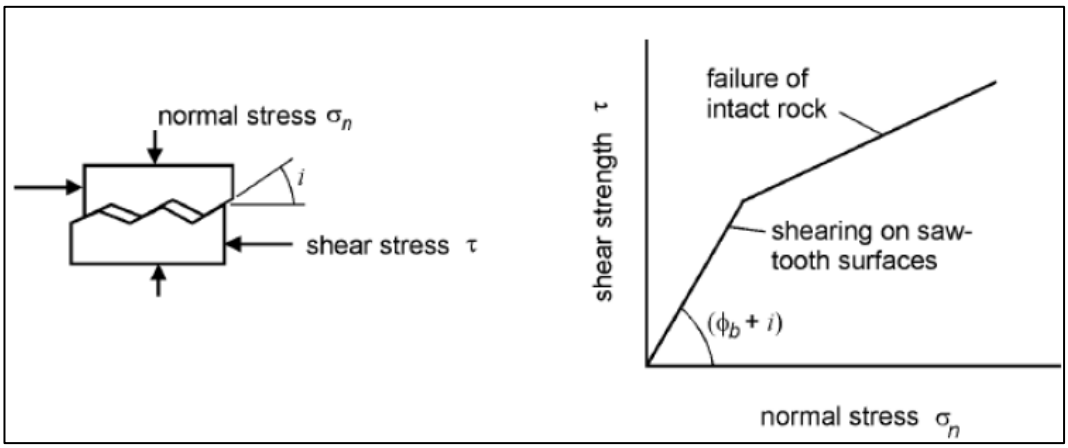


Figure 2-8: Patton's (1966) saw-tooth experiment (left) & bilinear shear strength model (right) (Joughin, et al., 2011)

Barton-Bandis shear strength model

The Barton-Bandis model (1990) was developed as an enhancement of Patton's approach where the change in shear strength with increasing normal strength is gradual rather than abrupt. Barton studied natural joint surfaces and developed simple practical methods that incorporated two additional parameters (JRC – Joint Roughness Coefficient and JCS – Joint-wall Compressive Strength) in the model to determine the shear strength of the joint (Joughin, et al., 2011). The Barton-Bandis model is expressed in Equation 2-10 as follows:

$$\tau = \sigma_n . \tan\left\{\varphi_b + JRC \log_{10}\frac{JCS}{\sigma_n}\right\} \qquad \text{Equation 2-10}$$

Where:		
	τ	Joint shear strength
	σ_n	effective normal stress
	φ_b	basic friction angle of a smooth joint surface
	JRC	Joint roughness coefficient
	JCS	Joint-wall compressive stress

The JRC and JCS parameters can be estimated in the field or a laboratory. The effective normal stress on a joint is considered an external parameter and can be reliably measured. The JRC is a measure of the asperities or undulations along a joint surface. The asperities have an interlocking effect during shearing that increases the friction angle to be greater than the base friction angle. JRC can be obtained by comparing the undulation profiles generated by Barton and Choubey (1977). Alternatively, the JRC can be back-calculated using an index test (to obtain JCS) by making JRC the subject of Equation 2-10 (Gumede, 2006).

JCS represents the condition of the joint walls and is affected by the influence of weathering, moisture, and permeability. When the joint surface is un-weathered, the JCS value is the same as the unconfined compressive strength of the rock material. As the degree of weathering or moisture content along the joint surface increases, the JCS decreases. The use of the Schmidt rebound hammer index test together with a base friction angle of a material determined from a tilt test can be used to estimate the JCS. This was initially proposed by Deer and Miller (1966), supported by Barton and Choubey (1977), and later endorsed by (Brown, 2003). The ISRM (1978) has also published suggested methods for estimating the JCS that are aligned with international standards.

The Barton-Bandis model ultimately is suitable for expressing pre-peak shear joint behaviour but is weak when describing pre-yield and post-yield joint shear behaviour (Joughin, et al., 2011). Barton-Bandis (1982) identified through extensive testing of joints, joint replicas, and review of the literature a scale effect on JCS and JRC estimates. Due to the greater possibility of weaknesses on a larger surface Barton-Bandis (1982) suggests an increased likelihood of the average *JCS* decreases with increasing scale. They proposed scale correction on JRC and JCS indicated by the following relationships in Equation 2-11 & Equation 2-12.

$$JRC_n = JRC_o \left\{\frac{L_n}{L_o}\right\}^{-0.02JRC_0}$$ Equation 2-11

Where: JRC_o & L_o refer to 100 mm laboratory scale samples

JRC_n & L_n refer to in situ block sizes.

$$JCS_n = JCS_o \left\{\frac{L_n}{L_o}\right\}^{-0.03JCS_0}$$ Equation 2-12

Where: JCS_o & L_o refer to 100 mm laboratory scale samples

JCS_n & L_n refer to in situ block sizes.

Barton model shear strength model

The Barton (2002) model is a calculation of joint friction angle expressed in Equation 2-13:

$$\varphi = \tan^{-1}(\mathrm{J}_r/\mathrm{J}_a)$$ Equation 2-13

Where:

φ	Friction angle
J_r	Joint roughness condition
J_a	Joint alteration condition

This model assumes that joints are cohesionless and provides a simple, easy, cheap method of estimating joint shear strength (Joughin, et al., 2011). The friction angle is determined using two Joint conditions (J_r & J_a) parameters. The joint roughness condition number is the degree of asperities and undulations along a joint surface. The joint alteration is dependent on the thickness of the infill material and water condition along the joint surface. These joint conditions are typically determined visually and through the touch and feel of the exposed joint surface.

2.2.10 Joint Mapping Techniques

Joint mapping is a process of observing and capturing data parameters of discontinuities from exposed rock mass or drilled core. It involves mapping discontinuities in terms of location, spacing, frequency, and orientation and may include capturing the condition of the discontinuity. This information is used to gain an understanding of the rock mass characterization, block kinematics, and mechanical behaviour of rock. There are 5 common types of exposure joint mapping techniques used discussed below:

1. Spot mapping - This is the selective sampling of only important discontinuities. The effects of a joint network on the mechanical rock mass behaviour are ignored. Brown (2003) however, indicated through various literature the significant influence random joints have on rock block formation.
2. Area (window mapping) - This involves the mapping of only the joints within a selected area shown in Figure 2-9. The orientations, lengths, spacings and roughness of the joints within the area are recorded. Joint trace lengths that fall outside the window are ignored. This reduces the sampling bias for orientation and size however is practically difficult to apply in narrow underground stopes (Joughin, et al., 2011). This is due to the limited height along the sidewall wall surfaces of stope excavations. The largest suitable and available area to map is across the stope hangingwall, however, obtaining an areal view that is essential when conducting area window mapping is nearly impossible in a narrowly confined stope where elongate support is in the way.

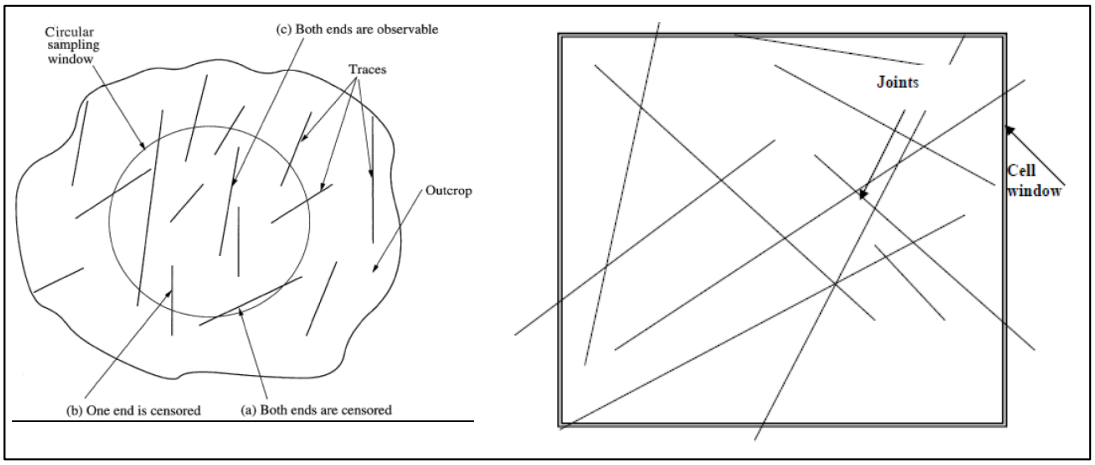


Figure 2-9: Area mapping (left) Zhang and Einstein (1998) (right) (Gumede, 2006)

3. Photogrammetric mapping – This requires the use of a high-resolution camera to produce point cloud-orientated joint mapping. Digital-resolution software is then required to interpret and create a 3D digital surface called the Digital Terrain Model (DTM) (Figure 2-10). The DTM is made of spatial data points that are used to characterize the rock mass in terms of joint dip direction, dip, and spacing measurements (Joughin, et al., 2011).

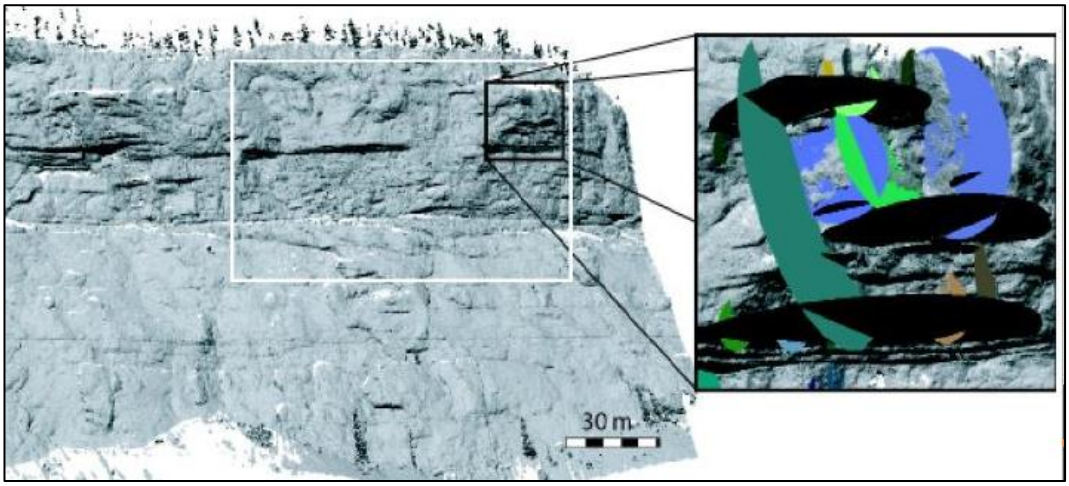


Figure 2-10: Photogrammetric mapping (Sturzenegger & Stead, 2009)

Photogrammetric mapping has limited use underground due to the low lighting environment, however, the technique is fast gaining entry as technology develops. The technology is relatively expensive. The major advantage is its usage in inaccessible areas as well as the ability to capture

joint-fracture networks include joint roughness properties over very large areas up 3 km (Song, et al., 2023). The technique does not require direct exposure to the rock surface being mapped and is said to be five times faster than manual data collection methods (Joughin, et al., 2011). A limitation however is the capturing of other joint properties such as infilling (thickness), joint wall strength, alteration or degree of weathering. These joint properties are usually obtained by direct observations in the field that include a touch and feel of joint planes. Developments in drone technologies are said to soon overcome these limitations (Tannant, 2015).

4. Core logging - This is an indirect method to measure orientations and joint spacings in the unexposed part of a rock mass. It requires the recording of the orientation and joint properties of joints along the retrieved borehole core. Its weakness when compared to the other mapping techniques lies in the inability to measure joint length (Gumede, 2006). It is therefore used in conjunction with scanline mapping to obtain a 3D view of the joint data.

5. Scanline mapping - This is a common joint mapping technique, known to be cheap and suitable for probabilistic key block analysis (Kemeny and Post, 2003). The method requires a straight line to be fixed across the rock surface and all the discontinuities that intersect the line are mapped as shown in Figure 2-11. Brady and Brown (2004) suggest the use of a measuring tape kept taut at all times pinned along the rock surface or a line drawn in with chalk on the rock surface. Only the properties of discontinuities that cross the tape are recorded. To obtain a 3D view of the joint data, two orthogonal scan lines (dip & strike) must be taken along the hangingwall and a vertical borehole into the hangingwall is used for the 3rd dimension. Circular scan lines used for joint mapping offer the advantage of eliminating orientation bias (Baecher and Einstein, 1977).

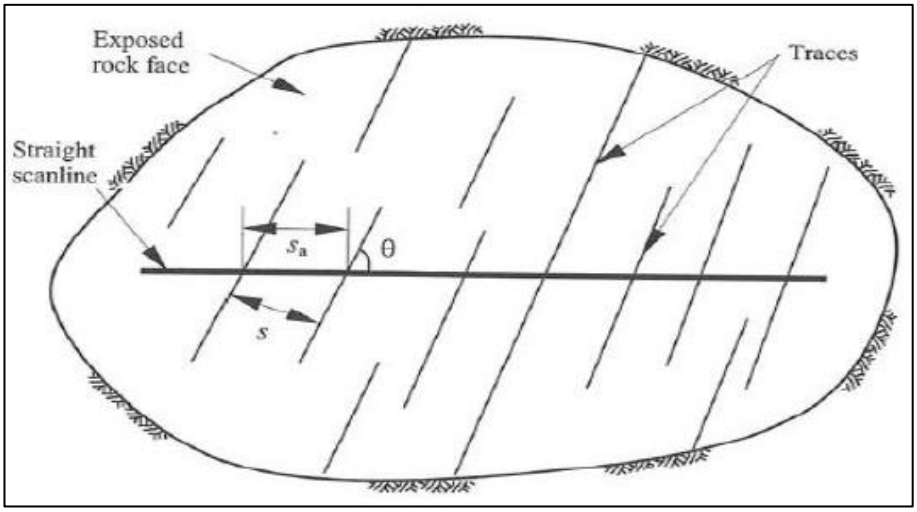


Figure 2-11: Straight scanline mapping

The scanline technique is however unreliable when mapping joint sets orientated at angles less than 20 degrees (<20^0) from the scan line. Priest (1993) suggested that there should be 150 (3 joint sets) – 350 (6 joint sets) observations to obtain sufficient data. Robertson and Mac (1970) suggested each joint set should have at least 100 observations to reduce the effect of potential errors. Call et al (1976) suggested that the number of observations is required to be a function of the degree of fracturing per joint set.

2.2.11 Joint mapping biases (errors)

Errors in joint mapping can arise from various sources such as human error, instrumentation error, joint length, orientation, censoring and truncation (Baecher & Lanney, 1978). These errors are discussed in detail below:

Joint length bias

Joint length bias occurs due to variations in the joint trace length. The probability that a particular discontinuity is intersected by the scan line depends on the orientation of the scan line and the length of the scan line. Larger discontinuities are more likely to be visible than smaller joints. In addition, longer trace lengths are more likely to intersect the scan line than short ones. The variation in joint trace length means some discontinuities are not accounted for during the scanline

mapping leading to a non-equal sampling bias (Joughin, et al., 2011). To overcome this, trace lengths are measured over their exposed length and the overall length can be statistically predicted (Gumede, 2006).

Joint censoring bias

Joint censoring bias is when joint trace length is cut off when the joint trace runs into the rock walls and the full length of the joint cannot be observed. This effectively reduces the length of the joint trace. Although difficult to overcome, censoring bias can be corrected by a method developed by Lasslet (1982) (Villaeuscusa, 1992). Villaescusa (1992) demonstrated this through a statistical method known as the maximum likelihood estimation applied to a distribution of the observed joint trace data. It was shown to correct simultaneously for joint censoring, truncation, and size bias (Villaescusa, 1992). The mathematics of this statical method are very long and complex and were not included in this literature review.

Joint truncation bias

Joint truncation occurs when discontinuities that fall below a pre-determined cut-off length (e.g. 0.5 m) are ignored. This may overestimate the spacing values due to the short discontinuities being omitted from the dataset. The truncation limit set depends on the purpose of the investigation (i.e. size of the unstable blocks being assessed). For example, assessing small blocks that can fall through safety net apertures will require a much smaller truncation limit than assessing large blocks that can fail, damage, or cause panel collapses. In the latter case, a high truncation limit is justified. Villaeuscusa (1992) suggested that the truncation bias can be corrected using a statistical method that makes use of the maximum likelihood estimator. This approach was also shown by Warburton (1980).

Join orientation (spacing) bias

Joints that are sub-parallel to the rock face have a lower probability of intersecting the scan line than joints perpendicular to the scan line. Terzaghi (1965) demonstrated this by showing that the number of joints that are sub-perpendicular

to the scan line are more likely to intersect the scan line than joints that are sub-parallel to the scan line (Figure 2-12). This error is reduced by having 3x mutually orthogonal scan lines in the same area however the vertical (borehole core) of sufficient length is often difficult to obtain.

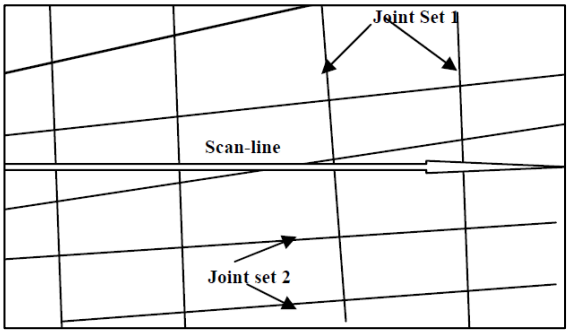


Figure 2-12: An illustration of joint orientation bias in a scan line survey (Gumede, 2006)

Terzaghi weighting method

A Terzaghi weighting method can be used to overcome biases associated with joint orientation. This method weighs the frequencies of the observed discontinuities by a bias compensation factor to reveal important data concentrations within a cell/mesh which may not be apparent on a normal (unweighted) stereographical projection. The bias compensation factor is the reciprocal of the sine of the intersection angle between the scanline and discontinuity expressed in Equation 2-14.

$$\text{Bias compensation factor} = 1/\sin\theta \qquad \text{Equation 2-14}$$

Where: θ is the angle between the scanline and the discontinuity introduced during data collection.

The Terzaghi method has been widely used by researchers, including Goodman (2013), Park et. al, (2005) and Fouche and Diebolt (2004). Tang et. al (2016), found

that the Terzaghi method involved some errors that persisted even when optimizing countermeasures were applied. The true source of this error is unknown however is suspected to be from the meshing effect (Tang, et al., 2018). Tang et. al (2018) presented the modified Terzaghi method that eliminates the meshing procedure improving the accuracy of the bias correction method. The modified Terzaghi method entails multiplying this bias compensation factor by counted frequencies that fall at the poles.

This modified Terzaghi weighting method is a feature built into the Rocscience DIPS software. The bias compensation factor is referred to as the geometric weighting factor, W shown in Figure 2-13. DIPS allows the user to set the "minimum bias angle" (recommended between 5^0 – 25^0) with the default setting of 15^0. This means that any planes that intersect the scanline at an orientation angle less than the "minimum bias angle", will be limited to the maximum weighting factor.

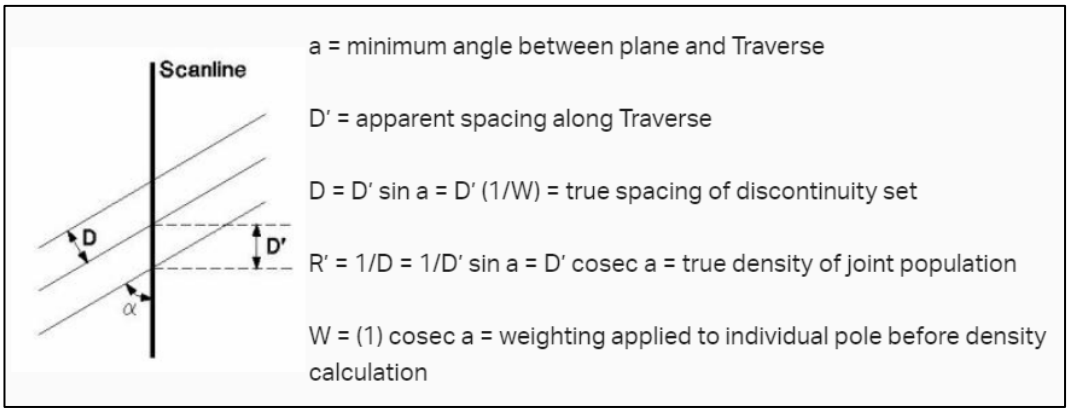


Figure 2-13: Terzaghi geometric weighting factor, W compensate for orientation bias

2.2.12 Other Rock Mass Mapping Techniques

Petroscope/Borehole camera mapping

There are other techniques available for mapping discontinuities deep in a rock mass not exposed to the naked eye. Besides the visual assessment from the retrieved borehole core, the inside of boreholes can be visually examined using instruments such as a Petroscope or Borehole camera. These instruments are

similar in principle with the latter being much more expensive (Ryder & Jager, 2002). A borehole camera is a battery-powered video camera and recorder that consists of a rugged camera head attached to a probe-length tube fitted on an extension reel or spool. The probe length tool allows the camera head to extend deep within the borehole providing visual recordings of the rock mass within the borehole (Ryder & Jager, 2002). Mapping discontinuity parameters is difficult, and the use is therefore mostly limited to identifying the position of structures and identifying variations in rock types.

Ground Penetrating Radar

Ryder and Jager (2002) describe Ground Penetrating Radar (GPR) as a rapid, non-destructive, high-resolution electromagnetic reflection-based geophysical tool. It makes use of high-frequency electromagnetic waves transmitted through the rock mass and reflected to the unit to build an image of the rock mass. Fractures, geological discontinuities, and variations in rock types around excavations can be mapped up to 30 m deep. The data captured by the GRP however needs processing and analysis done a on personal computer to build a representative image of the rock mass.

The effectiveness of the GPR device is affected when used in proximity to metallic objects (such as pipes, rock bolts and meshing) that reduce the reflectivity of geological structures in the rock mass. Grodner (1999) however demonstrated that useful results can still be obtained despite this challenge.

2.2.13 Wide Reef Mining

According to Jager (1999), wide reef mining is a term generally used in South African mines when the stoping width exceeds 2.5m. There are a variety of mining methods that are used for wide reef mining that include, conventional stoping, pillar mining, and double and multi-cut mining. In a conventional mining environment, the main limitation with increasing the stoping width is the decreased efficiency of stope support units such as mechanical props and timber elongates.

When the orebody necessitates that the stoping width be greater than 2.5 m then the double-cut method can be used. For example, a 5.0 m wide orebody can be

divided into 2x cuts. The uppercut is done first to create space for supporting and practical mining. In such cases where the stoping width exceeds 2.5 m and double-cut methods are used appropriately designed hangingwall bolts are recommended (Figure 2-14). Timber-based units such as packs and elongates become increasingly ineffective at a stoping width greater than 2.0 m. This is due to a loss in the initial stiffness of the timber unit as well as increased proneness to buckling (Jager & Ryder, 1999).

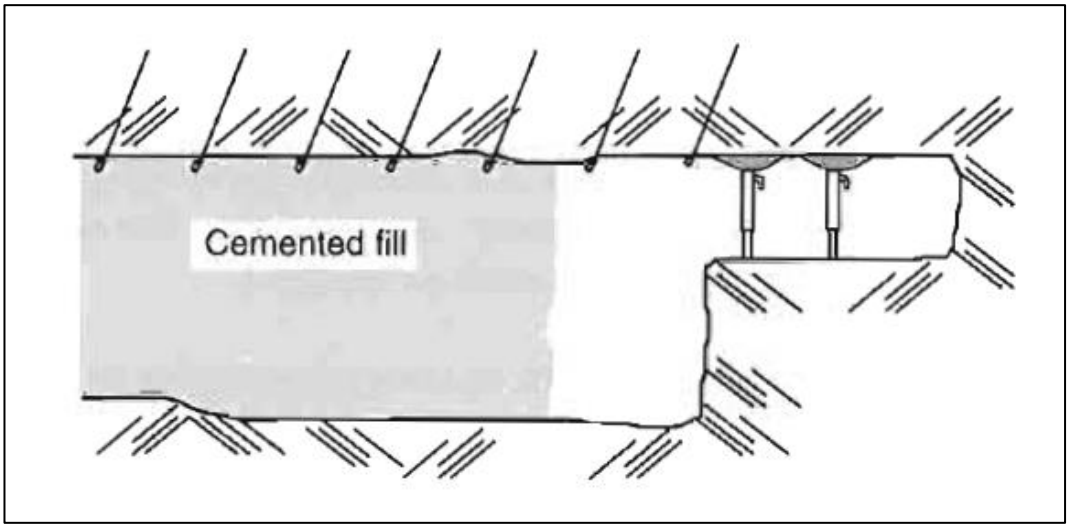


Figure 2-14: Double-cut mining layout and support (Jager & Ryder, 1999)

2.2.14 Cases of footwall extraction (multi-cut mining)

There are limited cases of footwall mining extraction being done from mined-out stopes. Footwall lifting is typically done to create infrastructure excavations. Winch beds and/or gully scraping paths are created from footwall lifting to facilitate normal stoping operations. Footwall mining done on a large scale occurs in unique circumstances where the orebody is wide (>2.0 m). This situation can occur where reef bands left in the footwall of mined-out stope later become desirable to mine.

More O'Ferrall (1981) refers to this scenario in a deep-level gold mine stope where the initial stope mined-out experiences total closure. The second phase of mining is carried out similarly to the initial cut. This is beneficial as the support in the second cut only needs to cater for the dead weight loaded onto the packs from the initial cut. When total closure has not occurred, a higher pack needs to be installed.

This may be problematic as a high pack generates lower load resistances than a low pack for the same closure.

When a critical span is reached the hangingwall will rapidly settle on the packs and may result in total loss of the panel. To address this, 5.0 m rib pillars or ridges are left intact and unmined. When total closure has occurred, the 5.0 m block left unmined can be assumed to act as a pillar. When total closure has not occurred the unmined block acts as a ridge with timber-based support on top of it. A 15.0 m–25.0 m span of the panel footwall is mined between the rib pillars or ridge as can be seen in Figure 2-15.

More O'Ferrall (1981) does not explain how he arrived at a 5.0 m wide rib pillar and the 15.0 m critical span. The author believes the 5.0 m wide pillar was selected to maintain an effective width-to-height ratio for the desired conditions. The critical span may be based on empirical evidence where rapid closure of the hangingwall occurs.

If the original timber support installed from the initial cut left on top of the ridge islands has decayed, it must be replaced by installing a new pack or stick-type support. The rib pillars or ridges can be removed when mining in a retreat direction allowing the stope to collapse (More O'Ferrall, 1981).

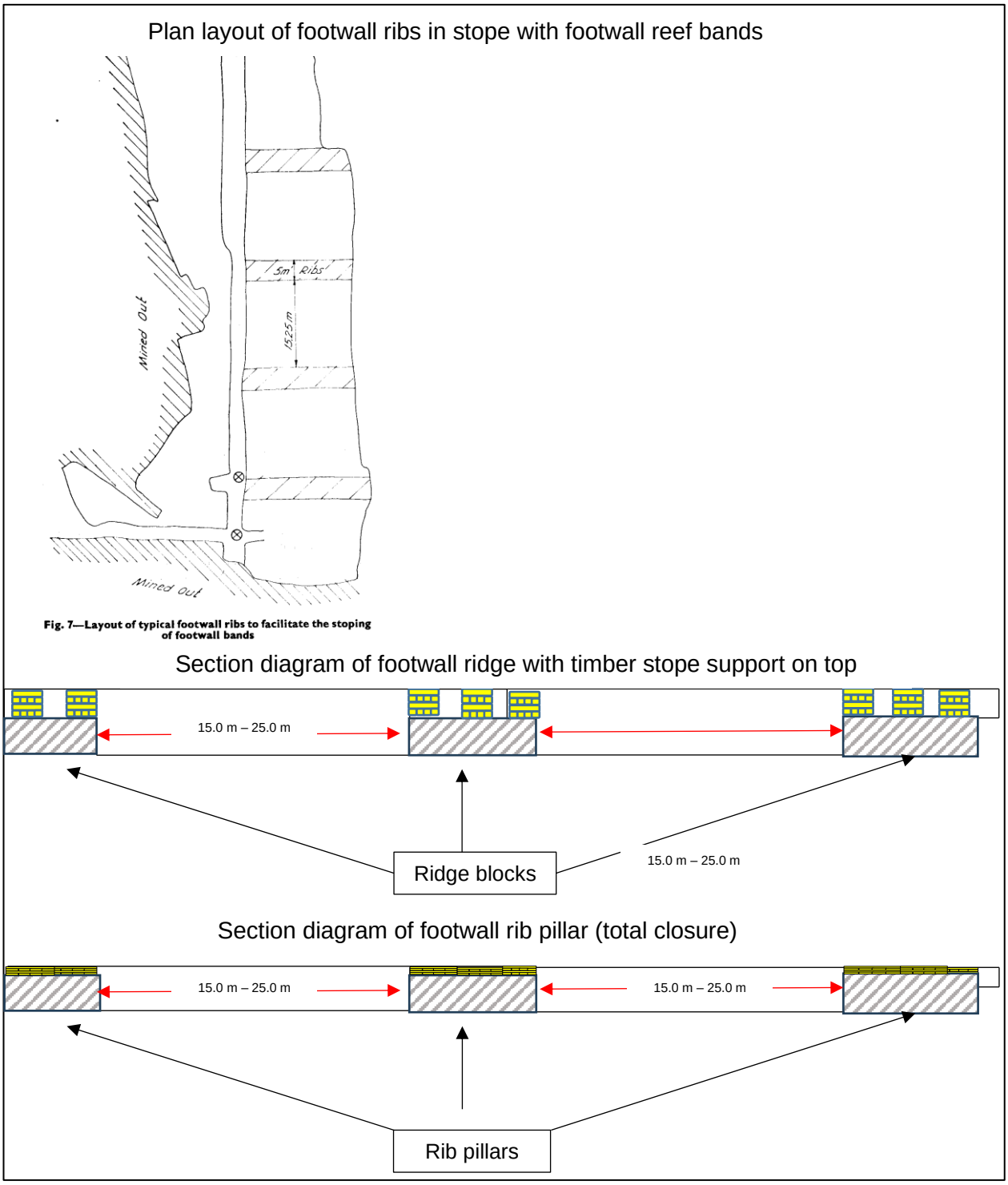


Figure 2-15: Layout (top) and section diagram (bottom) of footwall ribs for stoping of footwall bands (More O'Ferrall, 1981)

2.2.15 Wide reef mining at Impala No 2A shaft

Wide reef mining was conducted at the Impala No 2A shaft in early 2005. Two zones were identified with wide mineralised Pegmatoid below the top reef contact. The zones were located between raise lines 236 and 237 (zone 1) and between raise lines 337 and 338 at approximately 310 m below the surface (DuToit, 2009).

The 2A shaft high stoping width mining methodology made use of conventional stoping techniques. This included the use of Advanced Strike Gullies (ASGs) to scraper clean panels and slusher excavations to draw ore out of the stopes. The stopes were mined progressively downwards in 2-3 cuts of 1.0 m - 2.0 m increments from the top contact to create a 4.0 m - 6.0 m high stope excavation (Figure 2-16). These panels were between 15 m to 20 m in length with 6 m x 15 m grid pillars (Figure 2-17). The bolt support system made use of 1.8 m long Xpandabolts (Swellex) and 4.5 m long cable anchors (Appendix C and D).

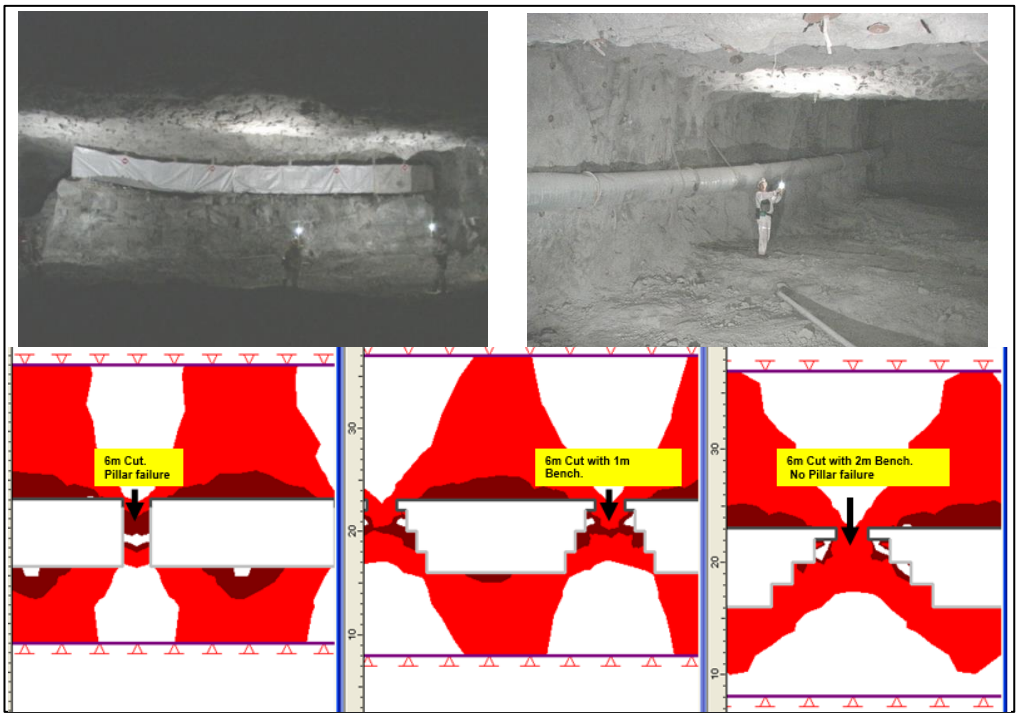


Figure 2-16: Photograph of 6.0 m high stope (top) and PHASE^2 model layout for 20.0 m wide x 6.0 m high stope (bottom) (DuToit, 2009)

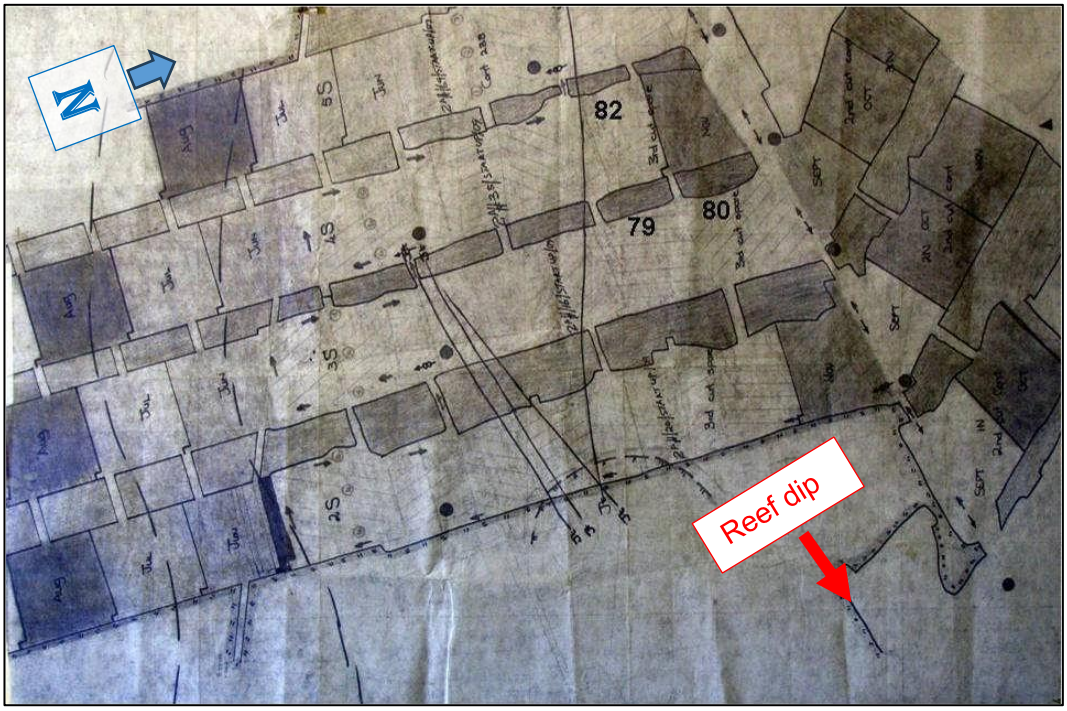


Figure 2-17: Copy of stope plan for 20.0 m wide panel with 6.0 m x 15.0 m planned grid pillars (Malan, 2009)

The 2A shaft high stoping width methodology and support system were successfully carried out up until 2010. This was impacted after 2 major falls of ground fatality accidents that occurred at Impala Platinum's (9-person fatality) and Aquarius Platinum's (5-person fatality) bord and pillar sections in 2009. The North-West Department of Mineral Resources and Energy (DMRE) inspectorate issued an instruction for all bord and pillar operations to reduce their spans to 6.0 m (Appendix E).

Although the instruction was specific to bord and pillar operations in the Northwest region, Impala Platinum decided to implement this change in the 2A shaft high stoping width section. This was done because the 2A shaft high-stoping method was a tendon-reliant support system much like a bord and pillar operation (Malan, 2011).

2.2.16 Timberless stoping Amandelbult

Timberless stoping has been carried out at Anglo Platinum's Amandelbult Dishaba mine since 2006. In this context, timberless stoping as the name suggests, entails

the supporting of stope panels with cable anchors as opposed to timber support units. This change was introduced following a series of FOGs that were encountered in their timber support system. In addition, a shortage of timber in the industry was experienced in 2005 and was expected to pose a significant risk to the mine's future mining operations (van Aswagen, et al., 2010).

Discussion with Prinsloo (2024) revealed that the timberless stoping was initially carried out only in UG2 panels but later was expanded to Merensky panels. The stoping heights were on average between 1.2 m to 1.8 m wide however wider stoping heights up to 3.0 m were later trialled in 2018 but mined on a much smaller scale.

The support system of timberless panels consists of 30.0 m wide panel spans supported on 3.0 m x 3.0 m chain crush pillars located on either side of the panels. Cable anchors of 3.0 m in length, were installed on a 3.0 m x 3.0 m pattern and RSS grout packs were installed, 3.0 m apart on the dip and 5.0 m apart in the direction of advance, in the back area. Notably, the reduction of FOGs that was achieved by this change was recently further improved by installing a permanent mesh areal coverage (van Aswagen, et al., 2010).

2.2.17 Rock breakage (blasting) in stopes

Rock breaking using explosives is the primary rock-breaking method used in Gold and Platinum conventional mining stopes. It requires shot holes to be drilled into the face and later charged (primed) with explosives. The drilling of shot holes is done under temporary support timeously and correctly installed in the face. Temporary support is installed directly in the face area and is later removed at the end of the shift before blasting takes place. Temporary support not withdrawn from the face will likely be taken out by the blast. Likewise, workers are required to evacuate the stope well before the blasting time which also puts constraints on other activities in the mining cycle (Daehnke, et al., 1998).

Blasting is violent by nature and involves the ejection of broken ore at high velocities from the face area much of which strikes permanent support units such as timber elongates. Permanent support units must therefore be built to resist or absorb the impact of the blast. The removal of temporary support from the face

means the newly installed permanent support must cater for the required support resistance. In addition, blasting also directly impacts the size and shape (stoping width) of the stope as well as rock mass conditions (degree of fracturing). The unsupported span after the blast is dependent on the rate of advance and together with the fracturing of the rock mass caused by the blast creates unsafe conditions that need to be remedied at the beginning of each shift (Daehnke, et al., 1998).

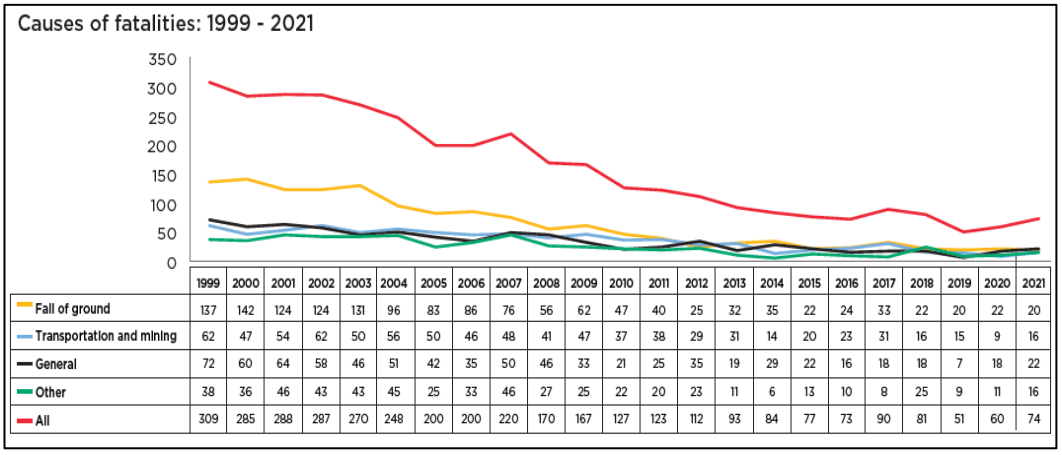
When selecting the choice of explosives, it is very important to consider the ground conditions, rock strengths and degree of stress fracturing in the rock mass. When the rock mass is severely fractured and/or weakened by geological disturbances, it is favourable to use low gas pressure emitting explosives rather than high gas content explosives. Strong high gas content explosives penetrate the crack openings and result in more damage to the host rock. Some explosives are not suited for wet rock mass conditions associated with groundwater (Mining Qualification Authority, 2006).

The most important parameters of the blast design are the burden of the shot hole which is dependent on the shot hole spacing. Excessive burdens often cause damage to the surrounding rock mass due to the extensive propagation of blast fractures. This is particularly exacerbated when the burden is increased in the direction perpendicular to the principal stress directions (Jager & Ryder, 1999).

2.3 Key Debates and Controversies

2.3.1 Fall of Ground Statistics

The mining industry has achieved revolutionary success with the reduction of FOG fatalities and injuries. FOG fatalities have reduced from 187 fatalities in 1999 to 20 fatalities in 2021 indicated in Figure 2-18. FOG injuries reduced from 1121 in 2003 to 277 in 2022 shown in Figure 2-19. This reduction in FOGs can be linked to some of the industry-adopted initiatives such as the Mining Occupation Safety and Health (MOSH). Early Entry Examination and Making Safe (EEMS), instope bolting and netting, Trigger Action Response Plan (TARP), and Ledging Leading Practice adoption (Figure 2-19). This trend is further emphasised in Figure 2-20 where FOG accidents have continued to decline at the Impala Platinum mine since 2012.



	1999	2000	2001	2002	2003	2004	2005	2006	2007	2008	2009	2010	2011	2012	2013	2014	2015	2016	2017	2018	2019	2020	2021
Fall of ground	137	142	124	124	131	96	83	86	76	56	62	47	40	25	32	35	22	24	33	22	20	22	20
Transportation and mining	62	47	54	62	50	56	50	46	48	41	47	37	38	29	31	14	20	23	31	16	15	9	16
General	72	60	64	58	46	51	42	35	50	46	33	21	25	35	19	29	22	16	18	18	7	18	22
Other	38	36	46	43	43	45	25	33	46	27	25	22	20	23	11	6	13	10	8	25	9	11	16
All	309	285	288	287	270	248	200	200	220	170	167	127	123	112	93	84	77	73	90	81	51	60	74

Figure 2-18: Causes of fatalities in the South African mining industry from 1999 to 2021 (Seccombe, A, 2022)

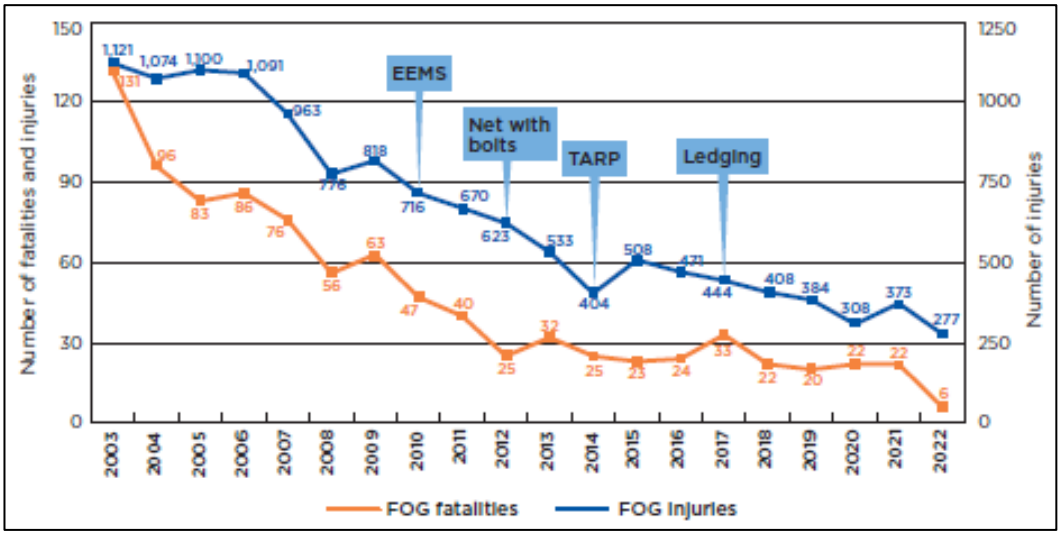


Figure 2-19: FOG-related reportable injuries and fatal accidents (Rakumakoe, O, 2023)

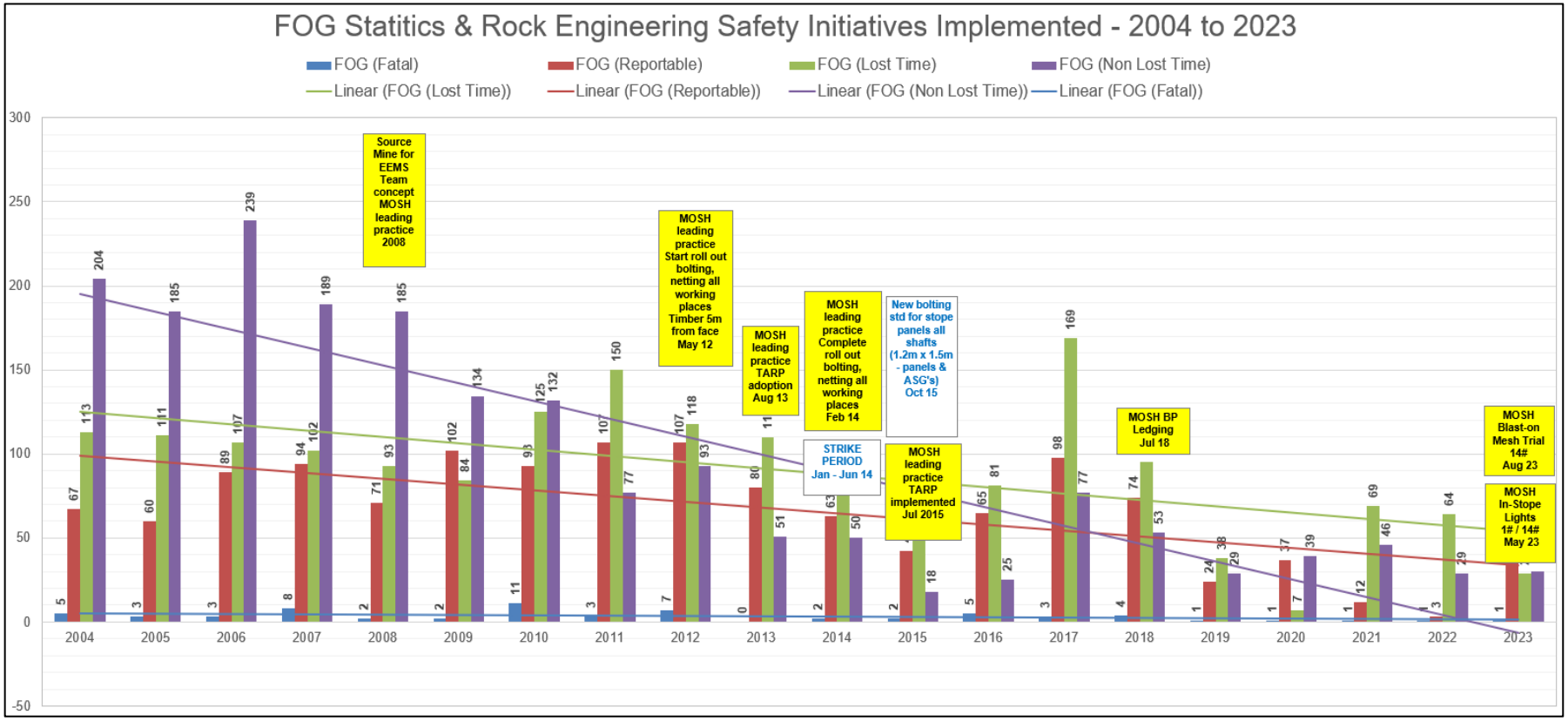
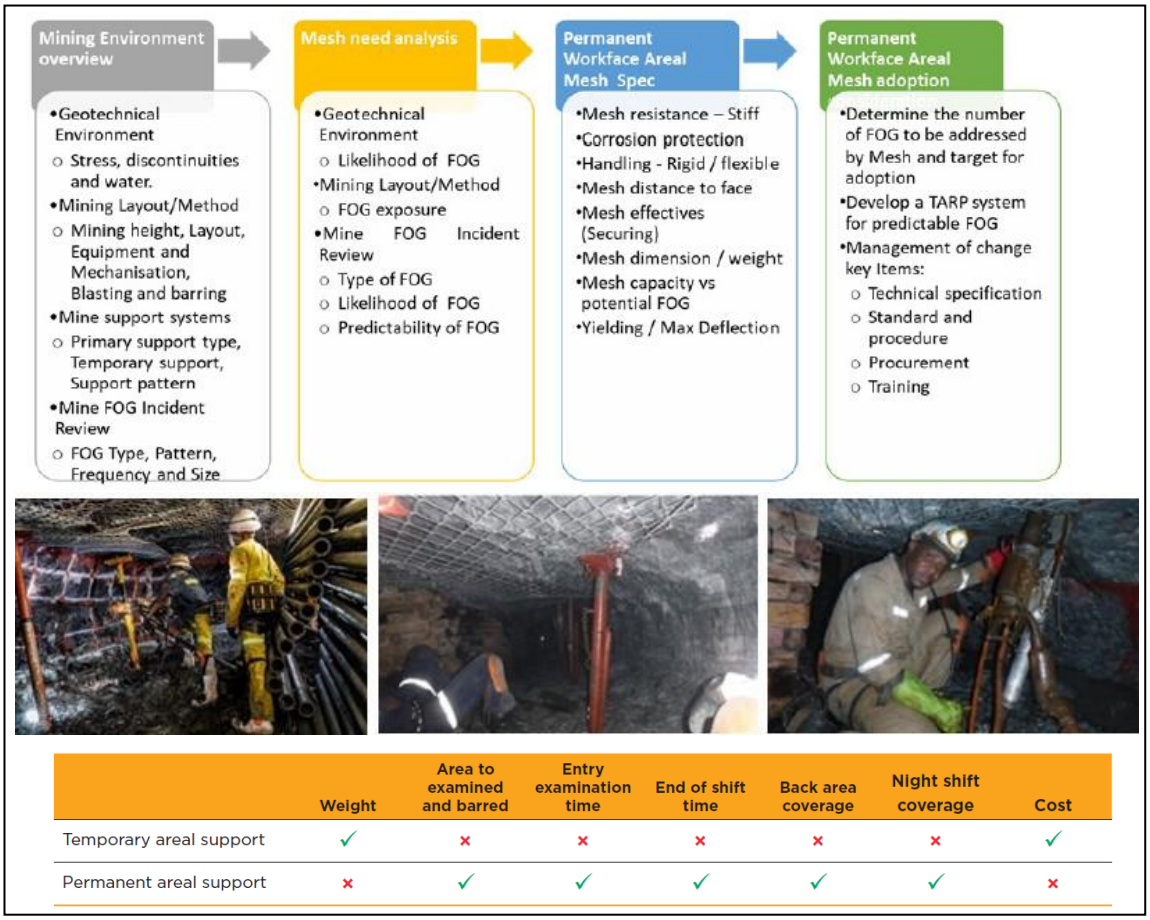


Figure 2-20: Impala Platinum FOG Statistics and Rock Engineering Safety Initiatives Implemented - 2004 to 2023 (Carollo, L, 2023)

2.3.2 Future support design improvements to reduce FOG accidents:

Despite this improvement over many decades, the number of FOG fatalities has plateaued and has not improved significantly since 2012 (Seccombe, A, 2022). The latest industry initiative to eliminate FOG fatalities is the adoption of permanent areal coverage mesh in stope panels. Figure 2-21 indicates the permanent work face areal mesh design process.



	Weight	Area to examined and barred	Entry examination time	End of shift time	Back area coverage	Night shift coverage	Cost
Temporary areal support	✓	×	×	×	×	×	✓
Permanent areal support	×	✓	✓	✓	✓	✓	×

Figure 2-21: MOSH permanent-workface-areal-mesh-adoption-process (Rakumakoe, O, 2023)

2.4 Chapter Summary

This literature study chapter of the research report discussed the deterministic support design where support resistance “demand” and “capacity” are evaluated against each other to obtain an acceptable FOS value. The tendon design philosophy was covered where suspension is accepted as the common and simplistic application of tendon support. There are a wide variety of tendon types available for use with unique characterises. The rock engineer must select the best-suited tendons to the geotechnical conditions.

The J-Block software was seen as a suitable tool that can be used for a probabilistic key block analysis approach to enhance the deterministic approach. A variety of joint mapping tools are available however all have their advantages and limitations. The scan line technique was deemed appropriate for J-Block. All the biases (errors) in a joint mapping exercise must be understood and corrected to accurately characterize the rock mass.

Wide reef mining entailing multiple cuts invariably eliminates the use of timber-based support where the stoping height exceeds 2.0 m due to the buckling effect. Reliance is consequently placed on tendon support-based systems to ensure stability.

Monitoring programmes are essential in providing an early warning system for underground workmen, particularly in the absence of timber-based support that normally provides warnings of imminent collapse. Stope closure meters would be best suited for identifying unusual deformation between the hangingwall and footwall.

Blasting and its influence on the stability of the rock mass are greatly affected by shot hole burdens in a blast design. These must be optimised to achieve the best stability results whilst obtaining the required fragmentation and advance.

Support design initiatives have made a significant impact on FOG accident reduction in the industry. Instope bolting and netting can be argued to be significant initiatives that have reduced FOG fatalities and injuries in the mining industry.

3 RESEARCH MODEL

3.1 Introduction

This chapter describes the research process that was followed throughout the project. It shows various stages of data gathering, analysis, evaluation and reporting that were done. The design of the research follows the project flow process provided in Figure 3-1 below.

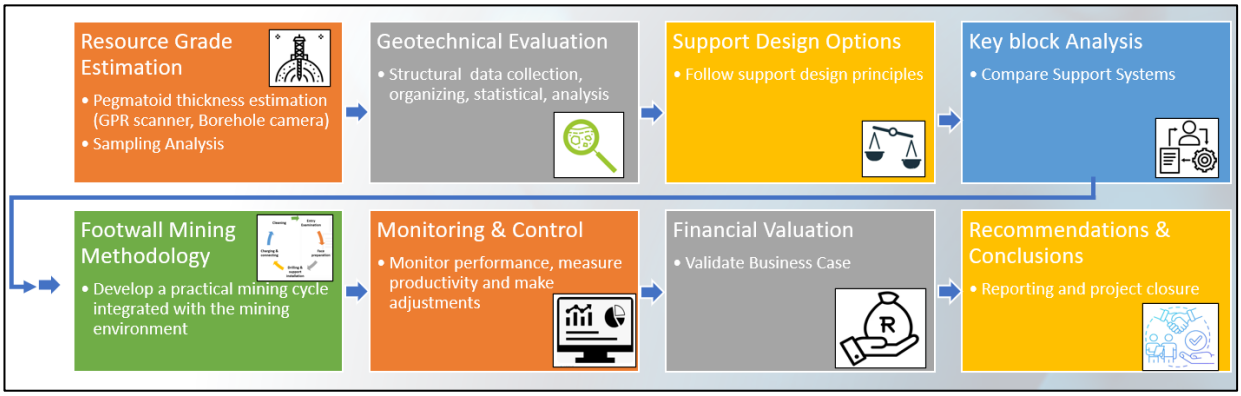


Figure 3-1: Research design process flow

The research began with a data collection phase where sampling data from the trial site was assessed to confirm and validate grade estimation values. These grade estimation values were used downstream in the project's financial valuation. The data collection also included geotechnical data captured through structural mapping, GPR scanning, and borehole camera assessments in the project trial site. Subsequently, there was a support design phase where two methods were considered for analysis. The first approach was a deterministic method that made use of the tributary area concept and Factor of Safety (FOS). The second approach was a probabilistic method that made use of statistical geotechnical information through a key block analysis program. The key block analysis program used was J-Block which simulated key blocks against the support design options (Esterhuizen, 2003).

3.2 Data Validation Process

A data validation process was carried out on the geotechnical structural data collected. The orientation of the structural data captured with the Apple device was checked and validated with a magnetic compass. The data was further validated by checking that the structural data was captured correctly in Excel.

The analyses of the results obtained from J-Block are described in Chapter 6. Tables and graphs were used to analyse the findings and trends, anomalies and correlations. The conclusions were based on these evaluations.

3.3 Chapter Summary

The research is structured in a format that follows a process flow with several stages. The project was scheduled into high-level activities that are explained on a Gantt chart timeline. This format enabled the various activities to be tracked and monitored. The research can be defined as a unique endeavour with a set of activities done with a defined timeline where budgeting and/or costing are factored (Association for Project Management, 2023).

4 DATA FOR THE STUDY

4.1 Introduction

Data collection was carried out in four main areas:

- Pegmatoid thickness analysis;
- Grade resource estimation; and
- Geotechnical structural mapping; and
- Support elements used in the trial stope.

4.2 Pegmatoid thickness analysis

The thickness of the H-reef varies across the mine and affects the depth of the footwall cut that was taken. To obtain an understanding of the Pegmatoid thickness, a Ground Penetration Radar (GPR) scanner was used to estimate the thickness at the project site.

The Pegmatoid and Footwall (FW1A or FW1B) lithologies were found to be visually distinguishable as can be seen in Figure 4-1. These lithologies also had significant differences in their Relative Densities (RD) as shown in Table 4-1. This difference in densities suggested that the GPR scanner could be used to determine the thickness of each lithology below the footwall when scanned.

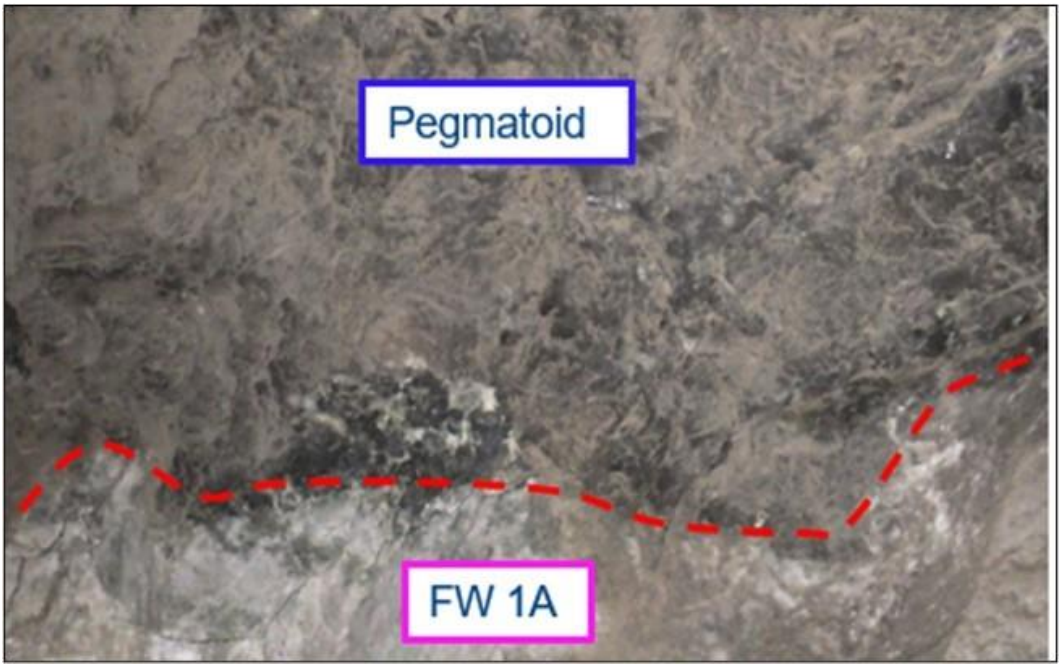


Figure 4-1: Photograph indicating the visual difference between Pegmatoid and footwall formations

Table 4-1: Relative in situ rock densities for rock-type units around the Merensky Reef horizon (Mans, P, 2020)

Merensky Reef	
Geological Unit	RD (t/m^3)
Pyroxenite	3.21
Chrome Straddler	3.19
Pegmatoid	3.15
Replacement Pegmatoid	3.15
Footwall 1	2.89
Footwall 2	2.89
Footwall 3	2.89

4.2.1 GPR Scanner Analysis

The GPR scanner used was the Sub Surface Profiler (SSP) developed by REUTECH Mining. The device collects data wirelessly, transmitting and

processing the data in real time, giving instant feedback on rock structures while scanning (Reutech Mining, 2016).

A total of four GPR scans were done at the trial site. The scanning of the footwall panels ranged between 16 m – 30 m long (measured linearly). Note that scanning was restricted to areas where there was no water or ore accumulation in the footwall away from ongoing drilling activities. The GPR scans indicated that the Pegmatoid thickness in the trial site was on average 2.0 m below the stope footwall and 1.5 m below the ASG footwall (Figure 4-2 & Figure 4-3). The thickness of the Pegmatoid varies in different parts of the stope which is associated with normal undulation of the lithology. The purple in Figure 4-2 & Figure 4-3 represents the Pegmatoid. The cut-offline placed just below the purple approximates the optimal extraction of 2.0 m below the footwall.

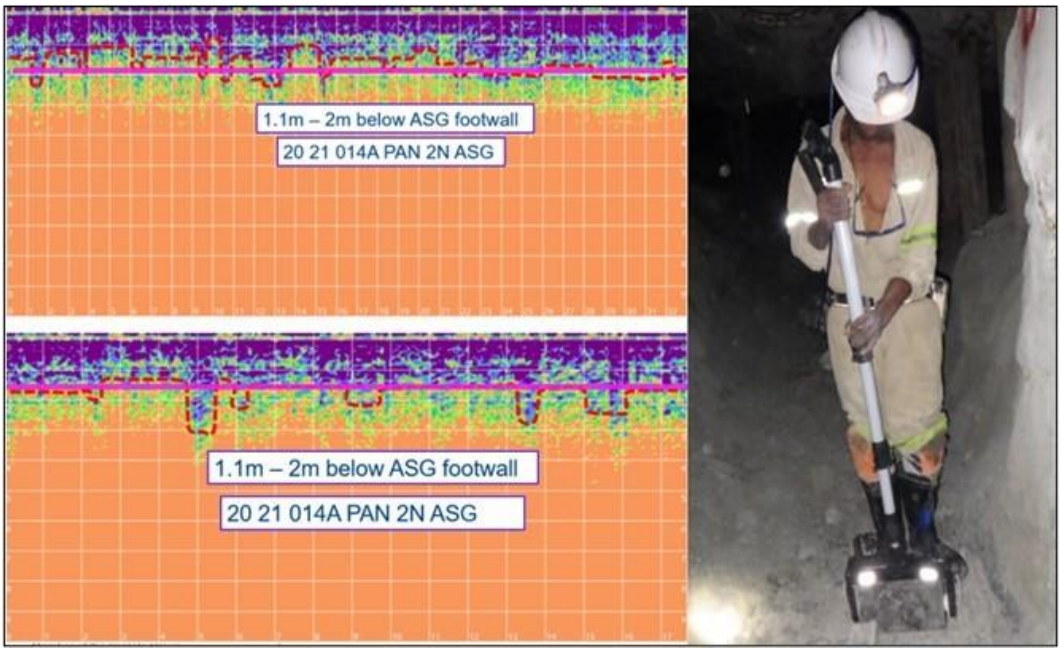


Figure 4-2: GPR scan results showing Pegmatoid thickness along 20 21 014A PAN 2N ASG trial site.

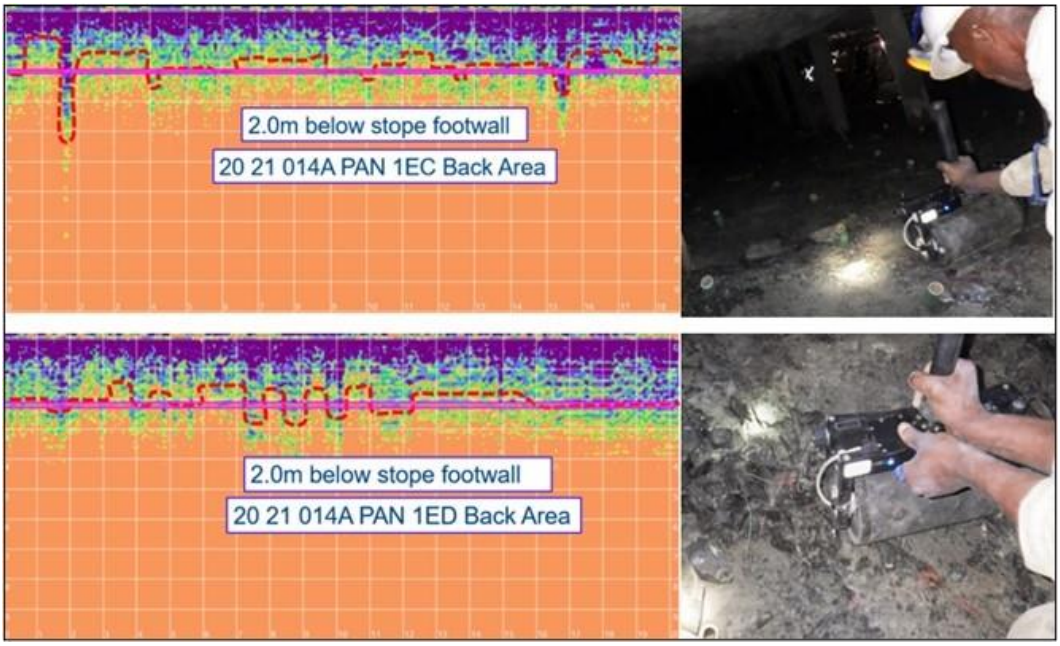


Figure 4-3: GPR scan results showing Pegmatoid thickness along 20 21 014A PAN 1EC and 1ED Back area.

4.2.2 Borehole Camera Analysis

A borehole camera was used to confirm and validate the scans done with the GPR scanner. A total of four borehole camera inspections were conducted in holes drilled into the Pegmatoid package. These inspection holes were drilled at angles of between 30^0 - 50^0 from the footwall surface.

Three 1.2 m long inspection holes were drilled into the stope footwall and one 2.0 m long inspection hole was drilled into the ASG footwall. One of the three holes drilled in the stope was flooded with water and could not be de-sludged/cleaned due to continuous water ingress. This water ingress is suspected to be from cracks or openings connecting to ponds of drilling water that accumulated along the stope footwall.

Pegmatoid was observed along the entire length (1.2 m) of the other two inspection holes drilled in the stope footwall. The longer 2.0 m inspection holes drilled in the ASG footwall intersected the F/W1 contact at 1.3 m along the hole length with the remaining 0.7 m in F/W1 rock-type formation. The sequence of steps that were followed when the borehole camera inspections were carried out were as follows:

1. Suitable positions to drill the inspection holes were identified;
2. The holes were drilled at the steepest possible angle using a 1.5 m long drill steel in the stope footwall. The length of drill steel was used in the ASG footwall were 1.8 m and 2.2 m long;
3. The holes were de-sludged using a compressed air pipe to remove water and grit from the holes;
4. The inspection hole angles and lengths were measured; and
5. The borehole camera was inserted into each hole to assess the Pegmatoid thickness and F/W 1 intersection point.

Photographs showing the various steps taken during the borehole camera assessment are shown in Figure 4-4.

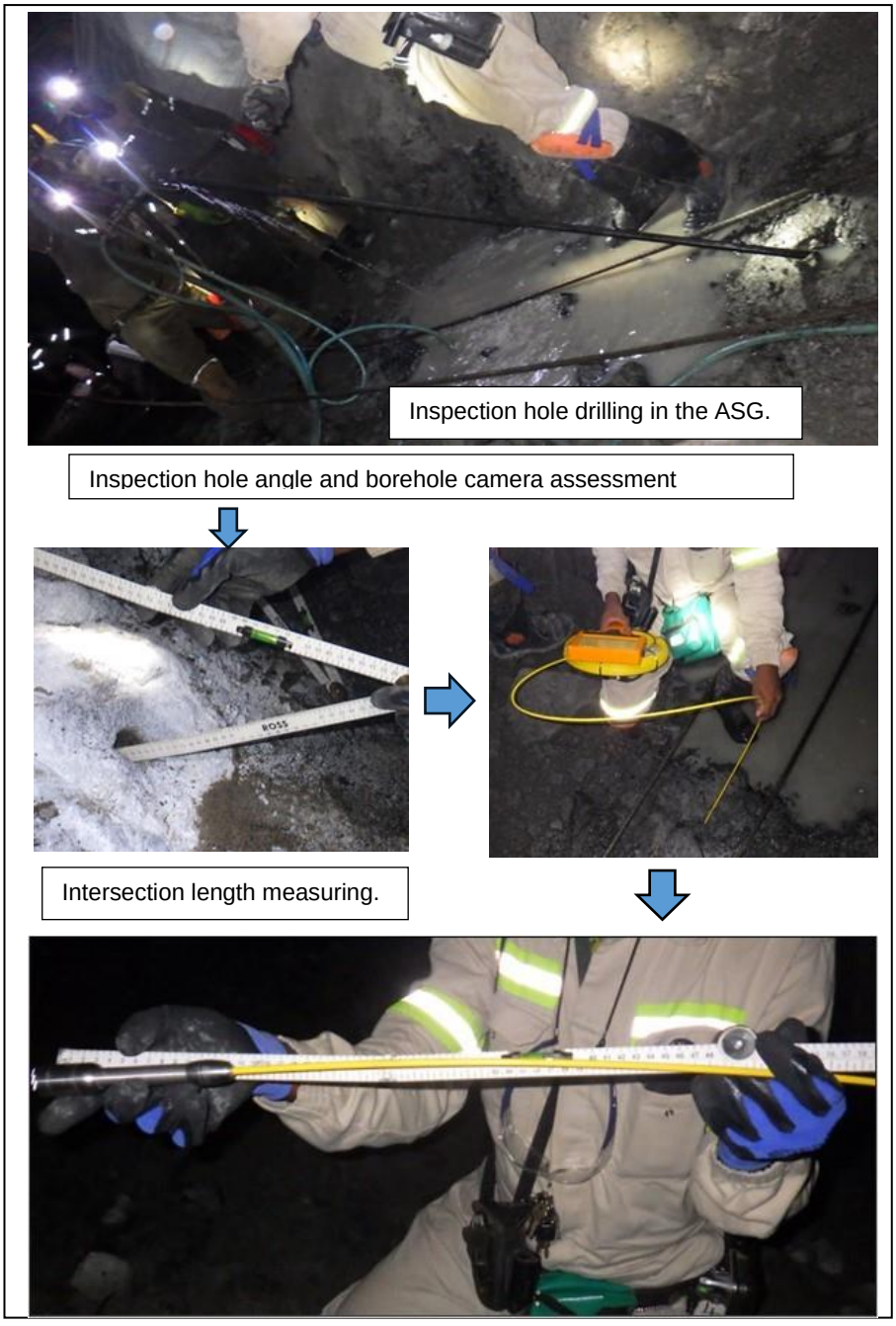


Figure 4-4: Photographs showing various steps in the borehole camera assessments

The borehole camera observations made inside the inspection holes are provided in Figure 4-5.

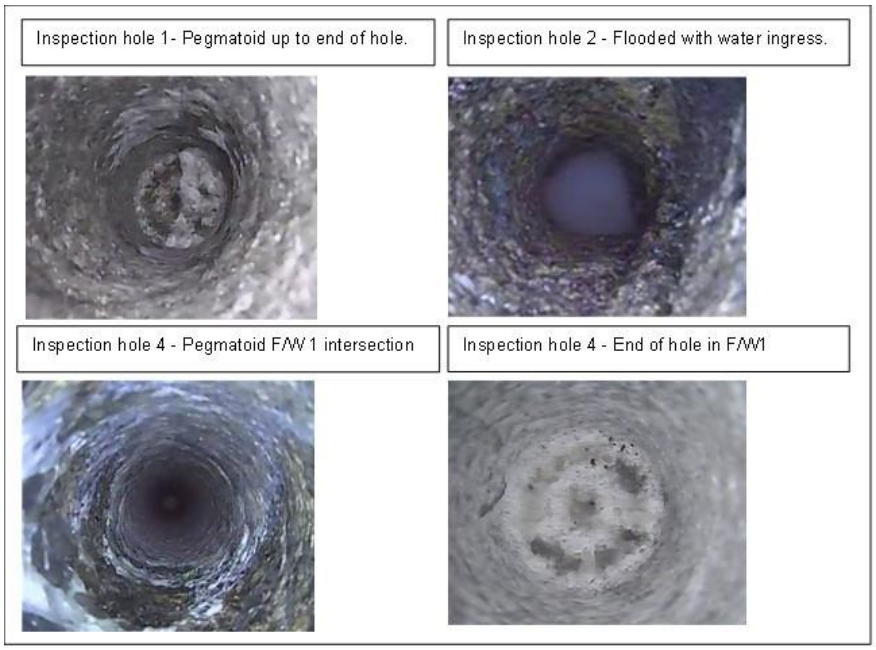


Figure 4-5: Photographs indicating images observed inside the various inspection holes

The Pegmatoid thickness was calculated using Equation 4-1.

$$Peg\ thick_{ASG} = Hole\ length\ to\ FW1\ int\ x\ Sin\ (hole\ angle) \quad \text{Equation 4-1:}$$

$$= 1.3\ m\ x\ Sin\ 50^0$$

$$= 0.99\ m$$

The total Pegmatoid thickness is calculated in Equation 4-2. This is the summation of the ASG shoulder heights with the Pegmatoid thickness below the ASG footwall. This is further illustrated in Figure 4-6. A summary of the borehole camera analysis is provided in Table 4-2.

$$\text{Total Pegmatoid thickness}_{\text{stope}} = ASG\ shoulder\ height + Pegmatoid\ thickness_{ASG} \quad \text{Equation 4-2}$$

$$= 1.2\ m + 0.99\ m$$

$$= 2.2\ m$$

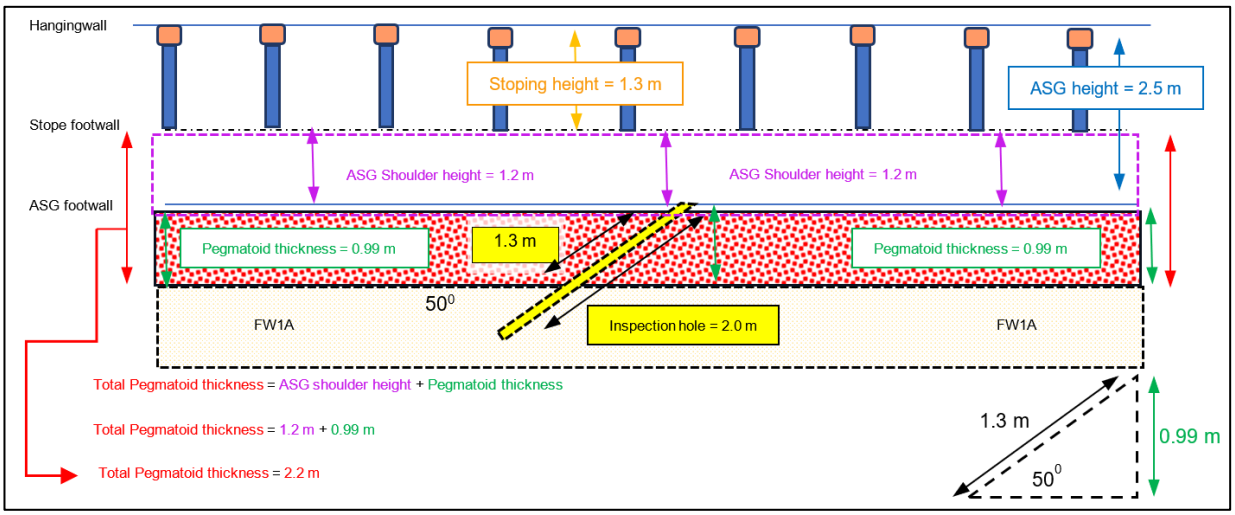


Figure 4-6: Diagram showing drilled inspection holes used to determine Pegmatoid thickness

Table 4-2 Summary of borehole camera assessment

No:	Location	Length of inspection hole	Angle of hole from footwall slope	Pegmatoid bottom contact	Pegmatoid true thickness (below f/w)	Comments
1	Toe of panel (1.3 m Stoping height)	1.2 m	40^0	n/a	>0.77 m	Bottom contact not intersected
2	Middle of panel (1.3 m Stoping height)	1.2 m	40^0	n/a	n/a	Hole flooded
3	Top of panel (1.3 m Stoping height)	1.2 m	30^0	n/a	>0.6 m	Bottom contact not intersected
4	ASG (2.5 m height)	2.0 m	50^0	1.3 m	0.99 m	Bottom contact intersected at 1.3 m

4.3 Grade Resource Estimation

Grade estimations at the project site were done through sample cutting along the exposed footwall segments. These samples were taken to improve the grade

confidence level for the footwall layer to be mined. All the actual cutting of the samples was done by the internal sampling department. These cut samples were then taken to an external sampling laboratory for analysis and processing.

A total of two sample cuts were taken using a pneumatically powered diamond saw grinder machine (Figure 4-7) along the ASG shoulder. Analysis of these cut samples confirmed an average grade of 0.88 g/t to be contained over 900 mm footwall Pegmatoid (Figure 4-8). Note however that the bottom contact of the Pegmatoid layer expected to have the higher concentration of PGM content was not exposed. An additional 0.99 m of Pegmatoid lies below the ASG footwall that would have to be exposed to sample the entire 2.2 m thick footwall package as described in Chapter 4.

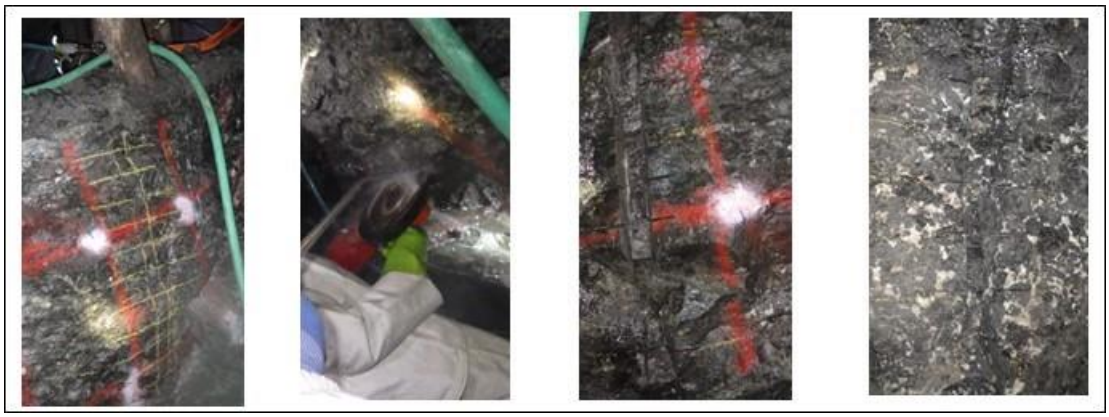


Figure 4-7: Sample cutting in the Merensky Pegmatoid footwall

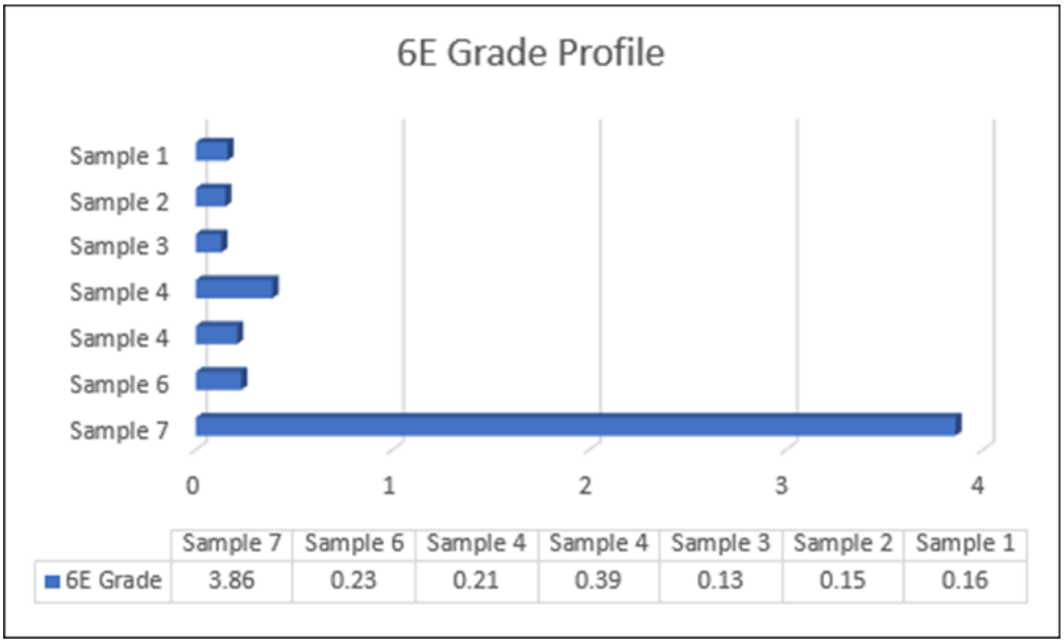


Figure 4-8: Merensky H -reef grade distribution results from cut samples

4.4 Geotechnical Structural Mapping

4.4.1 Geotechnical structural mapping technique

The following steps were used during the mapping process:

- Measuring the orientation (dip / dip-direction) of the scanline and discontinuities using the Apple electronic measuring device;
- Determining the trace length (persistence or continuity) of individual discontinuities which were measured as far as could be visibly traced in one direction within the exposed rock mass;
- The joint shear strength properties were recorded using the method described by Barton (2002);
- The joint conditions were determined visually and through the touch and feel of the rock mass. The roughness and alteration of the joint surfaces were recorded;

- Other discontinuity properties such as rock type, infill type, infill thickness and moisture content were recorded; and

- Blast fractures were excluded from the joint mapping exercise.

The scanline mapping was conducted in various panels along the trial site raiseline (20 21 014A). The mapping involved the use of a measuring tape aligned along the excavation hangingwall surface secured to existing bolts along the ASG hangingwall (in the direction of advance) and panel face or back area (perpendicular to the direction of advance). The scanlines ranged between 15 m to 20 m in length. Four areas were mapped in the three panels listed below as shown in Figure 4-9. The dataset of the structural mapping information can be observed in Appendix F. It must be emphasized that no time-dependent creep deterioration was observed in the rock mass or discontinuities mapped.

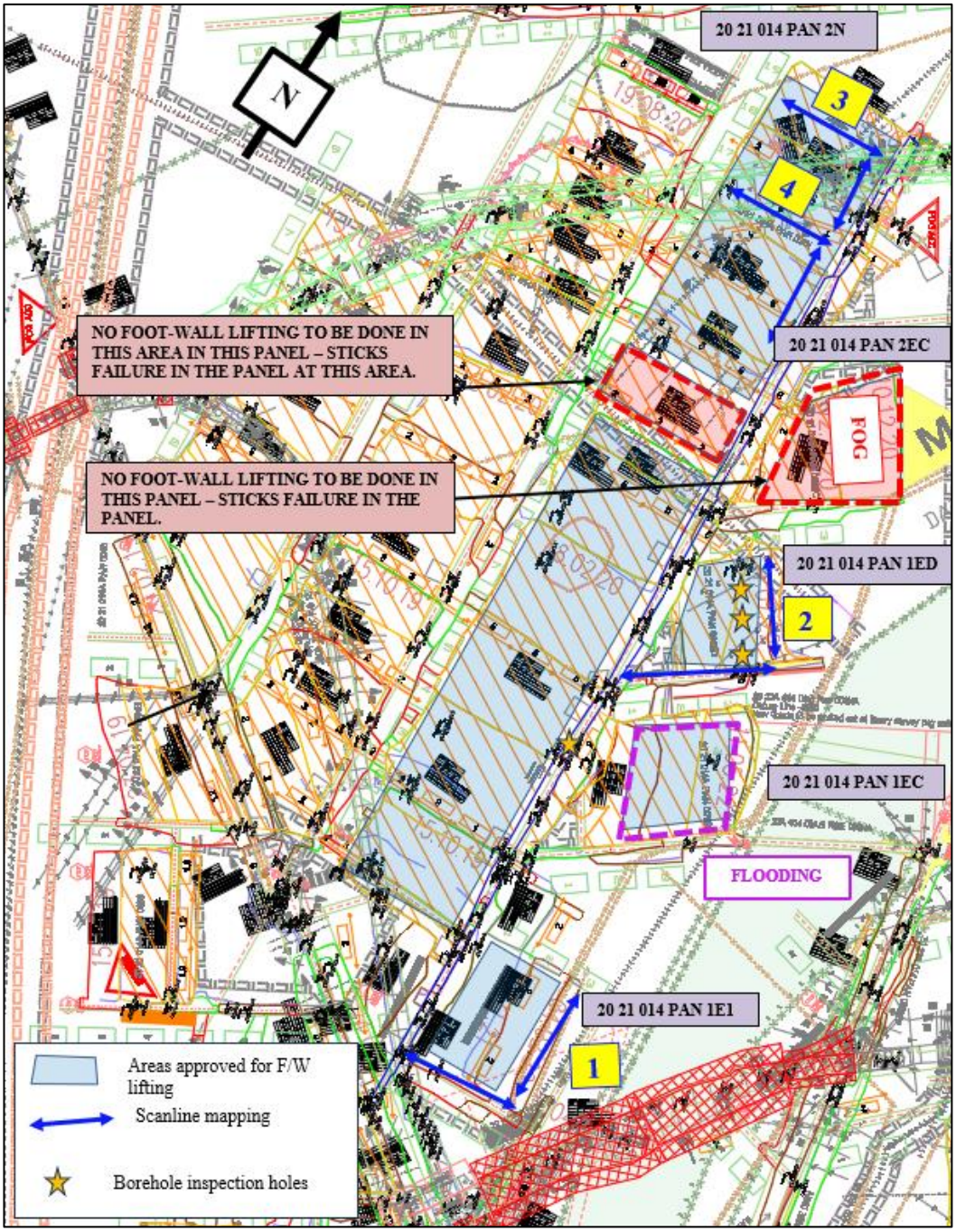


Figure 4-9: Copy of the mine plan showing scanlines, geology and Q-ratings and planned footwall extraction.

An Apple iPhone device installed with a specialised software application was used as an electronic measuring device. The Apple device was first calibrated, checked, and found to be in good agreement with a standard magnetic compass both on the

surface and underground. It was then used to measure the dip and dip direction of each scanline traversed. The iPhone was also used to measure the dip and dip direction of the structural discontinues. Photographs showing the iPhone device used to map the structural discontinuities are shown in Figure 4-10.

The benefit of using the Apple device is that each measurement taken is stored on the device as opposed to a compass that relies on the user to record the measurements on a logging sheet. In addition, a standard magnetic compass is strenuous and cumbersome in the underground stope environment compared to the iPhone. The compass usage was therefore limited to a few check readings for each scanline. Measurements were taken as far away as possible from metallic objects such as roof bolts that could influence the readings taken from the mapping device.

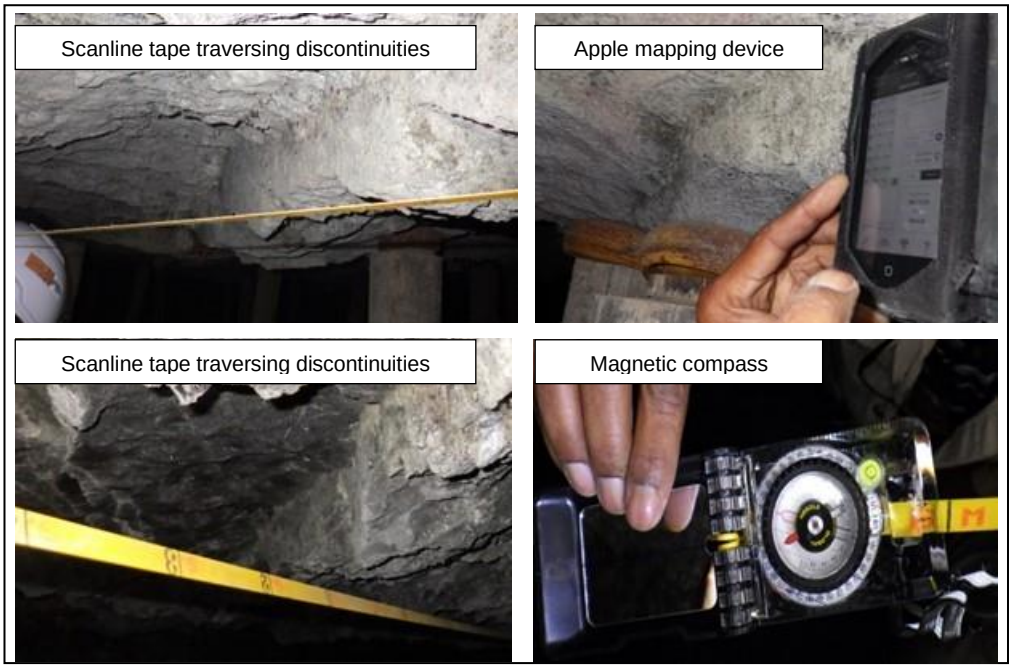


Figure 4-10: Photographs indicating the structural mapping done using an iPhone compared to a magnetic compass using the scanline technique

4.4.2 Assumptions & corrections for errors (biases) during joint mapping

The assumptions and correction factors applied are described below:

Correction for true joint spacing

Correction for joint spacing was accounted for by measuring the dip and orientation of the scanline. To obtain the true spacing, an orientation correction is applied using the relative angle between the joint set and the scanline. True joint spacing has been calculated using the Equation 4-3:

$$\lambda ti = \lambda ai * ABS(\cos(\beta i - \beta s)) * \cos\alpha s * \sin\alpha i \qquad \text{Equation 4-3}$$

Where:

$\lambda ti =$	true joint spacing between joint (i) and joint (i + 1).
$\lambda ai =$	apparent spacing between joint (i) and joint (i + 1), i.e. the linear difference between the intersection points along the scanline tape between joint (i) and joint (i + 1) of the same joint set.
$\beta i =$	dip direction of the joint (i)
$\beta s =$	azimuth of the scanline tape
$\alpha i =$	dip angle of the joint (i)
$\alpha s =$	the plunge of the scanline

The above formulas were used in an Excel spreadsheet (Appendix F) where the azimuth and dip for both scanline and discontinuities within a joint set were used to calculate the true joint spacing.

Correction for joint orientation bias

Two semi-orthogonal scanline traverses were mapped such that joints sub-parallel to one tape would be intersected by the other tape. This would serve to minimise orientation biases that would be associated with a single traverse scanline. The use of two orthogonal scanlines ensures that discontinuities that intersect the scanline at an angle of less than 20°, i.e. joints orientated sub-parallel to the scan

line are accounted for and not missed. Note however the 3rd dimension (vertical) was not mapped. An orientation bias correction therefore still exists for all the mapped joint data in the current study but to a limited scale.

The Terzaghi weighting method using a feature in DIPS was used to correct for joint orientation and spacing bias. The recommended range in DIPS is limited to angles between 5° to 25° with the default set at 15°. A minimum bias angle of 20° was applied in the study as this was observed to provide clearer contour concentration groupings for selecting the joint sets than the 15° default setting angle.

A magnetic delineation of 17 degrees was factored for using a magnetic compass. This ensured that all directional measurements were taken relative to true north.

Truncation limit error

A truncation limit of 0.5 m was used in the mapping procedure. Only joints greater than 0.5 m in length that traversed the scans were mapped for orientation and joint properties (roughness and alteration). This limit was based on the following factors:

- Block sizes formed from joints smaller than 0.5 m were deemed insignificant for the key block J-Block analysis; and

- The J-Block analysis was focused on assessing stability when the footwall is extracted, and timber elongates are removed;

Joint shear strength assumptions

Barton's (2002) model was used to estimate the joint friction angle (φ) used in J-Bock. Consequently, the approach becomes conservative as zero cohesion was applied to all joints. The net effect is to simulate a lower strength on all competent joints.

The joint friction angle (φ) of competent joints with no or negligible infill returns high friction angles which may be over-estimated. This has the potential to result in the

simulation of a rock mass that appears to be more competent than the actual rock mass behaviour. An upper truncation limit was therefore set to the base friction angle, as recommended by Barton. An upper truncation limit of 38° (base friction angle of Pyroxenite) was applied.

The log sheet in Figure 4-11 was used to record and capture relevant data for rock mass characterization and J-Bock evaluation. This log sheet prompts the mapper to capture the required information with necessary descript minimizing the probability of omission.

Essential Logging Parameters for Jblock Evaluation
Beneficial Data for Rock Mass Characterisation

Essential Logging Parameters for Jblock Evaluation																	Beneficial Data for Rock Mass Characterisation							
Location	Traverse ID	Scanline Peg Reference	Tape Azimuth (deg)	Tape Plunge (deg)	Joint No.	Joint Set	Distance on Scanline (m)	Rock Type	Dip (deg)	Dip Direction (deg)	Angle between Scanline and Strike of Structure	Add (+) or Subtract (-) 90deg for Dip Direction (?)	Persistence (m)	EndsVisible	Joint Roughness Number (Barton, 2002)	Joint Alteration Number (Barton, 2002)	JRC (Barton-Bandis, 1990)	Infill Type	Infill Thickness (mm)	Moisture	Wall Hardness	Separation	Thickness	Comments
Panel ID	ASG (a)	Peg AP 4579 - 12m	75	5	a1	J1	4.37	Harzburgite	39	54	23	+	5.2	1	2.0	3.0					56	3	2	
Panel ID	Face (a)	Peg AP 3722 + 3m	345	18	f1	Dome	8.11	UG2	67	211	56	-	3.5	0	0.5	6.0					1	3	3	
Panel ID	Top of Panel (a)	Peg AP 4656 + 4m	75	5	t1	J3	13.22	Pyroxenite	83	68	12	-	7.9	2	1.5	1.0								

Figure 4-11: Example of the structural data mapping sheet

Table 4-3 provides a summary of all the scan lines that were taken at the project trial site. All the collected geotechnical data is given in Appendix F. A total of 155 discontinuities were mapped and classified comprising of 3 main joint sets.

Table 4-3: Summary information of the Traverse Scan-Lines taken in the project trial site.

Workplace	Traverse ID	Scanline orientation (dip/dip direction)	Scanline direction start	Linear Traverse length
20 21 014A PAN 1EC	ASG H/W	06^0 / 341^0	Peg K16567 + 3.6 m	12.5 m
20 21 014A PAN 1EC	Stope H/W	12^0 / 259^0	Peg K16567 + 23 m	21.5 m
20 21 014A PAN 1EB	ASG	15^0 /353^0	Peg K12833 + 4 m	28.7 m
20 21 014A PAN 1EB	Stope H/W	15^0 / 042^0	Peg K12833 + 28 m	23.5 m
20 21 014A PAN 2N (1)	ASG	0^0 / 185^0	Peg K13868 +12.3 m	13.3 m
20 21 014A PAN 2N (1)	Stope H/W	6^0 / 291^0	Peg K13868 + 11.3 m	22.5 m
20 21 014A PAN 2N (1)	ASG	3^0 / 95^0	Peg K13868 - 3.5 m	10.4 m
20 21 014A PAN 2N (1)	Stope H/W	15^0 / 179^0	Peg K13868 - 4.5 m	20.3 m

4.4.3 Support Elements Used in the Trial Stope

The method of extracting the footwall required the removal of existing timber elongates in the mined-out stope. These support units had to be replaced with suitable alternatives to maintain back area stability. The use of longer timber elongates in the sliped zone to replace blasted-out units was considered unfavourable due to the following:

- Heavier mass of the timber that would impact productivity, and present a material handling safety risk;
- Increased potential for buckling where the w/h (width-to-height) ratio exceeds 10 (Ryder & Jager, 2002) resulting in instability in the back area; and

- The longer timber elongates could only be installed after blasting out the exiting units (i.e. cannot be pre-installed) presenting a FOG risk.

The use of a tendon support system to replace the blasted timber elongates presents the advantage of pre-installation before extracting the footwall layer. This ensures that the area is safely supported before any blasting activities taking place.

Tendon units such as mechanical anchors, grouted rebar (Shepherd Crooks), split-sets and Swellex bolts are unfavourable for pre-installation in an existing 1.35 m narrow stoping height. A coupling mechanism would be required for mechanical anchors used in a narrow stope where the segments are joined inside the support holes. An angled (bent) Swellex bolt would be required in a narrow stope where it is straightened once inside the support hole. These types of modifications present additional challenges and risks to the support installation process. For this reason, Cable Anchors (CAs) were selected due to their length, flexibility, and high-strength characteristics as suitable replacements for timber elongates.

Temporary Support (Safety Nets)

Since CAs were used in the sliped zone and the existing elongates were in place ahead of the advancing ledge, the only temporary support requirement was the safety nets. These 3.0 m x 2.5 m safety nets were installed between rows of existing elongates and attached to the bearing plates of the existing bolts. The safety net provided areal coverage for persons drilling the CA support holes. The existing elongates also provided sufficient support resistance to maintain stability in the area where CA support holes were drilled.

4.5 Chapter Summary

Data was collected in four main categories that were used throughout the research project:

- The first category of data collection was done to determine the Pegmatoid thickness. The GPR scanner estimated the Pegmatoid thickness to be 2.2 m thick below the mined-out stope footwall. This was later confirmed

through bore-hole camera analyses. An understanding of the Pegmatoid thickness enabled a decision to be made on the depth of cut to be taken as well as the number of cuts to be mined. The thickness was also essential in planning the potential tonnages produced.

- The second category of data collection was the grade sampling of footwall in the area of interest. An average grade of 0.88 g/t was sampled from two cuts.
- The third category of data collection was the geotechnical data collected through a structural mapping process. 155 structural discontinuities were mapped from 8 scanlines taken in 4 parts of the area of interest.

5 RESEARCH AND FINDINGS

5.1 Support Design Philosophy Deterministic Approach

5.1.1 Fall out Height

The support design philosophy followed suggestions from Daehnke, et al (2001) that consider the 95% cumulative FOH from a FOG database. The entire mined-out panel can be considered as the stope back area. The FOH of FOGs recorded in the stope back area would traditionally be considered in isolation for design purposes. However, there are too few FOG records for the back areas (approximately 4 FOGs to date) in the FOG database. As a result, the combined fallouts from the face area, ASG, and the back area were used. This combination resulted in a total of 60 records (Appendix G), which is still below the recommended 100 FOGs suggested by Jager & Ryder (1999). In such cases, mapped brow data can also be used where the brow thickness would be considered as a FOH. This was however not conducted in the study due to time constraints and limited resources available. The database was analysed to find the 95% cumulative FOH determined to be 1.4 m (Figure 5-1). This 95% cumulative FOH was used to determine the anticipated load and length requirements of the support units. The 5% outside of the support capacity was assumed to be recognised by the established TARP system and supported separately.

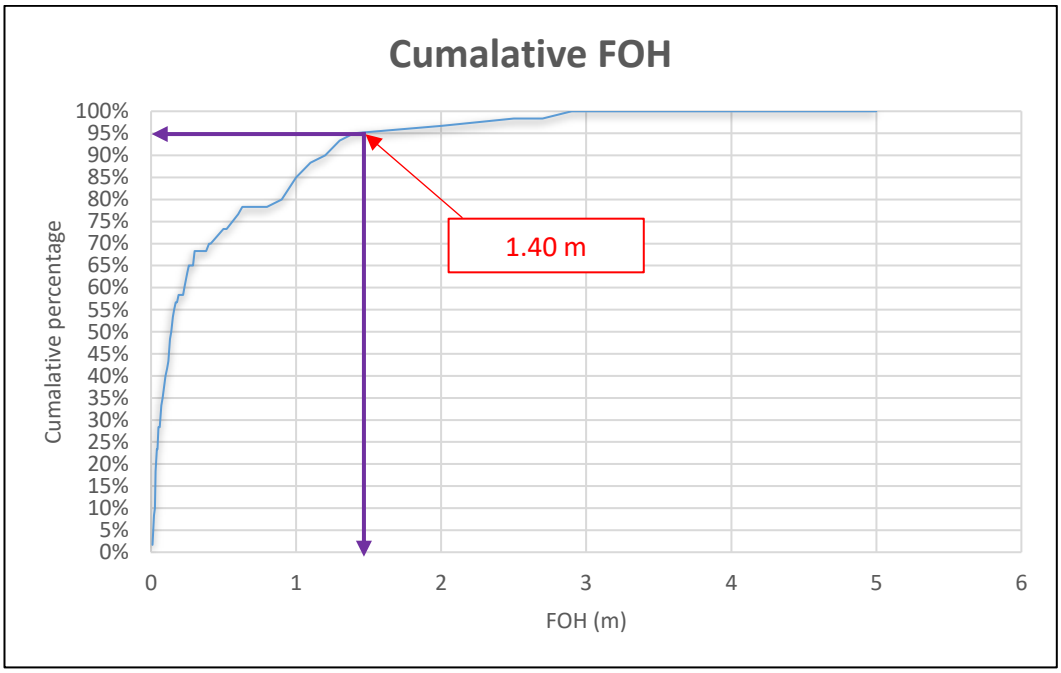


Figure 5-1: 95% Cumulative fallout height for stoping filtered for the back area, face area and ASG (Tati, 2023).

5.1.2 Empirical Barton fall-out-height

The Barton et al (1980) empirical fall-out-height was developed for tunnels but provides similar heights of unstable rock to the FOG analysis at Implata Platinum. It was therefore used as an additional measure to determine the reach and strength of the tendon support. The footwall mining that was done was considered the final stage of extraction in the mined stopes. The stope therefore only needed to remain stable for the duration of the footwall lifting. As a result, an ESR value of 3.0 was used. The anticipated fall-out-height from this analysis is given in Equation 5-1 (Barton, et al., 1980.):

$$L = \frac{2.0+0.15\times B}{ESR} \qquad \text{Equation 5-1}$$

Where:

B = 25.0 m — Excavation width

ESR = 3.0 — Excavation Support Ratio

$$L = \frac{2.0+0.15\times 25.0}{3.0} = 1.92 \text{ m}$$ — Anticipated fallout height

This FOH is inclusive of the critical bond length. A critical bond length of 200 mm was assumed and therefore, an actual **FOH of 1.72 m** was presumed.

5.1.3 Support Resistance Required (SR $_{required}$)

The required support resistance to support the "demand" is calculated using Equation 5-2:

$$SR_{required} = FOH\,(m) \times G\,(m/s^2) \times \rho\,(kg/m^3) \qquad \text{Equation 5-2}$$

Where:

FOH	*Fall out Height*	$= 1.72\ m$
G	*Gravitational Acceleration*	$= 9.81\ m/s^2$ *(Constant)*
ρ	*Rock Density*	$= 3\,200\ kg/m^3$

Using Barton's (1980) method of evaluating the length requirements of bolts, an actual FOH of 1.72 m was anticipated. The minimum tendon length of 2.0 m tendon is thus required that is inclusive of the bolt head. The SR requirements associated with the weight of the rock that must be supported were therefore determined to be 54.0 kN/m^2.

5.1.4 Height supported by existing timber elongate

The timber elongate support units in the mined-out stope currently support the back area. Although these support units have undergone a certain amount of creep/deformation, there is a height these units are currently catering for.

Laboratory press tests were done on five (160 mm - 180 mm diameter) 1.5m long timber elongates units (Figure 5-2). These laboratory-based strength values for timber press tests were done at a loading rate of 30 mm/min. The load-deformation curves for these tests are provided in Figure 5-3 where the average minus two standard deviations (95,5%) curve provides a peak strength of 450 kN.



Figure 5-2: Laboratory compression tests conducted on 1.5 m long timber elongates.

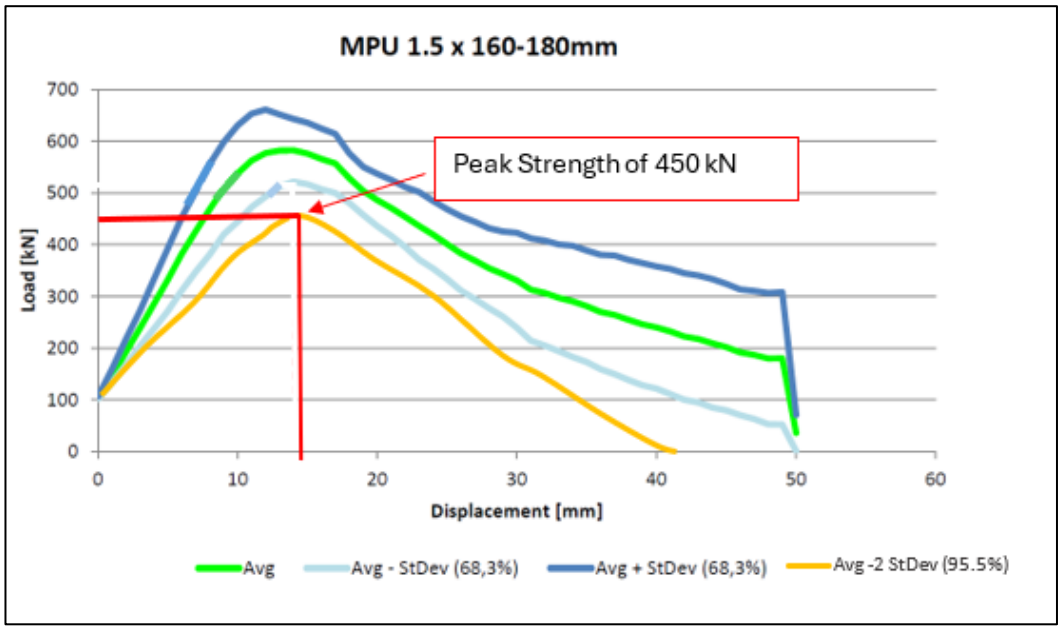


Figure 5-3: Load deformation graph for 1.5 m long timber (Rainbow Mining Support, 2023)

The above laboratory strength and deformation characteristics for the timber elongates were downrated for underground conditions as suggested by Daehnke et al (1998). An underground loading rate $V_{u/g}$ of 1 mm/day (0.000694 mm/min)

was assumed. When considering the laboratory loading rate (V_{lab}) of 30 mm/min, and Figure 5-4, the derating factor k becomes 0.6. using Equation 5-3, the underground timber strength ($F_{u/g}$) was downrated from the laboratory peak strength (F_{lab}) of 450 kN to ($F_{u/g}$) 270 kN.

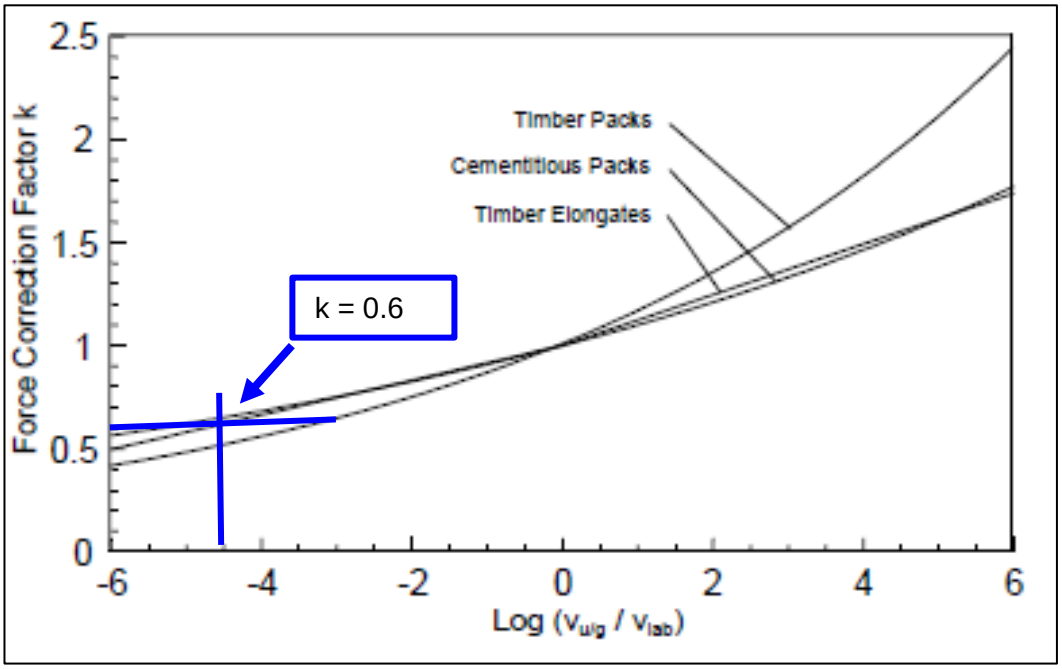


Figure 5-4: Graph for adjusting the load-deformation curves for different deformation rates (Ryder & Jager, 2002)

$$F_{u/g} = k \times F_{lab} \qquad \text{Equation 5-3}$$

Where:

k	De-rating factor
$F_{u/g}$	Timber strength downrated for underground loading
F_{lab}	Timber load generated in laboratory conditions

FOH supported by Timber Elongates:

The support resistance generated by a timber elongate was based on the derated strength of the timber elongate and the tributary area. The tributary area for a timber elongate support unit installed in the back area spaced 2.0 m (strike) and 1.5 m (dip) is shown in Figure 5-6. Therefore, FOH supported by timber elongate support units was calculated where:

$$FOH_{elongate} = SR \div (\rho \; x \; g) \qquad \text{Equation 5-4}$$

Where:

$SR = \frac{F}{A_T}$		Support resistance (kN/m^2)
F	270	Derated timber strength (kN)
A_T	dip x strike	Tributary Area (m^2)
ρ	3.2	Rock Density (t/m^3)
g	9.81	Gravitational acceleration (m/s^2)
A_T	=1.5 m x 2.0 m	= 3.0 m²
$SR =$	$\frac{270\ kN}{3.0\ m^2}$	=90 kN/m²
$FOH_{elongate}$	$\frac{90\ \mathrm{kN/m^2}}{3.2\ {}^{\mathrm{t}}/_{\mathrm{m}^3}\ \mathrm{x}\ 9.81\ \mathrm{m/s^2})}$	= 2.9 m height

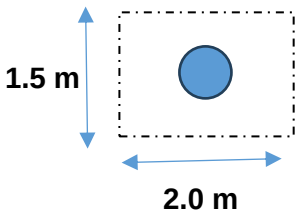


Figure 5-6: Timber elongate tributary area

The 2.9 m height supported by the timber elongates is much higher than the cumulative FOH (1.4 m) and the theoretical Barton FOH (1.72 m). However, there was no evidence that the support was carrying close to capacity.

5.1.5 Support Unit Specifications

Cable Anchor 18 mm diameter strands

The strength of a CA is determined from laboratory tensile strength testing. Four UTS tests were conducted at the Groundwork laboratory test facility shown in Figure 5-7.



Figure 5-7: Photographs indicating laboratory UTS tests conducted on 4.5 m long 18 mm diameter cable steel samples at the Groundwork testing facility (Matitsela, 2018)

The load-deformation curves for these four UTS tests are provided in Figures 5-8, 5-9, 5-10 and 5-11. The peak and yield loads for each test are shown in the graphs.

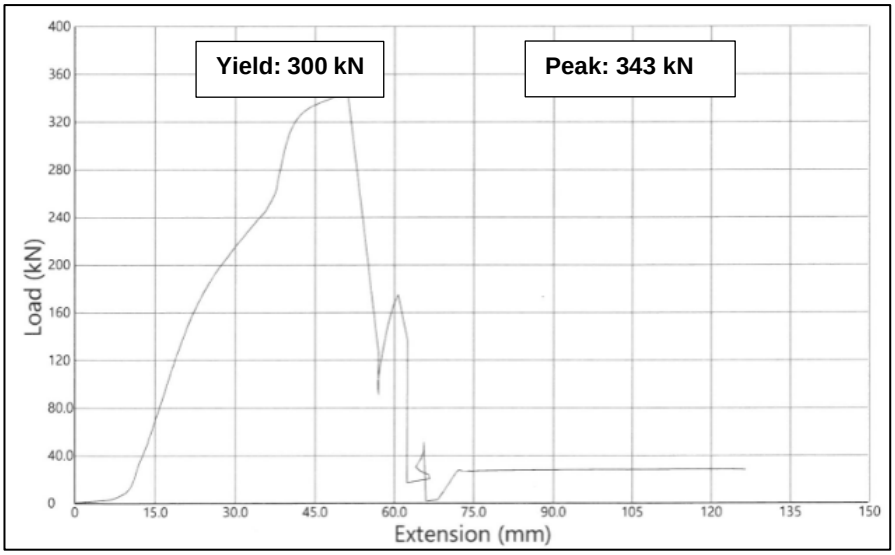


Figure 5-8: Test No.1 - Load deformation graph for 4.5 m long 18 mm diameter cable steel (Matitsela, 2018)

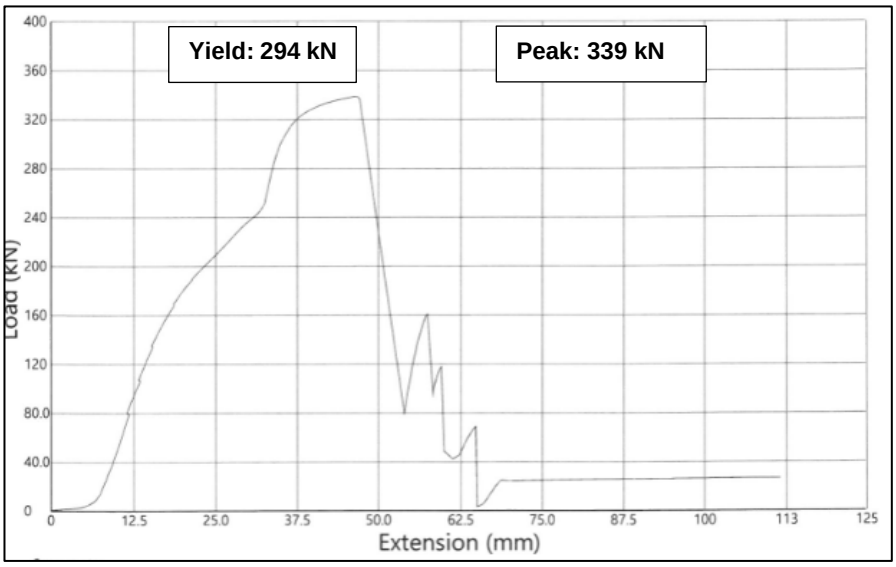


Figure 5-9: Test No.2 - Load deformation graph for 4.5 m long 18 mm diameter cable steel (Matitsela, 2018)

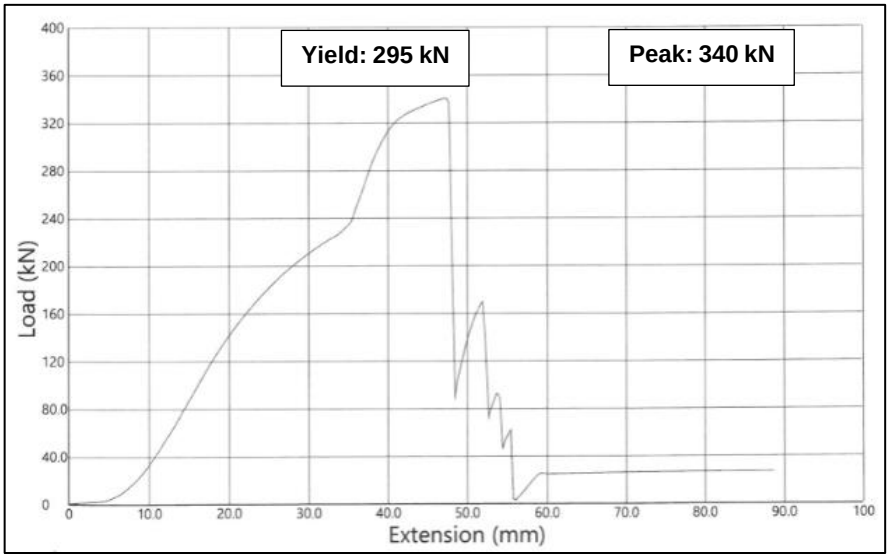


Figure 5-10: Test No. 3 - Load deformation graph for 4.5 m long 18 mm diameter cable steel (Matitsela, 2018)

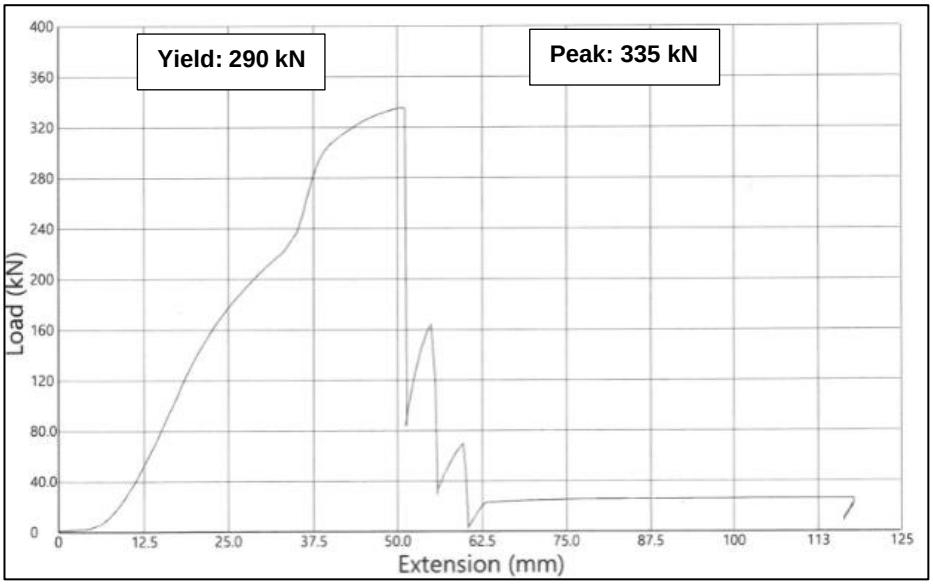


Figure 5-11: Test No. 4 - Load deformation graph for 4.5 m long 18 mm diameter cable steel (Matitsela, 2018)

Table 5-1 summarises the results shown in the graphs. The mean peak load for the tests was calculated to be 339 kN whereas the mean yield load is 295 kN (roughly 87% of the peak strength).

Table 5-1: Summary of UTS test conducted on four 18 mm diameter cable steel samples.

No	Sample Description	Peak Load/Yield Load (kN)		UTS (MPa)	Elongation at Max %
1	18 mm diameter CA	343	300	1350	7.3
2	18 mm diameter CA	339	295	1330	16
3	18 mm diameter CA	340	295	1340	6.8
4	18 mm diameter CA	335	290	1320	7.3
	Mean	339	295	1335	7.1
	Std dev (68% confidence)	336	291	1322	6.8
	Two Std dev (95% confidence)	333	287	1309	6.6

Dura-Pak 60-300

The load-deformation curve in Figure 5-12 shows a peak strength of 3600 kN. Table 5-1 suggests a yield load of 3000 kN for the equivalent Dura Unit, which will be used for design purposes.

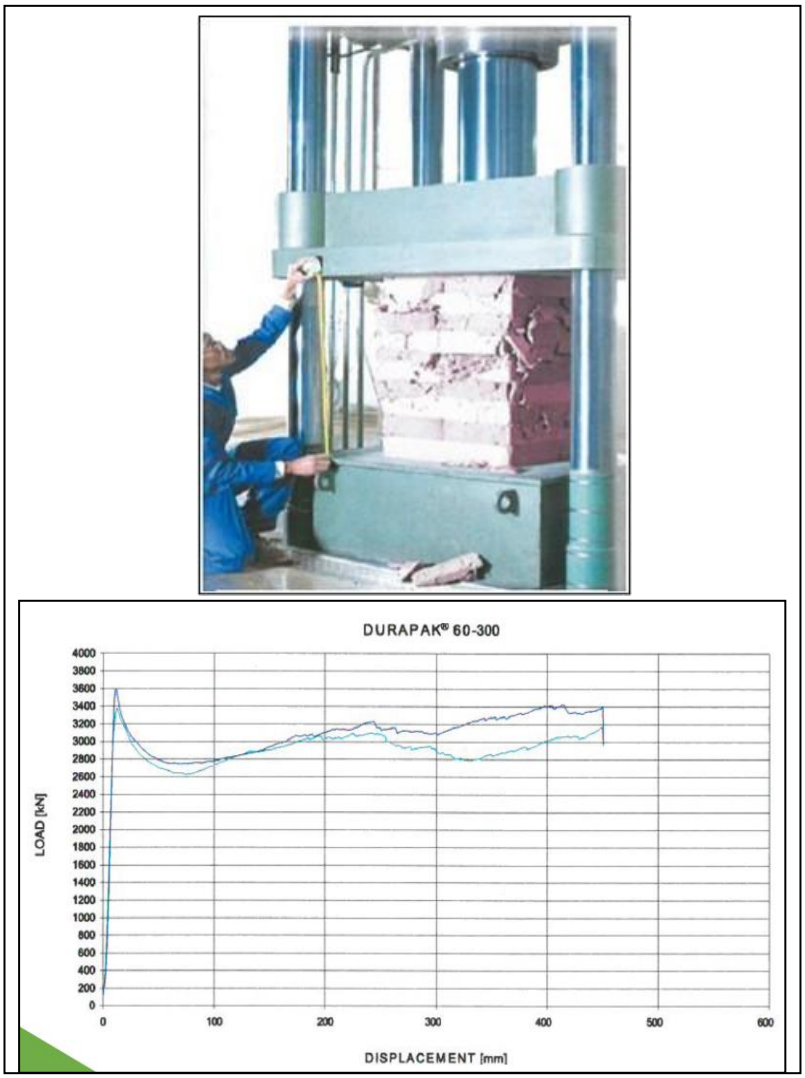


Figure 5-12: Dura-Pak press-test and load-deformation curve (Support, 2023)

Table 5-2: Static Yield Loads for various Dura-Pak sizes (Support, 2023)

PACK SIZE	MAXIMUM PACK HEIGHT (m)	UNITS PER LAYER (m)	STATIC YIELD LOAD (kN)
0.6 x 0.6	**1.5**	**2**	**3000**
0.6 x 0.9	**1.5**	**3**	**4000**
0.9 x 0.9	**1.8**	**4**	**5500**
0.9 x 1.2	**1.8**	**6**	**7000**

Permanent Support (Cable Anchors)

The permanent support that was assessed consisted of CAs that are installed to replace the blasted-out timber elongates. Various options were assessed against each other by varying CA length and spacing to determine the most optimal option. The support options were varied as follows:

A. Support Scenario “1” (SS1) - 1.5 m dip & 2.0 m strike; and
B. Support Scenario “2” (SS2) - 2.0 m dip & 2.0 m strike.

Dura-Pak Breaker line

Dura-Paks are cement packs that provide very high load-carrying abilities and are sufficiently stiff when adequately pre-stressed for this low-closure environment. These packs have proven successful support units in arresting large FOGs in stope panels in three instances on Impala No 20 Shaft. These large collapses were caused by low-dipping geological structures that extend as much as 10 m into the hangingwall where the Bastard Reef is located. Such an example is shown in Figure 5-13 (Impala Platinum, 2017). Significant amounts of stope closure can be seen to have taken place ahead of the Dura-Paks where elongates have cracked/failed. The Dura-Paks however, remain stiff and stable arresting the large FOG from propagating beyond the breaker line. There is no evidence of any large FOG incidents that have run beyond a Dura-Pak Breaker line on the No 20 Shaft.



Figure 5-13: Photographs of Dura-Paks arresting the propagation of large-scale collapses (Impala Platinum, 2017)

Dura-Pak support units were planned as breaker lines every 12 m of footwall retreat mining to compartmentalize the back area. This line of support units was a safeguard against the propagation of a large FOG. The packs would effectively contain any large FOG in a localized area, preventing it from propagating further towards the centre gully (which was the main access way).

5.1.6 Support configurations based on the 95% fallout height analysis

The layout for the two support systems options; Support Scenario 1 (SS1) and Support Scenario 2 (SS2) with the tributary areas in the stope panel are indicated

in Figures 5-14 and 5-15. The CA support spacing on strike was restricted to 2.0 m to conform with the timber elongate spacing. The drilling of the CA support holes was to be done between timber elongates under safe areal coverage. As a result, only the dip spacing could be varied for analysis purposes.

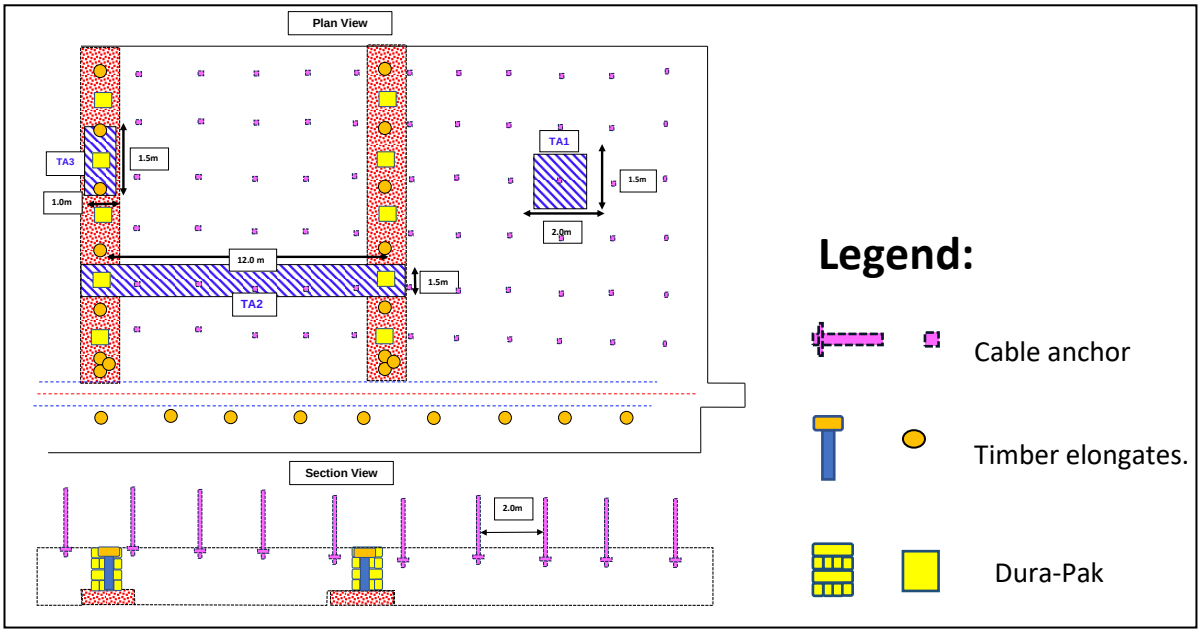


Figure 5-14: Support Scenario 1 - Layout configuration for CAs installed during the drilling shift (CAs at 1.5 m x 2.0 m pattern)

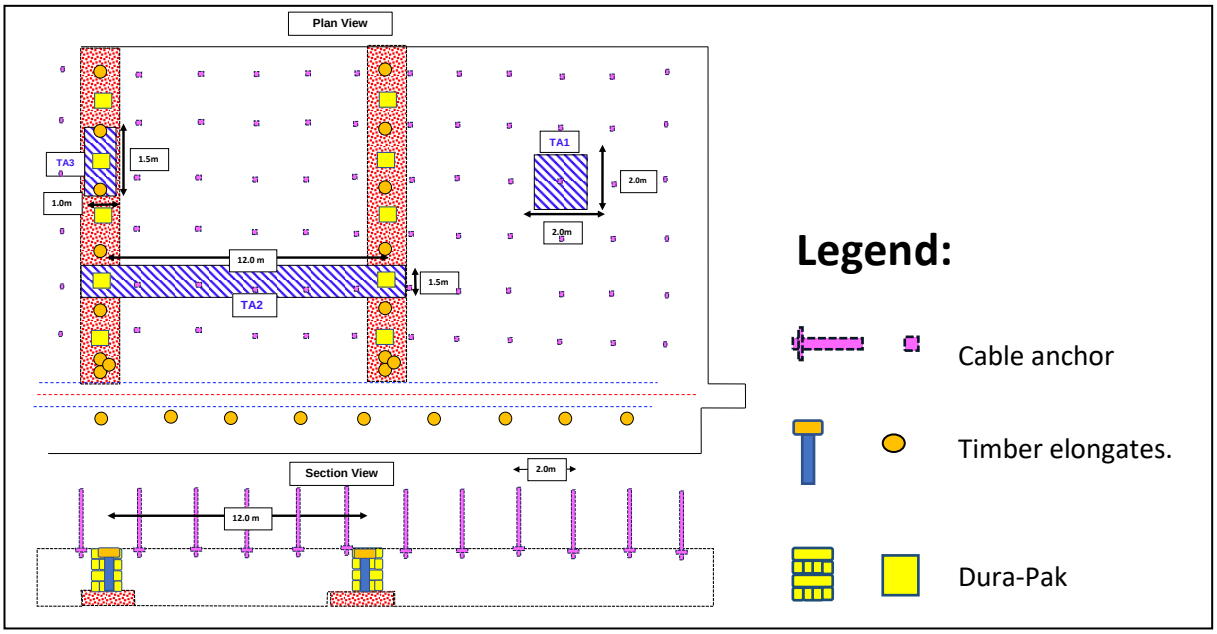


Figure 5-15: Support Scenario 2 - Layout configuration for CAs installed during the drilling shift (CAs at 2.0 m x 2.0 m pattern)

These tributary areas are delineated into two main zones of interest as follows:

- TA1 indicates the “new back area” where the footwall sliping was complete and the area was supported on CA’s. This tributary area only considers the CA.
- TA2 indicates the area between Dura-Pak breaker lines where the footwall has been mined out. This tributary area considers the Dura-Paks and anchors between the breaker lines.
- TA3 considers the Dura-pack acting in isolation.

The existing Hydrabolts and timber elongates were not considered in the Tributary area zones. This is because the support units have already been subjected to deterioration (corrosion) and deformation (creep), respectively, and their true strength was not known. The timber elongates however served as a warning system. Any cracks signs on the timber indicated possible instability and mining of the footwall in these areas was not carried out.

5.1.7 Support Design Results (Deterministic Approach)

Tables 5-3 and 5-4 provide various support resistance values for *demand* based on the 95% cumulative FOH and the Barton formula, respectively. The *capacity* was based on the support elements in the various tributary area zones. The various FOS values relating to each tributary area zone are also provided.

Table 5-3: SR and FOS for various tributary area zones (SS1 - 2 m x 2 m cable anchor pattern) based on the 95% FOH.

Tributary Area Zone	Span		TA	Support Type	Laboratory Support Capacity Results	No of units Installed	Total SR	Act. SR	Req. SR	FOS
-	dip	strike	m²	-	kN	-	kN	kN/m²	kN/m²	-
TA 1	2	2	4	35 ton 3.5m Cable Anchor	295.0	1	295.0	74	43.95	1.7
TA 2	3	12	36	35 ton 3.5m Cable Anchor	295.0	5	7475.0	208	43.95	4.7
				600mm 1.5m Dura-pak	3000	2				

The FOS for tributary area zones (TA1 & TA2) in SS1 were above the acceptable industry value of 1.5.

Table 5-4: SR and FOS for various tributary area zones (SS2 - 1.5 m x 2 m cable anchor pattern) based on the Barton et al (1980) formula.

Tributary Area Zone	Span		TA	Support Type	Laboratory Support Capacity Results	No of units Installed	Total SR	Act. SR	Req. SR	FOS
-	dip	strike	m²	-	kN	-	kN	kN/m²	kN/m²	-
TA 1	1.5	2	3	35 ton 2.5m Cable Anchor	295.0	1	295	98	54	1.8
TA 2	3	12	36	35 ton 2.5m Cable Anchor	295.0	5	7475	208	54	3.9
				600mm 1.5m Dura-pak	3000	2				

The FOS for tributary area zones (TA1 & TA2) in SS2 were well above the acceptable industry value of 1.5.

The support systems provide satisfactory FOS results for the two FOH calculations. SS1 and SS2 provided a FOS of 1.7 and 1.8, respectively. The industry standard is 1.5 (Stacey, 2001).

The database for the 95% FOH was too small to do a proper analysis of FOH and therefore the Barton et al (1980) formula was used as another measure to determine a possible FOH. For this reason, a probabilistic key-block analysis was considered important as a check. The key block analysis considers loose blocks that can fall out with the support units or fall between support units, as well as possible failure of the support elements.

5.2 Geotechnical Data Analysis

All the geotechnical data collected underground described in Chapter 4 was used as inputs into an Excel spreadsheet and the DIPSs program for interpretation. The DIPS program makes use of orientation-based geological data that is displayed on a stereographical net for analysis. DIPS was mainly used to group the plotted discontinuities on the stereographical projection into joint sets (Figure 5-16).

Although the size of the dataset was considered adequate for analysis (a total of 155 discontinuities mapped), a Terzaghi weighting analysis was done to account for possible biases that could have arisen during data collection. These joints are sorted accordingly in Excel, grouping all the joint sets. The standard deviation for joint dip direction was obtained using the Fisher distribution in DIPS whilst the standard deviation for the dip of the joints has been approximated using the normal distribution.

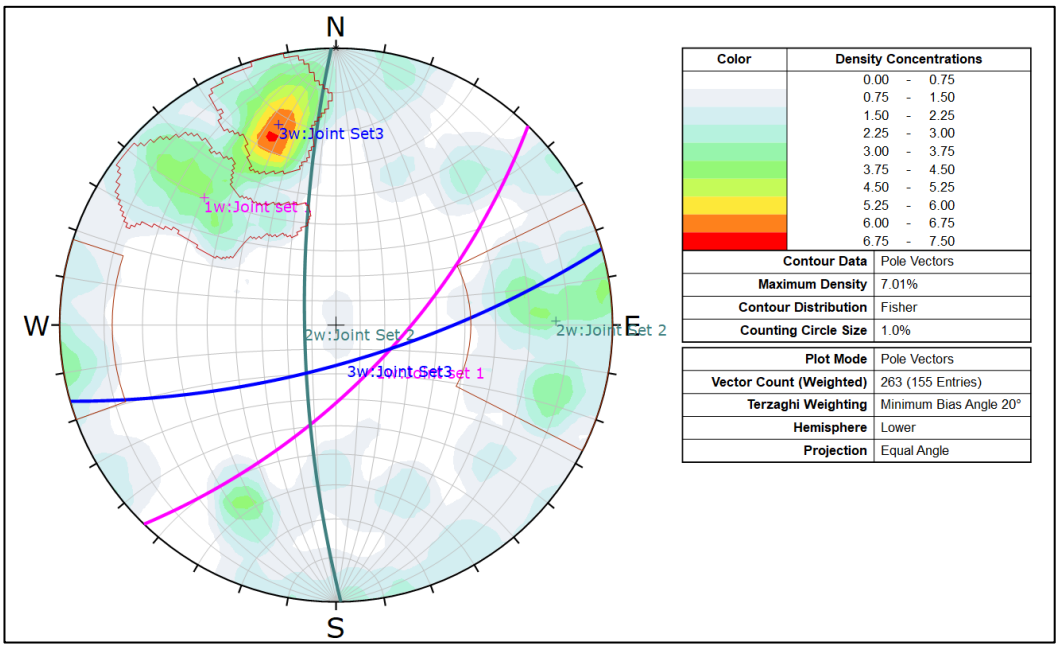


Figure 5-16: Dip stereo-net spatial plot of joints grouped into joint sets with Terzaghi weighted analysis.

Three main joint sets were identified from the collected field data with the rest of the joints forming random joints. These were arranged in Excel to determine the statistical distribution for each joint set. This information was later used as input data for J-Block key block analysis. Note that a conservative approach was used where the upper truncation limit for the friction angle was set at 38° (base friction angle of pyroxenite hangingwall). This was done to not exaggerate the strength of the joint surface as described in Chapter 2.

The statistical information on the various joint sets was done in Excel and arranged according to the inputs required by J-Block (Tables 5-5, 5-6, 5-7 and 5-8).

Table 5-5: Joint set 1 statistical data summary

Joint set 1	Dip (^{0})	Dip direction (^{0})	Friction angle (^{0})	Length/Persistence (m)	Spacing (m)
Interval	8	7	4	4	1.6
Min	45	135	9	0.8	0.12
Max	88	174	27	26.2	8.1
Count	27	27	14	27	19.0
Mean	69	151	24	7.37	2.1
St Dev	14	9	6	6.83	2.1

Table 5-6: Joint set 2 statistical data summary

Joint set 2	Dip (^{0})	Dip direction (^{0})	Friction angle (^{0})	Length/Persistence (m)	Spacing (m)
Interval	5.6^0	8^0	2	5	1.5
Min	53^0	262^0	27	0.8	0.02
Max	89^0	310^0	38	31	9.3
Count	44	44	44	44	37.0
Mean	77^0	285	36^0	6.8	1.1
St Dev	9.9^0	13	4^0	8.5	2.1

Table 5-7: Joint set 3 statistical data summary

Joint set 3	Dip (^{0})	Dip direction (^{0})	Friction angle (^{0})	Length/Persistence (m)	Spacing (m)
Interval	4.9	5	0	5	2.2
Min	61	170	27	1	0.1
Max	87	195	38	28	11
Count	21	21	9	21	15.0
Mean	75	182	27	5.8	3.2
St Dev	7.3	7	1	6.0	3.6

Table 5-8: Joint set 4 statistical data summary

Random	Friction angle (^{0})	Length/Persistence (m)	Spacing (m)
Interval	3	5	0.9
Min	7	7	0.1
Max	27	33	5.9
Count	31	63	54
Mean	22	7.0	1.4
St Dev	6	7.8	1.6

5.3 J-Block Analysis (Key block): Probabilistic Approach

5.3.1 Key block distribution

A key block analysis was carried out on the above-mentioned support systems using the J-Block key block analysis program. J-Block is a comparative assessment tool used to assess support scenarios. This probabilistic approach was a supplementary approach to the traditional deterministic method described in Chapter 5.1. It makes use of a statistical distribution of geotechnical data to test the support design against an array of scenarios. This is done by the program by forming various key blocks and testing the support in the area where the key block is formed.

The analysis of the statistical geotechnical data in Section 5.2 was used as inputs in the J-Block Geotechnical domain. Three main joint set parameters were defined as well as parameters for random joints. A distribution of key blocks indicated in Figure 5-17 was generated from the geotechnical data up to a 68% confidence level as only 1 standard deviation was considered in the joint set input data. The minimum number of recommended (100 000) discrete block formations was selected to get a suitable distribution of data.

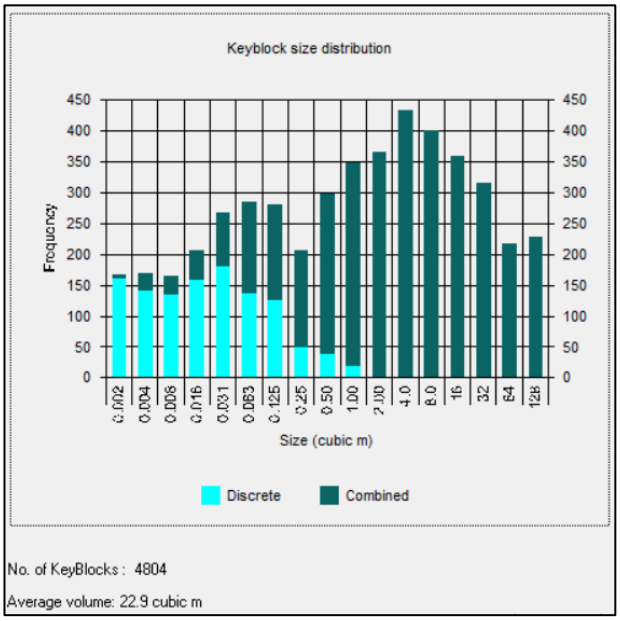


Figure 5-17: Graph showing the key block size distribution

A significant proportion of the discrete blocks formed lie between 0.002 m^3 to 0.25 m^3 (6.4 kg to 400 kg). This size range of discrete blocks has a higher potential to fall between the tendon support units rather than failing the support units. These are however expected to be easily catered for through the barring and making safe process in EEMS.

A smaller population of larger discrete blocks ranging from 0.25 m^3 to 1 m^3 (800 kg to 3200 kg) were also formed and are also expected to be easily supported by the CA (34-ton) support units.

A larger population of the blocks were combined with sizes greater than > 1 m^3. These combined blocks did not form discrete blocks and are not expected to be as prone to fallouts as the discrete blocks. A total of 4804 blocks were formed in the key block distribution.

5.3.2 Mining Excavation

These key blocks were generated within a defined stope excavation outline created in J-Block (Figure 5-18). The excavation outline of the workplace that was created represents a 28.0 m (skin-to-skin) panel with a 50.0 m back length. The excavation surface was made to dip at 10^0, which is equivalent to the reef dip in the project trial site.

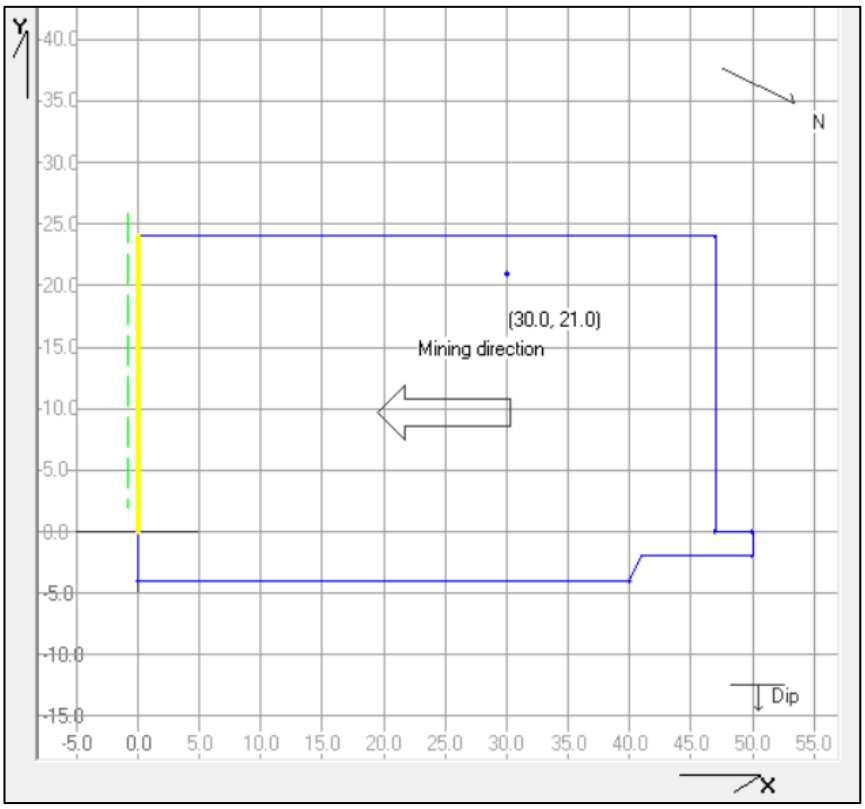


Figure 5-18: 28 m panel excavation outline with 50 m back length

The stope excavation outline is representative of a breast panel that was initially advanced Northwards however the direction of mining for the *footwall mining project)* is in a retreat direction (Southwards). The face area line (yellow line) depicted at X = 0 represents the *footwall mining* front that is being advanced in a retreat direction. This footwall mining methodology is discussed in greater detail in Section 5.4.

5.3.3 Support System Scenarios

Two Support Scenario spacings with four varying CA lengths were tested for the excavation profile that included the following support elements. A total of 8 support scenarios were thus simulated. The rated strength of the 18 mm cable strands was provided by the OEM supplier and determined in the UTS test results where the average strength was 339kN. Therefore 339kN ÷ 9.81 m/s^2 = 33.9 tons (34 tons). The rated strength for a 60cm x 60cm pack at 1.5m height is 3000 kN.

Support Scenario 1

The support elements in this evaluation are shown below specifying the peak strength, tendon length, and support spacing as follows:

- 34-ton CA's installed in a 2.0 m strike x 1.5 m dip pattern are pre-installed in the hangingwall to ensure back area stability. Four CA support lengths were simulated for Support Scenario 1:
  - 1.0 m long CA spaced at "SS1"
  - 1.5 m long CA spaced at "SS1"
  - 2.0 m long CA spaced at "SS1"
  - 2.5 m long CA spaced at "SS1"
- A breaker line of Dura-Pak support units spaced 3.0 m apart on dip and 12 m apart on strike.

Support Scenario 2

The support elements in this evaluation are shown below specifying the peak strength, and tendon support spacing as follows:

- 34-ton CA's 2.0 m strike x 2.0 m dip are pre-installed in the hangingwall to ensure back area stability. Four CA support lengths spaced were simulated for Support Scenario 2:
  - 1.0 m long CA spaced at "SS2".
  - 1.5 m long CA spaced at "SS2"
  - 2.0 m long CA spaced at "SS2"
  - 2.5 m long CA spaced at "SS2"

- A breaker line of Dura-Pak support units spaced 3.0 m apart on dip and 12 m apart on strike.

The rationale for comparing these 8 support scenarios was to assess the influence of CA length and spacing on the effectiveness of the support system.

- The 1.0 m CA lengths were simulated to test the validity of the 95% cumulative FOH. These support scenarios tested the “reinforcement” tendon philosophy.
- The 1.0 m and 1.5 m long CAs are both shorter than the theoretical Barton et al (1980) based FOH of 1.76 m. These support scenarios tested the “reinforcement” tendon philosophy under the Barton et al (1980) FOH conditions.
- The 2.0 m and 2.5 m long CA units are sufficient to cater for the theoretical Barton et al (1980) based FOH of 1.76 m with sufficient bond length (>200 mm). These support scenarios tested the “suspension” tendon philosophy under the 95% FOH and Barton et al (1980) based FOH.

5.3.4 Support Specifications

For each support scenario, the support specifications were defined. This includes the rated strength of point support (such as elongates) and area support units (such as packs). Note that, although the CA’s are grouted in practice, grouting was not included in the J-Block simulation as a conservative approach.

The tendon (CA) installation angle relative to the excavation surface was specified in Figure 5-19. The length of the support tendons as well as the spacing between support is specified. A support spacing variance of 0.05 m was applied to account for human errors during installation. The CA support holes in the panel hangingwall were drilled with an instope bolting drill rig capable of drilling holes vertically. As a result, the CA’s were installed at angles greater than 70^0 to the hangingwall.

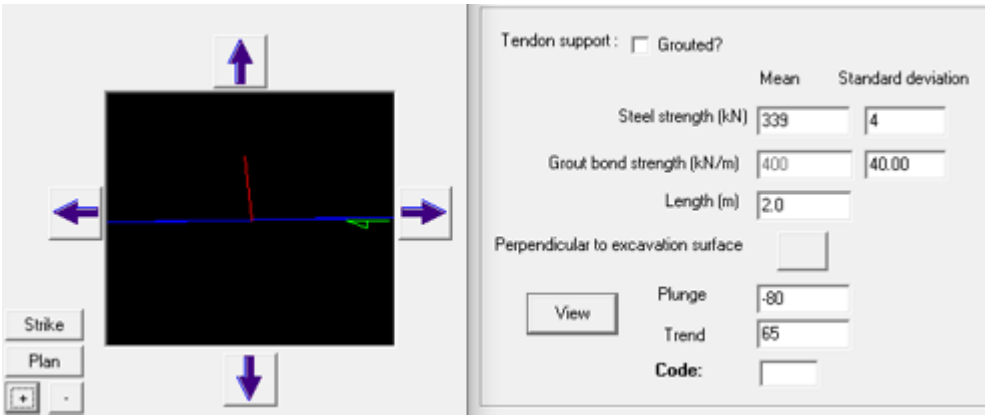


Figure 5-19: Installation angle for CAs along the panel back area

5.3.5 Support Zones

Three support zones indicated in Figures 5-20 and 5-21 were defined as follows:

- Zone 1, was defined as the face area where the footwall blasting front takes place and consists of the pre-installed cable anchors.
- Zone 2 is defined as the back area that starts 12 m from where footwall mining is taking place up to the stopped panel face. Zone 2 consists of cable anchors and Dura-Pak units.
- Zone 3 is defined as the ASG and siding forming the access-way for men and material into the panel. It consists of timber elongates, installed along the siding as well as tendon units along the ASG hangingwall.

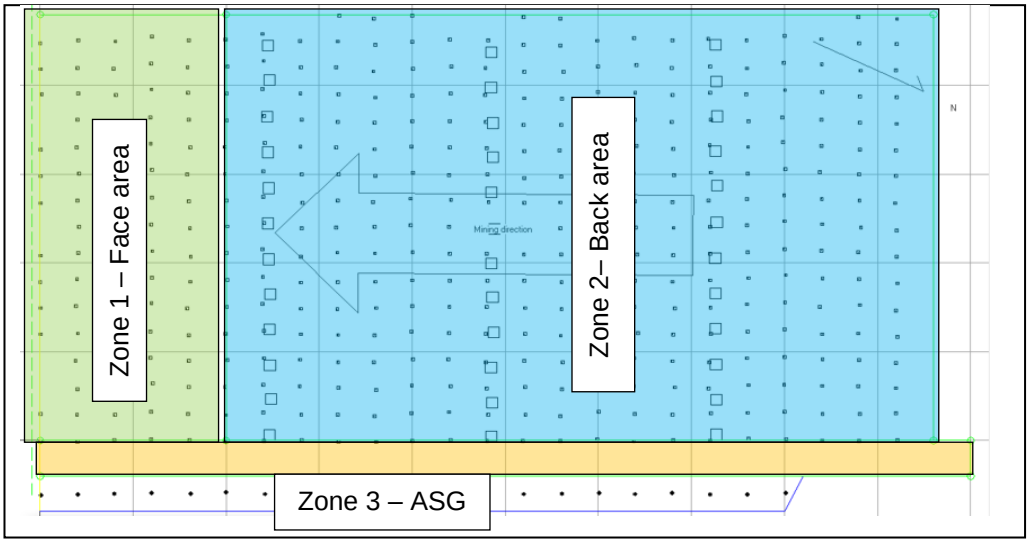


Figure 5-20: Support Scenario 1 – 34 ton – CA in 1.5 m dip x 2.0 m strike, Dura-Paks 3.0 m x 12 m apart.

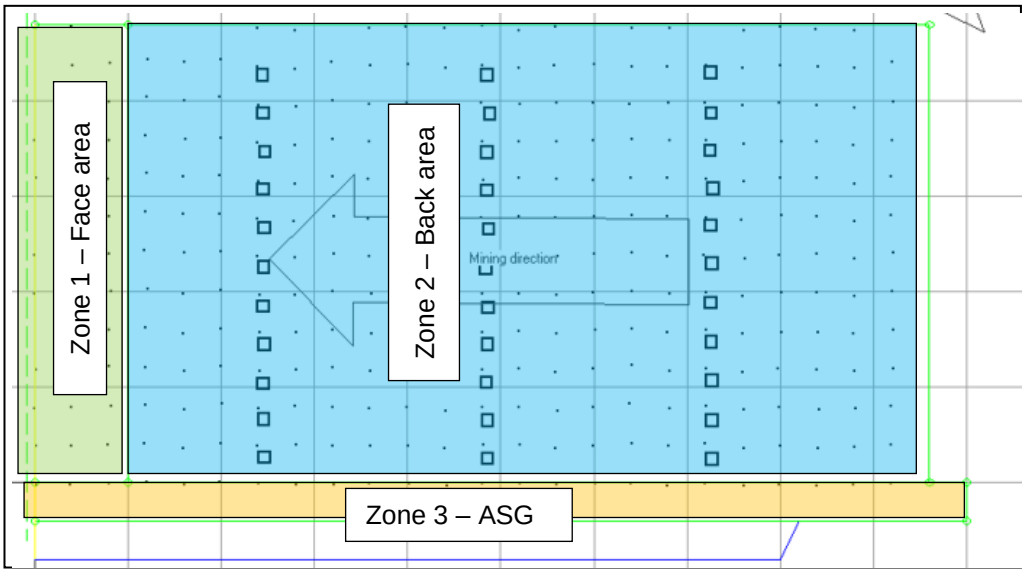


Figure 5-21: Support Scenario 2 – 34 ton CA in 2.0 m strike x 2.0 m dip, Dura-Paks 3.0 m x 12 m apart

5.4 Footwall mining methodology and mining sequence

5.4.1 Footwall mining philosophy

The philosophy of the footwall mining methodology entailed mining the panel out in a retreat direction. The mining started from the stopped panel face progressing backwards towards the centre gully. This was done to ensure that any instability that could occur in the mined-out area was away from the main access centre gully to prevent other panels from being impacted. The stoping width progressively increased as the re-treating mining front advanced creating a wide stope excavation.

The method entailed blasting out of existing timber support units which were replaced with long CAs. CAs were selected as the suitable replacement support unit due to their flexible characteristic enabling longer units to be pre-installed in a 1.35 m stoping height. In addition, CAs have less cumbersome logistical requirements than the longer heavier timber elongates.

The design of the support system and mining methodology required that the CAs be pre-installed before blasting the footwall. In doing so, this enabled a greater

extraction of footwall. In addition, there was no need to enter the blast-out area to install a new support unit after each blast as the cable anchors were pre-installed.

5.4.2 Footwall mining sequence: (support installation, drilling and cleaning process)

The following sequence was followed when trialling the footwall support and extraction methodology:

- Rows of 3.5 m long CA's were pre-installed for at least 6.0 m ahead of the retreat footwall mining face.

- All drilling of the long CA holes was done under the cover of safety nets installed across the hangingwall between rows of timber, attached to exiting bolts with S-hooks.

- The drilling of the footwall shot holes took place between existing elongates under the hangingwall supported with cable anchors.

- The footwall layer was extracted in 4.0 m segments drilled and blasted according to the OEM (Enaex) blast design specifications. A maximum of two rows of timber support was allowed to be blasted out at a time.

- 400 mm – 500 mm cuts were initially extracted by using short 700 mm long shot holes drilled with a 0.9 m drill steel jumper positioned at an angle 45^0 toward the ASG (Figure 5-22). A 500 mm burden-spacing was used between the production shot holes.

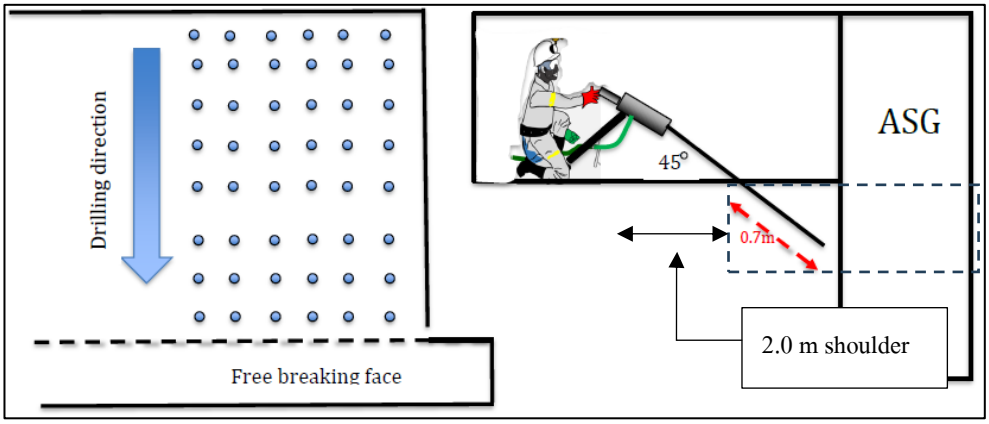


Figure 5-22: Diagram indicating the drilling direction of footwall mining shot-holes (Nel, 2022)

- The mining of the 400 mm – 500 m cut footwall layer resulted in a 2.0 m wide stoping height.

- The drilling of the footwall shot holes took place from the bottom of the panel at the ASG and progressed upwards up to 2.0 m from the top pillar. A 2.0 m shoulder was left at the top of the panel to maintain the instope pillar height-to-width ratio.

- The blasted footwall area was cleaned using scraper winch cleaning methods where blasted ore was pulled from the blasted footwall along the panel into the ASG and then into the main centre gully.

  The above sequence for footwall mining and support methodology are illustrated in diagrams Figures 5-23, 5-24, and 5-25:

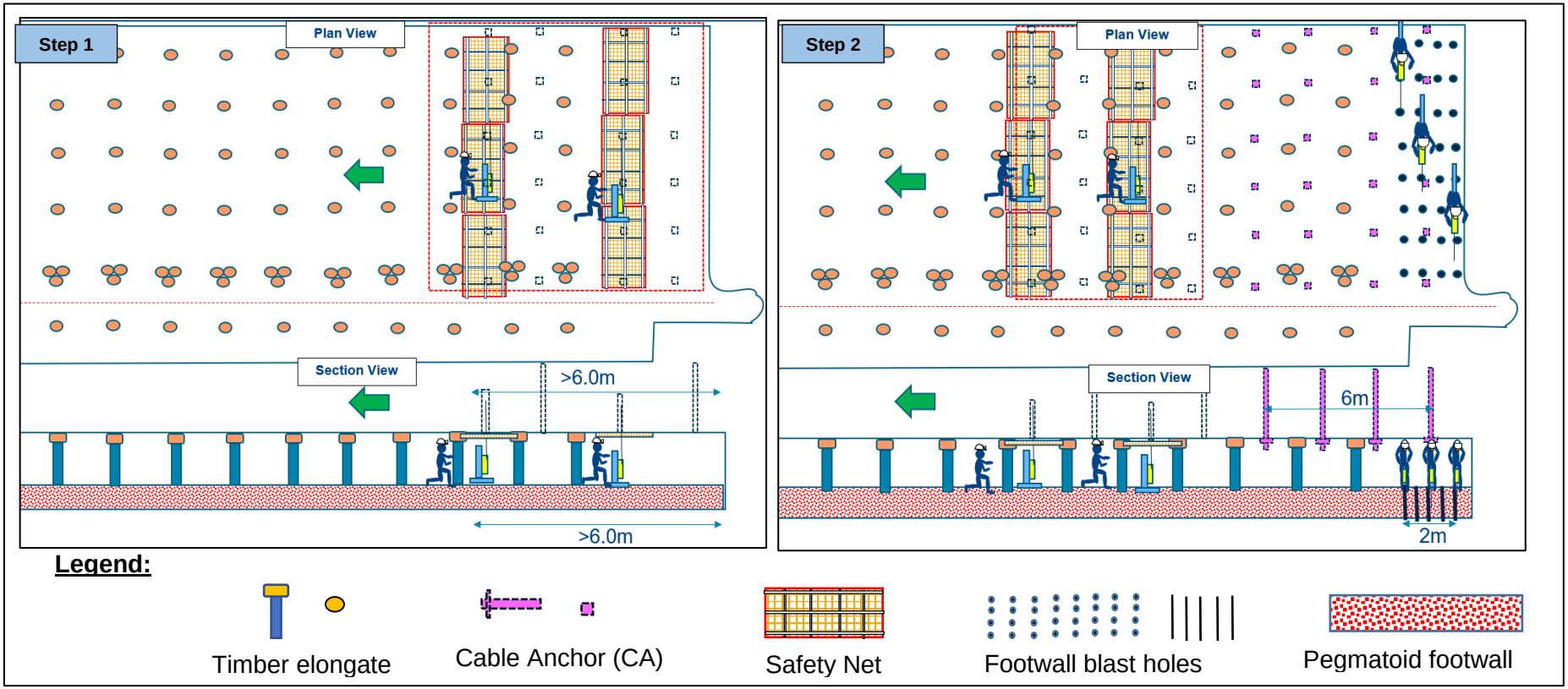


Figure 5-23: Cable anchor pre-support work and footwall drilling to establish the trench (Tati, 2022)

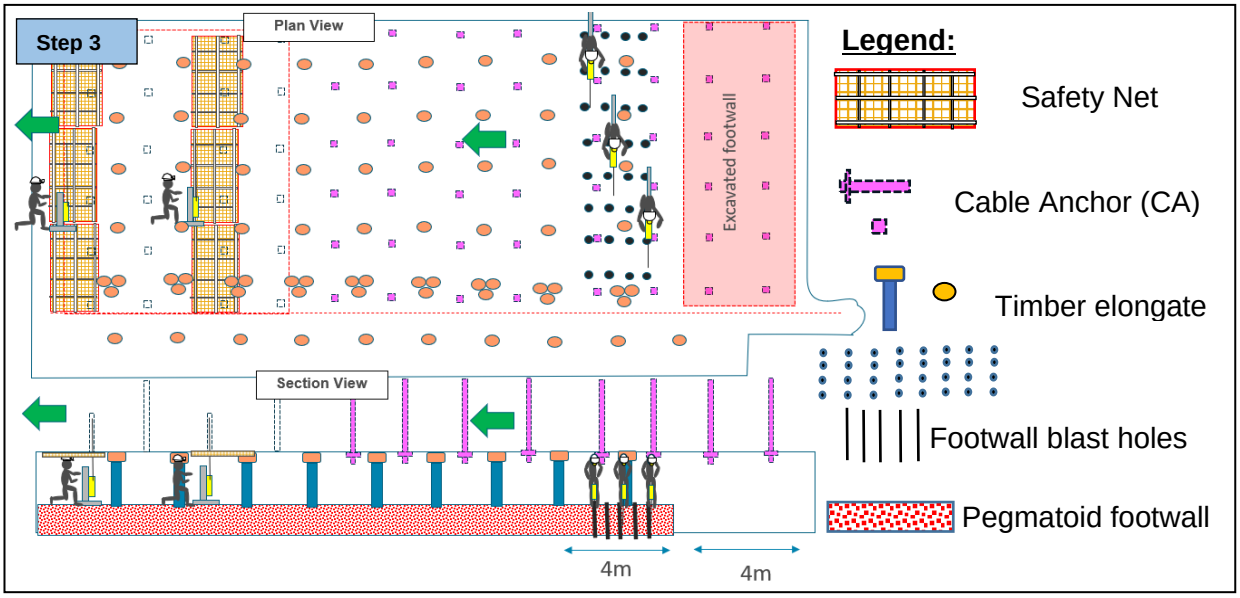


Figure 5-24: Blasted footwall after cleaning and next portion of cable anchor pre-supporting and footwall drilling (Tati, 2022).

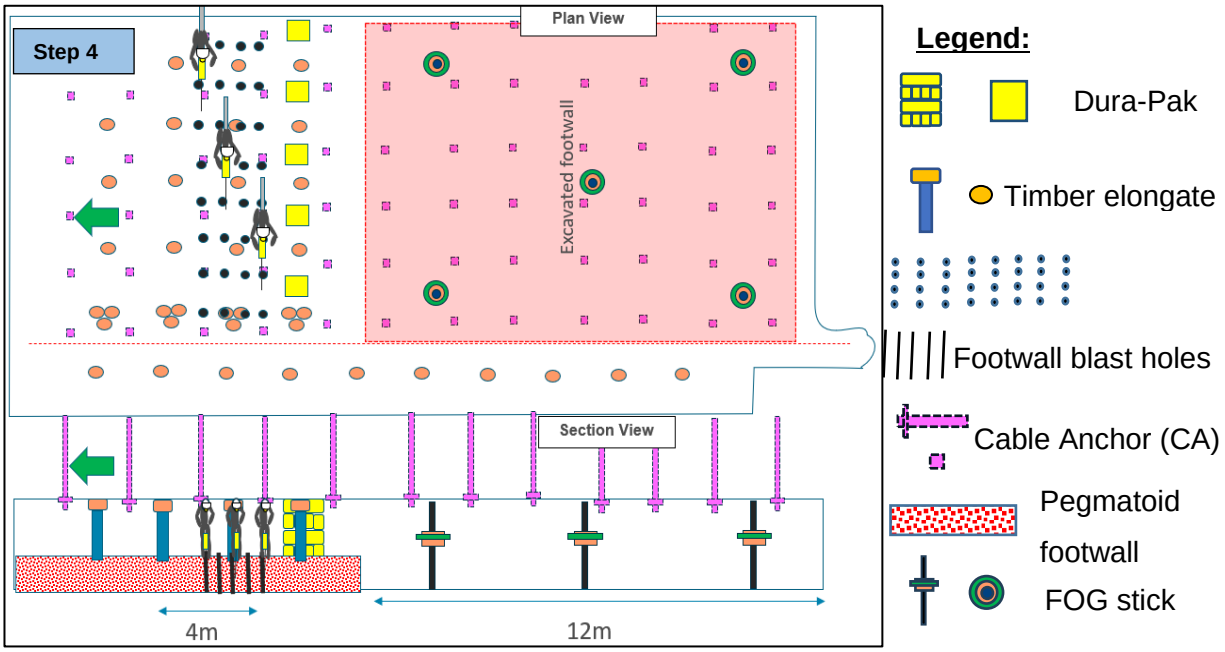


Figure 5-25: Dura-Pak breaker line installed at 12 m intervals, footwall drilling to leapfrog ahead of Dura-Pak breaker line (Tati, 2022).

Figure 5-26 shows photographs taken during the implementation of the footwall mining method.

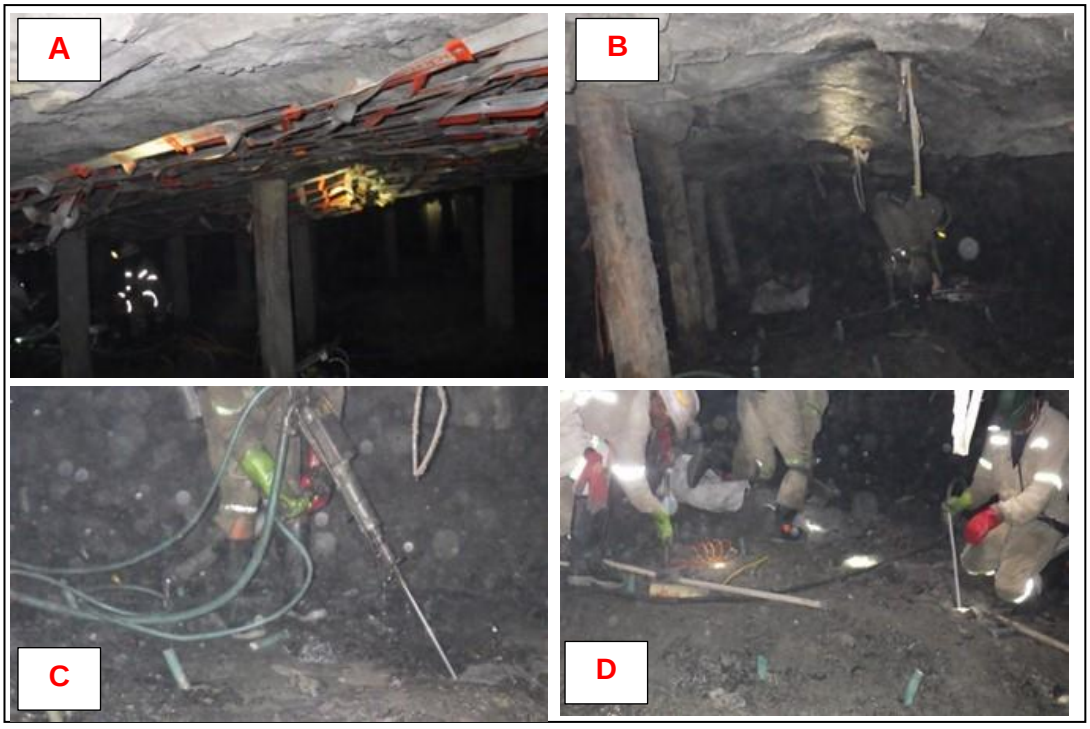


Figure 5-26: Photographs showing cable anchors pre-installed and footwall drilling.

Photographs showing the implementation of the support and mining activities carried out at the footwall lifting trial site as described in section 5.4.2 are indicated in Figure 5-26 as follows:

- Photograph A indicates the safety net installed between rows of timber during the pre-drilling of CA holes.
- Photograph B indicates the CA installed between rows of timber prior to the footwall lifting.
- Photograph C indicates the footwall drilling by the RDOs to create the trench in the face area.

- Photograph D charging-up of the drilled footwall to prime the holes with explosives.

5.5 Monitoring and Control

5.5.1 Teething Issues:

Various teething issues that affected mainly the RDOs drilling the production shot holes were encountered during the implementation of the project trial. These issues included the following:

- The confined space in the initial stoping height created challenging conditions for RDO to drill shot holes downwards.
- The productivity of the RDOs was affected as they were unable to complete all the footwall shot holes over the 4.0 m distance (two rows of elongates) in a given shift.
- The rock drill machine drilling angle (45^0) and air-leg restricted the length of drill steel that could be used. The depth of drilling of the first cut was limited to 0.5 m. Therefore, multiple cuts in the same area had to be taken where Pegmatoid thickness was greater than 0.5 m.
- The footwall sustained cracks and blast damage after blasting the first 0.5 m cut. This resulted in an increased number of drill bits getting stuck when drilling the subsequent cuts.
- Areas where the ASG depth capacity was insufficient (<1.0 m) created a restriction to the depth of the footwall cut. For practical cleaning reasons, the panel footwall could not be mined lower than the ASG footwall position.
- Relatively large rocks were formed from this footwall extraction method than a normal advancing stope face. This is believed to be due to the 3 breaking faces associated with the footwall mining method in an already fractured footwall with no in situ confinement.

5.5.2 Adjustment Controls:

To address the teething issues affecting the RDOs from drilling the production shot holes, an alternative approach (*trench and retreat method*) was developed and tested. An alternative blast design that suited the *trench and retreat method* was developed by an Enaex site consultant on the mine.

5.6 Alternative trench and retreat footwall mining methodology (support installation, drilling and cleaning sequence)

The alternative sequence for the trench and retreat footwall mining methodology was done as follows:

- A 2.0 m wide trench was created using the same drilling and blasting methodology explained in chapter 5.5.2 *Footwall mining sequence: (support installation, drilling and cleaning process)*. A second cut was taken in the same 2.0 m area to establish a 1.0 m deep trench.
- Once the above-mentioned trench was cleaned, a shoulder was established that formed the free-breaking face. The RDOs could then drill standing upright from the trench footwall shotholes according to the OEM (Enaex) blast design. The free-face shoulder was drilled into using 1.5 m long drill steel.
- Where the gully depth capacity in the ASG was less than the depth of footwall mining to be done, the gully depth was lowered first before any other footwall mining activities were carried out in the panel.

The above sequence for the trench and retreat footwall extraction methodology is illustrated in diagrams Figures 5-27,5-28, and 5-29:

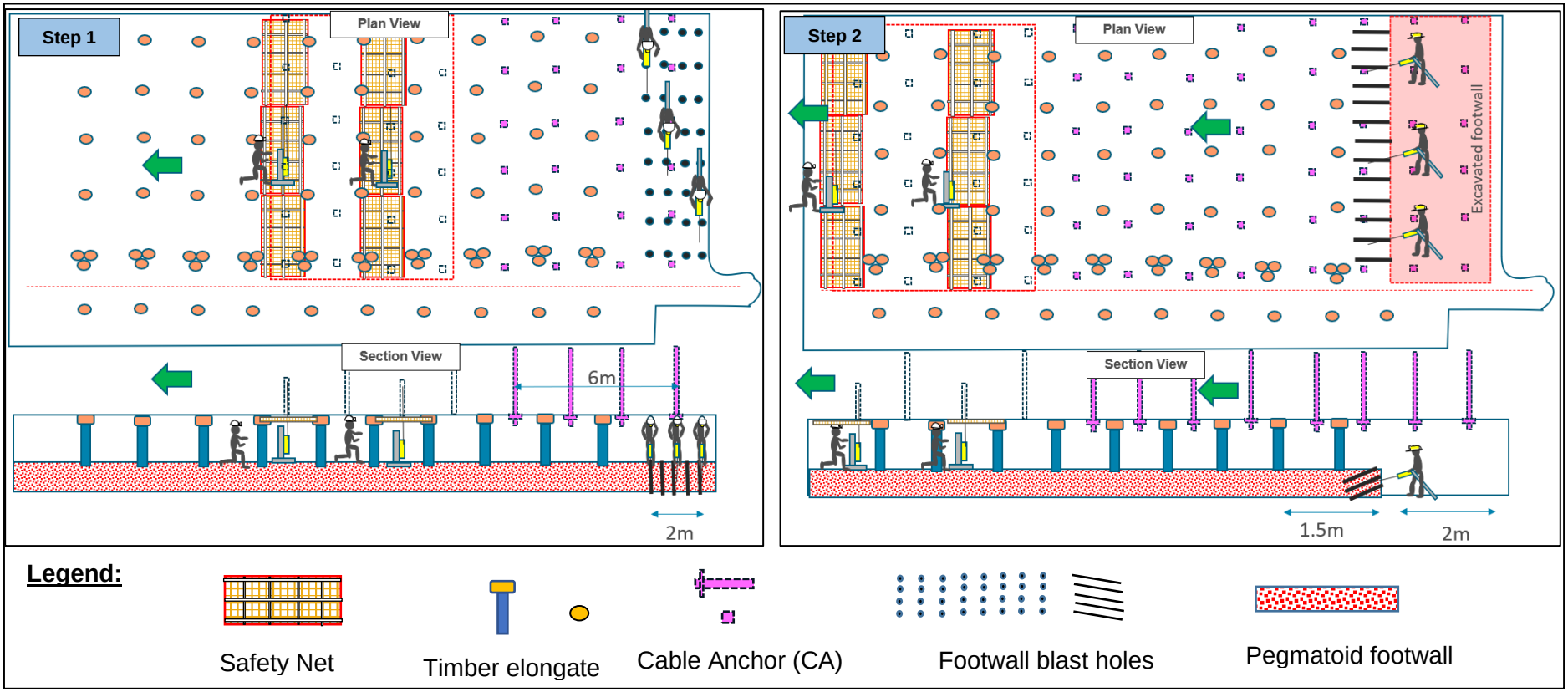


Figure 5-27: Trench creation and retreating mining sequence in the alternative footwall mining method.

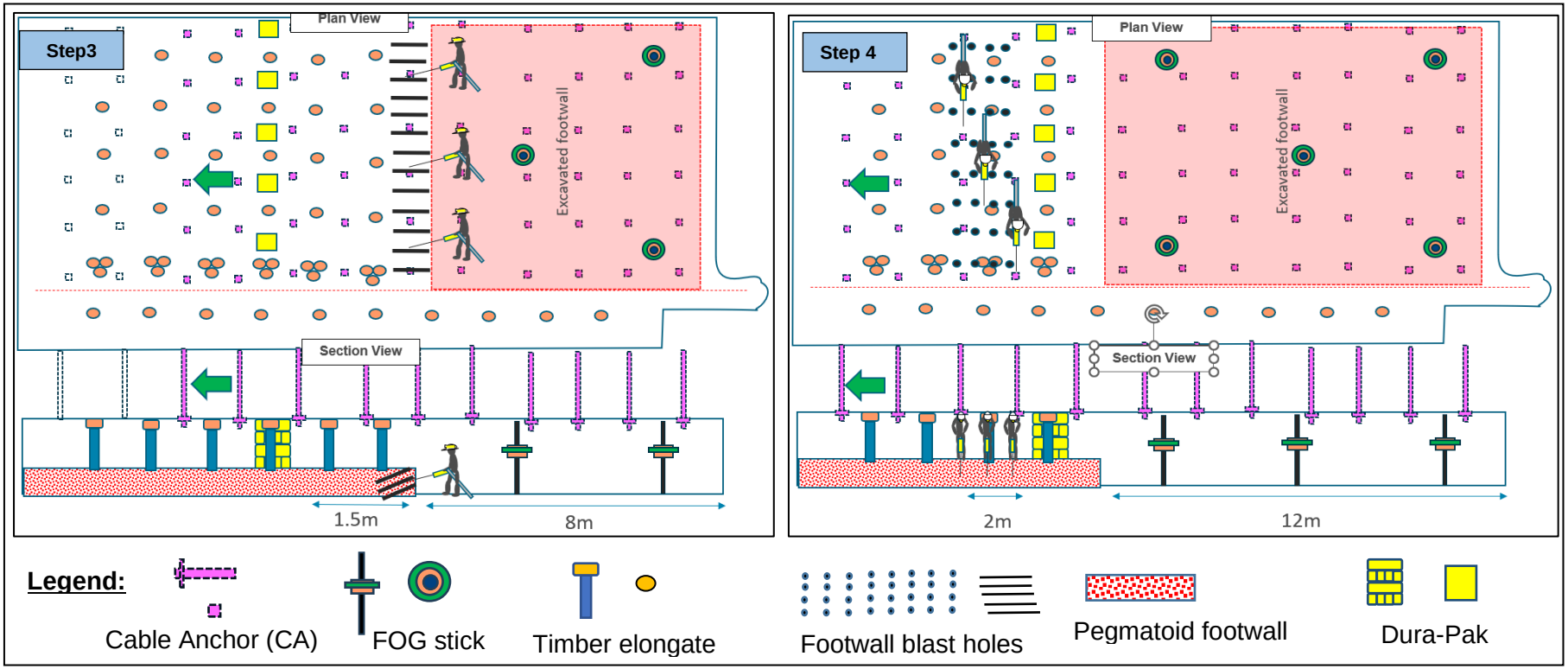


Figure 5-28: FOG stick monitoring devices installations and RDO's leapfrogging the retreating face to create a new trench

5.6.1 Alternative drill and blast design

Figure 5-29 is a section (front) view diagram of the alternative blast design for the trench and retreat method.

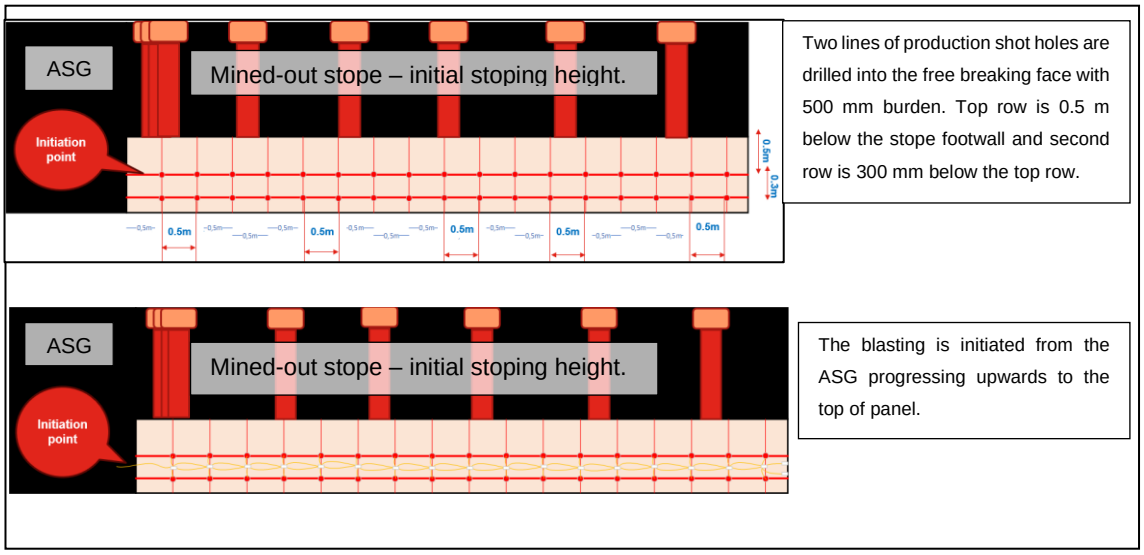


Figure 5-29: Section view diagram showing the alternative drill and blast design from an established free-breaking face (Eanaex, 2023)

Figure 5-30 is a diagram showing the top and side view for the alternative blast design for the trench and retreat method.

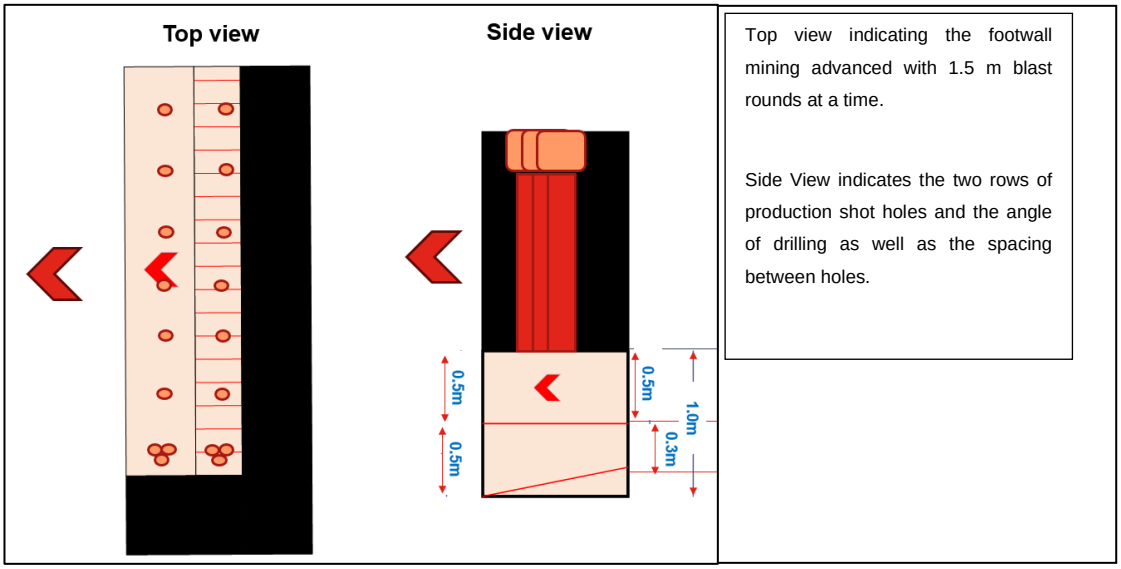


Figure 5-30: Diagram indicating top view and side view of alternative blast design (Eanaex, 2023)

Figure 5-31 shows photographs taken during the implementation of the alternative trench and retreat footwall mining method.



Figure 5-31: Alternative trench and retreat method being implemented.

5.4.4 Alternative trench and retreat methodology summary

The alternative “trench and retreat method” provided improved efficiencies and higher productivity of the crew. The approach was found to be more systematic with the crews blasting daily. Cleaning the panel, however, remained a challenge as blasted ore was thrown back into the back area. This delayed the systematic installation of FOG stick monitoring devices in the back area which are vital in the absence of timber elongates.

5.7 Stability Monitoring

A total of three FOG sticks were installed in 20 21 014A PAN 1ED where an area of 290 m^2 of footwall was extracted. The FOG sticks were installed in the pattern and spacing depicted in Figure 5-32. The initial measurements were recorded at each installation site and are summarized in Table 5-11. The FOG sticks provided continuous monitoring of back area stability by emitting a flashing light. A green flashing light was emitted from the FOG stick when there was little (< 7 mm) to no movement between the hangingwall and footwall. If the displacement between the hangingwall and footwall exceeded 7 mm, a red flashing light would be emitted from the FOG stick warning personnel not to enter that area.

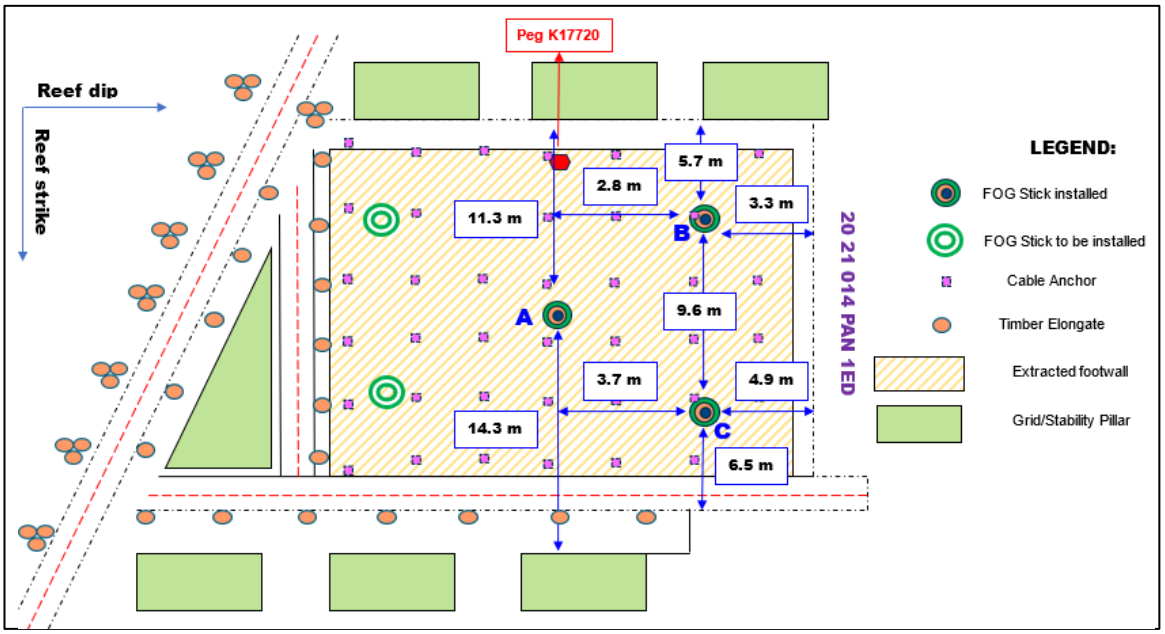


Figure 5-32: Diagram indicating FOG stick installation positions in 20 21 014A PAN 1ED

Table 5-9: Summary of FOG stick installation position & readings

FOG Stick Name	A	B	C
Peg position	K11720 -5.6 m dip K11720 +0.0 m strike	K11720 -1.3m dip K11720+2.8m strike	K11720 -10.9m dip K11720+3.7m strike
FOG stick initial reading (25/10/23)	No gauge reading	172 mm	156mm
FOG stick final reading (13/11/23)	No gauge reading	172 mm	156mm

Although the panel (2021 014A PAN 1ED) was not completely clean, these FOG sticks were installed on the solid footwall indicated in Figure 5-33. These FOG sticks were installed to assess the stability in the area where timber elongates were removed where cleaning and further mining activities are planned to continue.

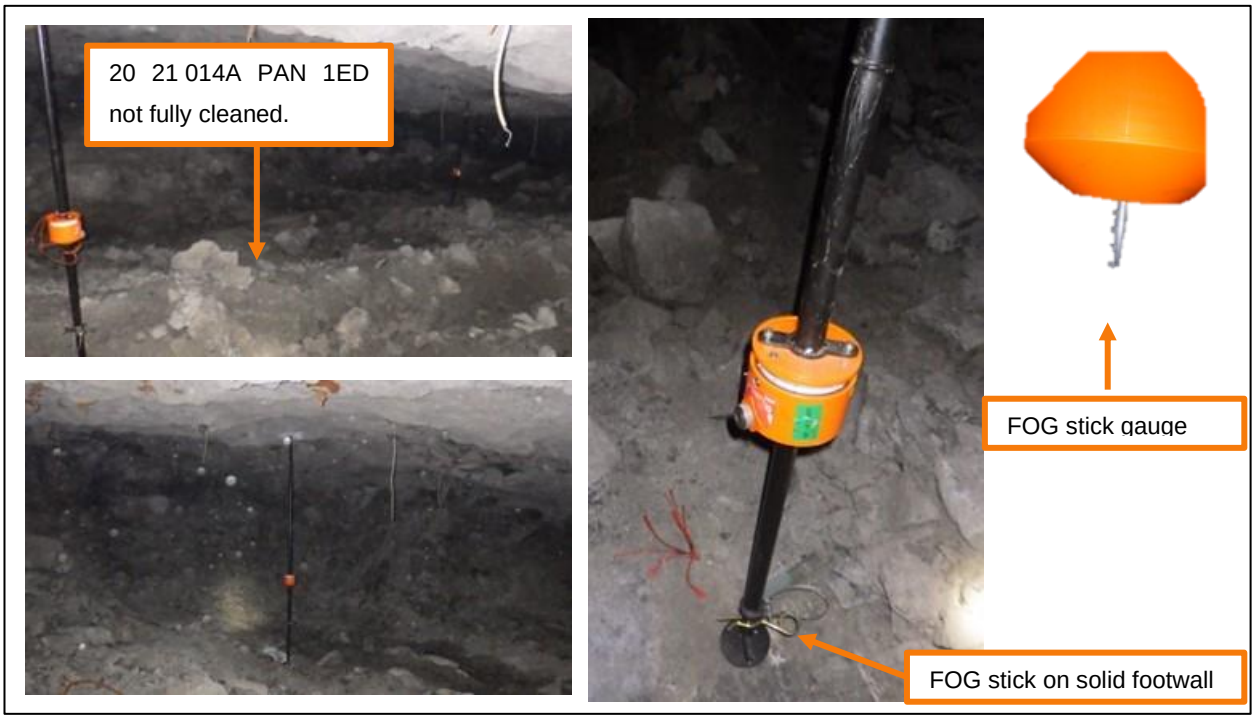


Figure 5-33: Photographs of FOG stick installation in 20 21 014A PAN 1ED Production output

The production output from the footwall mining 20 21 014A PAN 1ED is indicated in Table 5-12. The production output was measured by the Survey department and indicates the cubic volume that was extracted. Over the three-month trial period, a total of 1172 tons was mined which translates to 36 ounces. Note that the production was steadily increasing from Aug 23 to Oct 23 however had a subsequent drop in the Nov 23 month. This drop was due to a major shaft conveyance incident that occurred on the Impala operations affecting all other operational shafts.

Table 5-10: Footwall mining 3-month production output

Workplace	20 21 014A PAN 001ED			Cubics M3				Grand Total
RespMM	RespMO	PersonSS	RespWG	Aug 23	Sep 23	Oct 23	Nov 23	
20# PROJECTS	2015(MMM)	S. Sibiya	20-T034D	0	62	246	64	372
Pegmatoid density (t/ı	3.15			Tons				Grand Total
				Aug 23	Sep 23	Oct 23	Nov 23	
Grade (g/t)	0.88			0	196	774	202	1172
Ounce per gram (Oz/g)	0.035274			Ounces				Grand Total
				Aug 23	Sep 23	Oct 23	Nov 23	
				0	6.1	24.0	6.3	36

5.8 Chapter Summary

Chapter 5 of the research report details the research and findings of the trial project. The deterministic support design process was carried out for the footwall mining project trial area. Two support systems were defined, followed by a delineation of 2 main support tributary areas for the footwall mining panel. The support requirements were established by determining the FOH thickness. Support resistance equations were used to determine support resistance for the demand and capacity and ultimately determine the FOS for both support systems. The outputs of the two support system design calculations indicated that both support systems provided the required SR and stable FOS values >1.5 provided that the 95% FOH is assumed. However, the support spacings need to be 2 m x 1.5 m to satisfy the Barton et al (1980) equation.

The analysis of the results from the geotechnical structural mapping data was processed through Dips and Excel. This data analysis produced statistical data for three main joint sets including a set for random joints. This data was later used as inputs in the J-Block key block analysis program. The support design was further enhanced through a probabilistic key block analysis approach that made use of the J-Block program. The statistical geotechnical results were used as input data for the J-Block analysis. A standard 28 m wide x 50 m long excavation stope profile was created where the desired support system was placed. Three zones and an

area of interest were defined in the excavation profile where the simulations were processed. A total of 8 support scenario simulations were run in J-Block for comparison. The results from the J-Block simulations are analysed in Chapter 6.

Chapter 5.4 covered the footwall mining methodology (with the newly integrated support system) in detail describing the steps followed at each stage of the mining cycle. The initially proposed mining methodology was found to be practically cumbersome and inefficient. An adjusted “trench and retreat method” provided a more effective means for mining out the mineralized layer at improved efficiencies.

This was supported by production output results which increased from 196 tons in October to 774 tons in November 2023. The production output results demonstrate a proof of concept for the methodology. This suggests that the project is viable from a practical and operational point of view with minor teething issues still to be resolved.

6 ANALYSIS OF RESEARCH FINDINGS

This analysis chapter aims to bring together the findings from the deterministic approach and the probabilistic approach. The probabilistic approach was used to validate the deterministic approach. The two FOHs (cumulative FOH of 1.4 m and Barton et al (1980) FOH equation of 1.72 m) were used to determine the extremities of support length and resistance requirements. The analysis is illustrated and explained through a series of tables and graphs.

6.1.1 Key-block fall simulation outputs.

Table 6-1 provides a summary of the key block results for the various support scenario J-Block simulations. It shows the number of key blocks created, key blocks failed, as well as rockfalls per mining step.

Table 6-1: Statistical outputs result for the carious support scenario simulations.

Support Standard (SS1) - 1.5 m x 2.0 m	1.0 m CA
Simulation Statistics	
Total simulations area	4524
Percent area that is a keyblock	79.80%
Total no of keyblocks	142 692
Total no of failed keyblocks	75 725
Average rockfalls per mining step	16.45

Support Standard (SS1) - 1.5 m x 2.0 m	1.5 m CA
Simulation Statistics	
Total simulations area	4540
Percent area that is a keyblock	79.90%
Total no of keyblocks	144 153
Total no of failed keyblocks	75 671
Average rockfalls per mining step	16.73

Support Standard (SS2) - 2.0 m x 2.0 m	1.0 m CA
Simulation Statistics	
Total simulations area	4540
Percent area that is a keyblock	80.10%
Total no of keyblocks	134508
Total no of failed keyblocks	77 772
Average rockfalls per mining step	17.19

Support Standard (SS2) - 2.0 m x 2.0 m	1.5 m CA
Simulation Statistics	
Total simulations area	4540
Percent area that is a keyblock	82.30%
Total no of keyblocks	153111
Total no of failed keyblocks	77 750
Average rockfalls per mining step	17.57

Support Standard (SS1) - 1.5m x 2.0 m	2.0 m CA
Simulation Statistics	
Total simulations area	4540
Percent area that is a keyblock	82.10%
Total no of keyblocks	125336
Total no of failed keyblocks	74 764
Average rockfalls per mining step	16.4

Support Standard (SS1) - 1.5 m x 2.0 m	2.5 m CA
Simulation Statistics	
Total simulations area	4540
Percent area that is a keyblock	82.20%
Total no of keyblocks	125007
Total no of failed keyblocks	74 780
Average rockfalls per mining step	16.6

Support Standard (SS2) - 2.0 m x 2.0 m	2.0 m CA
Simulation Statistics	
Total simulations area	4540
Percent area that is a keyblock	80.10%
Total no of keyblocks	145 884
Total no of failed keyblocks	76 351
Average rockfalls per mining step	16.88

Support Standard (SS2) - 2.0m x 2.0m	2.5 m CA
Simulation Statistics	
Total simulations area	4540
Percent area that is a keyblock	82.10%
Total no of keyblocks	146 136
Total no of failed keyblocks	76 373
Average rockfalls per mining step	16.9

The key block failure results in J-Block were of key concern and are shown in a graphical format in Figure 6-1.

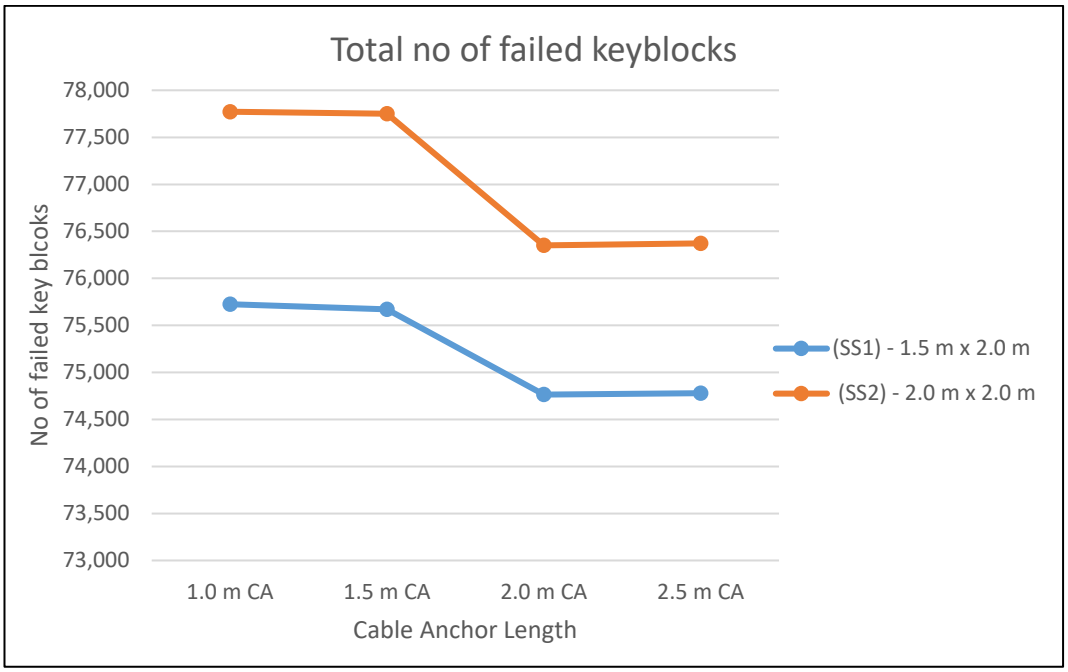


Figure 6-1: Graphical comparison of the number of failed tendons for various CA lengths and spacings

Figure 6-1 shows how there is a higher number of failed key blocks for 1.0 m and 1.5 m long CAs than longer CA lengths (2.0 m and 2.5 m). This can be argued to be associated with the 95% cumulative FOH (1.4 m) and Barton et al (1980) FOH equation (1.72 m). The number of key blocks that fail is expected to increase when tendons are too short for the key block created or too short for the FOH. The number of key block failures reduced and plateaued when CA was (2.0 m and 2.5 m), i.e. longer than the FOH analysis. It suggests that the Barton et al (1980) analysis provides a reasonable estimate for the length and spacing of the support elements.

6.1.2 Tendon Performance Results

Tendon failure analysis

Table 6-2 compares the tendon performance results for both support systems in the J-Block simulations. The results from the J-Block simulations show the number of successful tendons, failed tendons as well as short tendons. Successful tendons are those that have successfully supported a key block and prevented it from falling out. Failed tendons are those where the steel has failed either in tension or by rotation. Short tendons are those that did not have sufficient reach to penetrate through the key block.

Table 6-2: Tendon performance results,

Evalatuion criteria	Support Standard (SS1) - 1.5 m x 2.0 m			
Cable Anchor Length	1.0 m CA	1.5 m CA	2.0 m CA	2.5 m CA
Tendons successful	9165	9132	9976	11057
Tendons too short	15927	9140	8005	7572
Tendons failed	664	692	698	702
Evalatuion criteria	**Support Standard 2 (SS2) 2.0m x 2.0 m**			
Cable Anchor Length	**1.0 m CA**	**1.5 m CA**	**2.0 m CA**	**2.5 m CA**
Tendons successful	6249	6679	7565	8170
Tendons too short	8939	8406	6062	5424
Tendons failed	635	682	685	688

By comparing the columns between the support systems in Table 6-2, one can evaluate the effects of CA spacing on the support system. Conversely by comparing the rows in Table 6-2, one can evaluate the effects of CA length on the support system. Figure 6-2 shows a comparison of successful tendons for various CA lengths in both support scenarios (SS1 & SS2). The number of successful tendons gradually increases as the CA length is increased. Of particular interest here is that the denser support scenario SS1 has significantly more successful tendons than the more sparsely spaced support (SS2), up to a height of 1.5 m. Above a height of 1.5 m, the two support lines are parallel, and

the difference is only the number of installed support elements. There will always be some blocks that are above the reach of the tendons, but generally, these blocks are self-supporting. The issue of short tendons is also reflected in Figure 6.3. The analysis suggests a decline in short tendons above a height of 1.5 m.

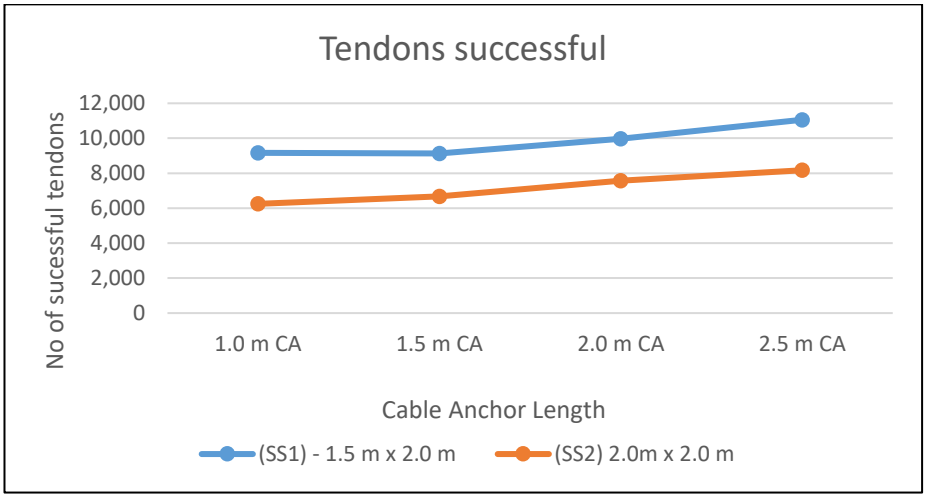


Figure 6-2: Graphical comparison of successful tendons for various cable anchor lengths and spacings

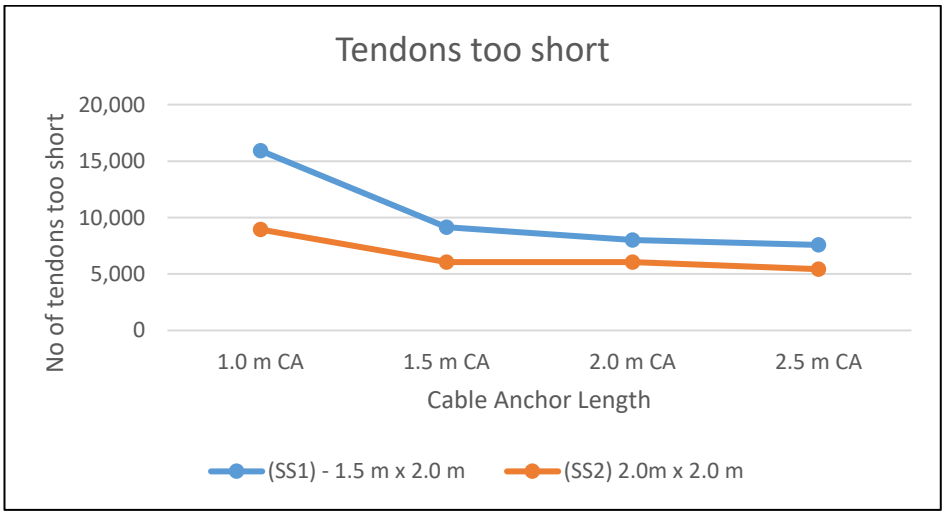


Figure 6-3: Graphical comparison of short tendons for various cable anchor lengths and spacings

The sharp change in slope when CA are less than 1.5 m shows a strong relationship to the 95% cumulative FOH (1.4 m) described in Section 5.1.1. An increased number of FOGs is expected for tendons shorter than the FOH. Furthermore, Figure 6-3 shows that there is little to no benefit in increasing the CA length beyond the FOH. The denser support scenario (SS1) also has more tendons that are "too short" than SS2 simply because more units are installed in SS1.

Figure 6-4 shows a sharper increase in support failure below a cable length of 1.5 m for the sparser pattern of support (SS2) than for the closer-spaced elements. The steeper slope suggests that the spacing of 2 m x2 m may not be of sufficient support resistance to meet the demand. The change in slope for both support scenarios at 1.5 m suggests that the reach of the bolts may not need to extend significantly beyond 1.5 m.

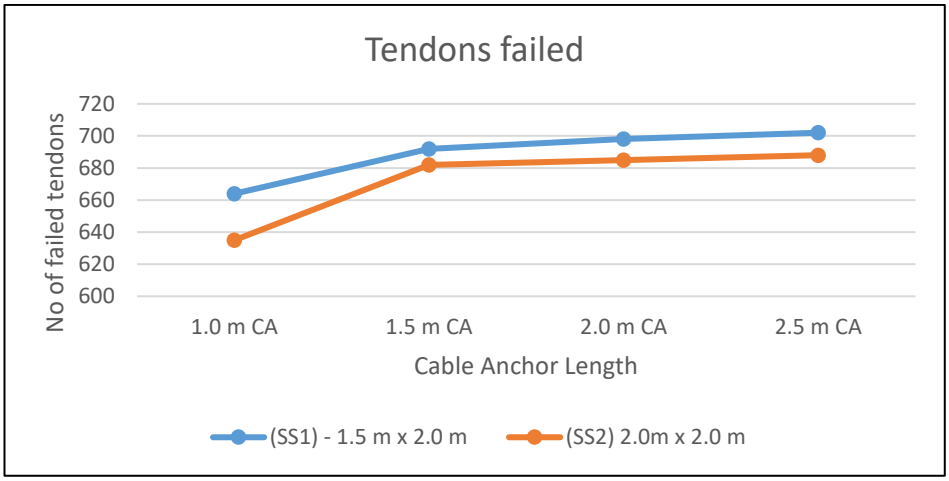


Figure 6-4: Graphical comparison of failed tendons for various cable anchor lengths and spacings.

There are fewer failed tendons for 1.0 m long CAs than the other CA lengths (1.5 m, 2.0 m and 2.5 m). This can be linked to the tendons that are too short in Figure 6-3. When tendons are too short, they cannot be tested for failure. The number of CA that fail plateau and remain relatively constant for CA lengths

(2.0 m and 2.5 m) that are greater than the 95% cumulative FOH (1.4 m) and Barton et al (1980) based FOH (1.72 m).

Summary of J-Block results

The J-Block results showed that CA lengths that were less than FOHs (1.4m and 1.72 m) experienced a significant increase in the number of fallouts. This brings justification and validity to the FOHs determined in the deterministic approach. There was an improvement in key block fallouts and successful tendons when CAs were 2.0 m long. Increasing the length beyond 2.0 m to 2.5 m had a marginal benefit in reducing the number of key block fallouts. The denser support scenario (SS1) made a significant improvement in the reduction of key block fallouts and successful tendons than the wider support scenario SS2. Therefore, the optimal support configuration amongst the options considered was a 2.0 m long CA spaced at 1.5 m (dip) and 2.0 m strike spacing, and a strength of 34 tons. The length of the cables is “in the hole”, and there is a requirement for an additional 0.5 m for tensioning. Thus, the actual length of the cables needs to be 2.5 m.

It is clear from the J-block analysis that the original support resistance provided by the mine poles was more than sufficient. It would account for the very few failed poles that were observed in the old stopes. The majority of the few failed poles appear to have been damaged by the blast, and therefore weaker than the calculated strength. While the tendon support resistance is lower than the original support system, the rigorous analysis shows that it is sufficient. Although longer bolts were used at the trial site, the support resistance was the same as suggested by the research, which confirms the research results. It appears that shorter bolts can be used in future trials.

7 CONCLUSIONS AND RECOMMENDATIONS

7.1 Introduction

An extraction methodology together with an integrated support design were trialled at an underground trial site for three months. The conclusions and recommendations were therefore based on results obtained during the 3-month trial period.

7.2 Summary of Conclusions

The following conclusions were drawn from the trial project:

a. The deterministic support approach suggests that stability can be achieved with both support systems (SS1 and SS2) with the FOS values above the industry-recommended value of 1.5. Careful considerations, however, must be made on the Barton et al (1980) based theoretical FOH which could have overestimated the support requirements.
b. For the reason in point “a”, the key-block probabilistic approach based on mapped structural data provided more detailed insight into the support systems' likely performance.
c. The area of interest has 3 main joint sets defined with random joints that formed both stable and unstable key blocks.
d. The effects of increasing the CA length improved the number of “successful tendons” tested by 14% on average for both support systems (SS1 & SS2).
e. Increasing the support length beyond 2.0 m had a marginal benefit to reducing key-block fallouts.
f. CA space closer together significantly improved the number of successful tendons tested than SS2.
g. A 2.0 m long CA length longer than the FOH at a spacing of 1.5 m dip and 2.0 m strike was found to be the optimal configuration for this mining

configuration. (An additional 0.5 m length needs to be added to allow for tensioning).

h. A reasonable production output was obtained from the trial which can improve as the crew becomes more attuned to the methodology.
i. Cleaning of the panel was a challenge as a significant amount of blast ore was thrown into the back area. Blasting barricades were not used during the trial and are recommended as an area for improving the methodology.
j. The footwall mining was carried out on a selective basis where the ground and support conditions were not compromised by time-dependent creep effects.
k. A practical extraction and support methodology was successfully trialled over 3 months. Safe production was realized over this period with the crews gaining more confidence and buy-in into the methodology.

7.2.1 Key findings and observations

The following key findings and observations were made during the research period:

- 2.0 m long cable anchors on a 1.5 m x 2.0 m spacing were determined to be the optimal support configuration for stability.
- The denser support pattern in SS1 provided more stable conditions than SS2 even though both support systems provide acceptable FOS values.
- The Pegmatoid package in the mined-out footwall was found to be much wider than initially anticipated at the trial site. Borehole data have indicated that there are other H-reef areas where the mineralization lies closer to the current stope footwall.

7.3 Research Contributions

The research has provided Impala Platinum with some insight into how the mineralized footwall layer can be safely extracted.

7.4 Research Limitations

The recommended 2.5 m long anchors were not available on the mine at the time of the trial. CA's with a length of 3.5 m were therefore used on the same spacing. The impact of drilling the additional length holes and the added cost of the longer cables affected the profitability of the exercise.

7.5 Recommendations for Future Research Work

The main object of the research project was to develop a viable proof of concept for the safe extraction of the mineralized layer immediately below the mined-out Merensky Stopes. This was reasonably achieved through the trial project. However, to gain a complete understanding of the method before rolling out, the following is recommended for future work and research:

I. The trial period should be extended further for an additional 3 months to obtain more data and test the shorter CAs.
II. Areas where the old mine pole support has deteriorated should be cordoned off (compartmentalized with Dura-Paks) leaving islands of unmined footwall in the stope.
III. Cleaning of the blasted ore can be optimized by using properly designed blasting barricades that are suspended from the CAs.
IV. The gullies in the project site should be deepened first to the bottom contact of the Pegmatoid to enable sampling of the entire footwall package to be done.
V. Training manuals and documentation for standards and procedures must be assembled on the learnings gained from the trial.

8 References

Association for Project Management, 2023. *What is project management?.* [Online] Available at: https://www.apm.org.uk/resources/what-is-project-management [Accessed 1 November 2023].

Baecher, G., 1983. *Statistical Analysis of Rock Mass Fracturing Geology.* s.l., Journal of Mathematical .

Baecher, G. & Lanney, N., 1978. *Trace length biases in joint surveys.* Nevada, In: Proceedings 19th U.S. Symposium on Rock Mechanics.

Balakrishna, A., 2022. *White area management standard.* Rustenburg: Impala Platinum, Geology Department, Internal and Confidential. Republic of South Africa.

Bandis, S. C., Lumsden, A. C. & Barton, N. R., 1983. Fundamentals of rock joint deformation. *International Journal of Rock Mechanics and Mining Sciences and Geomechanics Abstracts,* Volume 20, p. 249–68.

Barton, N., 1976. The shear strength of rock and rock joints. *International Journal of Rock Mechanics and Mining Sciences and Geomechanics Abstracts,* Volume 13, pp. 1-24.

Barton, N., 1995. *The influence of joint properties in modelling jointed rock masses.* Tokyo, Keynote Lecture, 8th ISRM Congress.

Barton, N., 2002. Some new Q-value correlations to assist in site characterisation and tunnel design. *International Journal of Rock Mechanics & Mining Sciences,* Volume 9, pp. 185-216.

Barton, N. & Bandis, S., 1982. *Effects of block size on the the shear behaviour of jointed rock.* Berkeley, 23rd U.S. Symposium on Rock Mechanics.

Barton, N. & Bandis, S., 1990. *Review of predictive capabilites of JRC-JCS model in engineering practice.* Rotterdam, Proceedings. International Symposium on rock joints, pp. 603-610.

Barton, N. & Choubey, V., 1977. The shear strength of rock joints in theory and practice. *International Society of Rock Mechanics,* Volume 10, pp. 1-54.

Barton, N., Lien, R. & Lunde, J., 1974. *Engineering Classification of jointed rock masses for the design of tunnel support..* s.l.:Rock Mech 6.

Barton, N., Løset, F. & Lunde, J., 1980.. *Application of the Q-System in Design Decisions Concerning Dimensions and Appropriate Support for Underground Installations.* New York: Pergamon.

Barton, N. R., Bandis, S. & Bakhtar, K., 1985. Strength, deformation and conductivity coupling of rock joints. *International Journal of Rock Mechanics and Mining Sciences and Geomechanics Abstracts,* Volume 22, p. 121–40.

Brady, B. & Brown, E., 2004. *Rock Mechanics for Underground Mining.* 3rd ed. s.l.:Springerlink.

Brown, E., 2003. *Block Caving Geomechanics.* Brisbane: Julius Kruttschnitt Mineral Research Centre.

Call, R. & Nicholas, D., 1978. *Prediction of step-path failure geometry for slope stability.* Nevada, Proceedings19th US Symposium on Rock Mechanics.

Call, R., Savely, J. & Nicholas, D., 1976. Estimation of joint set characteristics from surface maping data. *17th US Symposium on Rock Mechanics,* pp. 2B2-1-2B2-9.

Carollo, L, 2023. *FOG statistics & safety iniatives implemented.* Rustenburg: Impala Platinum - Rock Engineering Department, Internal and Confidential. Republic of South Africa.

Carollo, L, 2023. *Mandatory Code of Practice to Combat Rockfall and Rock Burst Accidents in Tabular Metalliferous Mines.* Rustenburg: Impala Platinum - Rock Engineering Department, Internal and Confidential. Republic of South Africa.

Coulomb, C. A., 1776. Essay on a application of the rules of maximum and minimum to problems of static relative to the architecture. *French Academy of Sciences,* Volume 7, p. 343–82.

Daehnke, A. et al., 1998. *Stope face support systems Final Report for SIMRAC Project GAP 330,,* Pretoria: CSIR: Division of Mining Technology..

Daehnke, A. et al., 2000. *The design and development of an effective support system for tabular stopes in gold and platinum mines,* Pretoria: CSIR: Division of Mining Technology, University of Pretoria.

Daehnke, A., van Zyl, M. & Roberts, M., 2001. Review and application of stope support. *The Journal of The South African Institute of Mining and Metallurgy,* 101(3), pp. 135-164.

Deere, D. & Miller, R., 1966. *Engineering classification and index properties of rock,* Albuquerque: NM: Air Force.

Dershowitz, W. & Einstein, H., 1988. Characterizing Rock Joint Geometry with Joint System Models. *Rock Mechanics and Rock Engineering,* Volume 21, pp. 21-51.

Dunnicliff, J. & Green, G., 1988. *Geotechnical Instrumentation for Monitoring Field Perfomance.* New York: John Wiley & Sons.

DuToit, E., 2009. *Design considerations for 338 mined-out area for wide reef mining – 2A Shaft,* Rustenburg: Impala Platinum, Rock Engineering Department, Internal & Confidential, Republic of South Africa.

Eanaex, 2023. *Revised Footwall Lift Design.* Rustenburg: Enaex Africa, Internal and confidential presenatation.

Esterhuizen, G., 2003. *JBlock User's Manual.* Colorado: Goodman & Shi, 1980.

Fouche, L., 2019. *Memorandum: 20 Shaft H-reef, 1500mm maximum stoping width recommendation.* Rustenburg: Impala Platinum, Geology Department, internal and Confidential. Republic of South Africa.

Fouche, O. & Diebolt, J., 2004. Describing the geometry of 3D fracture systems by correcting for linear sampling bias. *Mathematical Geolog,* 36(1), p. 33–63.

Glamheden, R. & Hökmark, H., 2010. *Creep in jointed rock masses State of knowledge.* Stockholm: Swedish Nuclear Fuel and Waste Management Co.

Goodman, R., 2013. *Topling: A fundamental failure modein discontinuity materials: Descriptin and analysis.* San Diego, Proceedings of Geo-congress.

Goodman, R. & Shi, G., 1985. *Block theory and its application to rock engineering.* New Jersey: Prentice-Hall.

Grodner, M., 1999. *Determination of the fracture pattern of rockbursts..* Paris, IRSM: 2nd Proceeding, international Workshop on the Application of Geophysics to Rock Eng .

Gumede, H., 2006. *Development of data sets on joint characteristics and consideration of associated instability for a typical South African gold mine.* Johannesburg: University of the Witwatersrand.

Gumede, H. & Stacey, T., 2007. Measurement of typical joint characteristics in South African gold mines and the use of these characteristics in the prediction of rock falls. *The Journal of The Southern African Institute of Mining and Metallurgy.*

Impala Platinum Limited, 2006. *Geology & Valuation Sub-Team Report.* Rustenburg: Impala Platinum - Geology department, Internal & Confidential. Republic of South Africa.

Impala Platinum, 2017. *FOG report at 20 23 012 PAN 6S.* Rustenburg: Impala Platinum Limited, Rock Engineering Department, internal and confidential.

Impala Platinum, 2022. *Bolting Principle Presentation.* Rustenburg: Impala Platinum Ltd, Rock Engineering Department, Internal & Confidential.

ISRM Commission on Standardization of Laboratory and Field Tests, 1978. Suggested methods for the Quantitative Description of Discontinuities in Rock Masses. *International Journal of Rock Mechanics and Mining Sciences,* Volume 15, pp. 319-368.

Jager, A. & Ryder, J., 1999. *A handbook on Rock Engineering practice for tabular hard rock mines.* Johannesburg: The Safety in Mines Research Advisory Committee (SIMARC).

Joughin, W., Jager, A., Nezomba, E. & Rwodzi, L., 2012. A risk evaluation model for support design in Bushveld Complex undergound mines: Part I - Description of model. *Southern African Institute of Mining and Metallurgy,* Volume 112, pp. 1-4.

Joughin, W., Nezomba, E., Rwodzi, L. & Jager, A., 2011. *Rock Elimination Track B - A Risk Based Approach to Enhancing Support Design in Bushveld Underground Mines,* Johannesburg: Safety in Mines Research Advisory Committee.

Kemeny, J. & Post, R., 2003. Estimating three-dimensional rock discontinuity orientation from digital images of fracture traces. *Computers and Geosciences,* Volume 29,, pp. 65-77.

Kotze, G., 2012. *J-Block training course.* Johannesburg: Open House Mining Solutions.

Lasslet, G., 1982. Censoring and edge effects areal and line transect sampling of rock koint traces. *Mathematical Geology,* 14(2), pp. 125-139.

Mabogo, S., 2021. *Grade Block Model.* Rustenburg: Impala Platinum, Geology Department, Internal and Confidential. Republic of South Africa.

Mabogo, S., 2022. *H-Reef mining project.* Rustenburg: Impala Platinum, Geology Department, Internal and Confidential. Republic of South Africa.

Malan, D., 2009. *Numerical Modelling of the High Stoping Width Areas at 2A SHAFT (Phase 1),* Johannesburg: Groundwork Consulting (pty).

Malan, D., 2011. *Investigation of the revised layout at 2A Shaft,* Johannesburg: Groundwork Consulting (pty).

Mans, P, 2020. *STD 18.13.01 Relative Densities.* Rustenburg: Impala Platinum - Geology department, Internal & Confidential. Republic of South Africa.

Matitsela, L., 2018. *Tensile Testing of 18 mm,* Auckland Park: Groundwork Consulting.

Mining Qualification Authority, 2006. *Demonstarte Knwoeldge and Understanding of Strata Control.* s.l.:Mining Qualification Authority.

Mooketsi, L., 2023. *Financial Valuation Footwall Lifting Project.* Rustenburg: Impala Platinum Limited, Finance Department, Internal and Confidential.

More O'Ferrall, R., 1981. The reworking of old mines - a rock mechanics challenge. *The South African Institue of Mining and Metallurgy,* pp. 311-312.

Napier, J. & Malan, D., 2012. Simulation of time-dependent crush pillar behaviour in tabular platinum mines. *The Journal of The Southern African Institute of Mining and Metallurgy.*

Nel, P., 2022. *Merensky footwall mining extraction.* Rustenburg: Enaex Africa.

Park, H., West, T. & Woo, I., 2005. Probabilistic analysis of rock slope stability and random properties of discontinuity parameters. *Engineering Geology,* 79(3-4), p. 230–250.

Patton, F., 1966. Multiple modes of shear failure in rock. *Proceeding. 1st congression, International Society of Rock Mechanics,* Volume 1, pp. 509-513.

Piper, P. & Malan, D., 2013. The In-situ Perfomance of Elongate Support Myths and Realites. *The Journal of The Southern African Institute of Mining and Metallurgy.*

Potvin, Y. & Hadjigeorgiou, J., 2020. *Ground Support for underground mines.* Crawley: Australian Centre for Geomechanics.

Priest, S. D., 1985. *Hemispherical Projection Methods in Rock Engineering.* London: Allen and Unwin.

Priest, S. & Samaniego, J., 1983. *A model for the analysis of discontinuity characteristics in two dimensions.* Melbourne, International Society for Rock Mechanics Congress, pp. F199-F207.

Prinsloo, L., 2024. *Timberless stoping at Amandabult.* Rustenburg: Personal commuincation.

Rainbow Mining Support, 2023. *Laboratory Testing Report - 160-180 Mine Pole Slow Compression Tests For Sebesta Mining,* Westonaria: Rainbow Mining Support.

Rakumakoe, O, 2023. *Permanent workface areal mesh leading practice.* Johannesburg: Minerals Council South Africa.

Reutech Mining, 2016. *SSP Brochure - The Sub Surface Profiler (SSP).* Stellenbosch: Reutech Radar Systems.

Roberds, W. & Einstein, H., 1978. Comprehensive Model for Rock Discontinuities. *Journal for the Geotechnical Engineering Division,* Volume 104 (5), pp. 553-569.

Robert, M., 1995. *Stope and gully support - Final Report for SIMRAC Project GAP 032,* Pretoria: CSIR: Division of Mining Technology.

Roberts, D., Roberts, M. & Achaempong, E., 2002. *Improved understanding of the use of short tendons for stope support under rockfall and rockburst conditions (Phase I),* s.l.: Safety in Mines Research Advisory Committee.

Robertson, A. & Mac, G., 1970. *The Interpretation of Geological factors for use in Slope Theory.* Balkema, Proceedings, Symposium on the Theoretical Background to the Planning of Open Pit Mines with Special Reference to Slope Stability.

Ryder, J. & Jager, A., 2002. *A text book on Rock Mechanics for tabular hard rock mines.* Johannesburg: The Safety in Mines Research Advisory Committee.

Seccombe, A, 2022. *Fact sheet / August 2022.* Johannesburg: Minerals Council South Africa.

Song, J. et al., 2023. Drone Photogrammetry for Accurate and Efficient Rock Joint Roughness Assessment on Steep and Inaccessible Slopes. *MDPI.*

Spearing, A., 1995. *Handbook on Hard-Rock Strata Control.* Johannesburg: The South African Institute of Mining and Metallurgy.

Stacey, T., 2001. *Best rcok engineering practice for other mines.* Braamfontien: Safety in Mines Research Advisory Committee.

Stacey, T., 2008. *Rock Engineering MINN 4010 Course notes.* Johannesburg: University of the Witwatersrand.

Stacey, T. R., 2001. *Best practice Rock Engineering handbook for "other" mines,* Johannesburg: Safety in mine Research Advisory Committee - SRK Consulting.

Sturzenegger, M. & Stead, D., 2009. Quantifying discontinuity orientation and persistence on highmountain rock slopes and large landslides using terrestrial remote sensing techniques. *Natural Hazards and Earth System Sciences,* Volume 9, p. 267–287.

Support, R. M., 2023. *Durapak 60 - 300.* Westonaria: Rainbow Mining Support.

Tang, H., Huang, L. & Juang CH, .. Z. J., 2017. Optimizing the Terzaghi estimator of the 3D distribution of rock fracture orientations. *Rock Mechanics and Rock Engineering,* Volume 50, p. 2085–2099.

Tang, H. et al., 2018. *Correction of Line-Sampling Bias of Rock Discontinuity.* [Online]
Available at: https://www.hindawi.com/journals/ace/2018/1629039/ [Accessed 21 Februaury 2024].

Tannant, D., 2015. Review of Photogrammetry-Based Techniques for Characterization and Hazard Assessment of Rock Faces. *International Journal of Geohazards and Environment,* p. 82.

Tati, B., 2022. *Extraction & support methodology for footwall mining in mined-out Merensky stopes.* Rusternburg: Impala Platinum, Rock Engineering Department, Internal and Confidential. Republic of South Africa..

Tati, B., 2023. *20 Shaft FOG database.* Rustenburg: Impala Platinum - Rock Engineering Department, Internal and Confidential. Republic of South Africa.

Terzaghi, R., 1965. Sources of error in joint surveys. *Geotechnique,* 5(3), pp. 287-304.

van Aswagen, L., Johnson, R. & Smith, G., 2010. Introduction of 3 m cable anchors as face support in 'timberless at Dishaba Mine. *The Southern African Institute of Mining and Metallurgy,* pp. 157-167.

Villaescusa, E., 1992. Maximum Likelihood estimation of joint size from trace length measurements. *Rock Mechanics and Rock Engineering.*

Villaeuscusa, E., 1992. *A Review and Analysis of Rock Discontinuity Mapping Methods.* [Online]
Available at: https://www.issmge.org/uploads/publications/89/99/6ANZ_046.pdf [Accessed 21 February 2024].

Warburton, P., 1980. A stereologicla interpretation of joint trace data. *International Journal of Rock Mechanics, Mining Society, and Geomechanics Abstracts,* Volume 17, pp. 181-190.

APPENDIX A. FOOTWALL MINING BLOCK & GRADE RESOURCE ESTIMATION

Table A1: Total H-reef grade & resource estimation figures

Legend
- Green colour = more than 1.75 g/t and more than 40cm channel width
- Yellow colour = less than 1.75 g/t
- Blue colour = less than 40cm channel width

RSE line	Channel Width	Resource grade (6E) g/t	Area (m^2 85% extraction rate)	Density (t/m^3)	Tonnes (t)	6E (kg)	6E (Oz)	Refined ounces
24 003	40	2.82	4 832	3.05	5 895	16.62	420	403
24 005	50	2.33	9 734	3.05	14 844	34.59	874	839
25 006	50	2.2	6 877	3.05	10 487	23.07	583	560
25 006	50	1.8	11 781	3.05	17 966	32.34	817	785
25 007	50	1.12	10 886	3.05	16 601	18.59	470	451
24 009, 26 009 & 25 009	50	1.62	81 411	3.05	124 151	201.12	5 083	4 880
24A 006	40	2.96	15 493	3.05	18 902	55.95	1 414	1 357
26 009	50	1.53	6 759	3.05	10 307	15.77	399	383
25 007 & 24 007	40	2.28	57 676	3.05	70 365	160.43	4 055	3 893
22 004	50	5.08	14 934	3.05	22 775	115.70	2 924	2 807
23 005	40	5.96	19 081	3.05	23 279	138.75	3 507	3 366
22A 005	40	7.45	5 578	3.05	6 805	50.70	1 281	1 230
23 006	40	3.55	12 274	3.05	14 974	53.16	1 344	1 290
23 007	20	2.06	12 115	3.05	7 390	15.22	385	369
24A 006	40	3.58	6 129	3.05	7 478	26.77	677	650
23 009 & 23 010	40	2.34	31 055	3.05	37 887	88.66	2 241	2 151
24 011	40	1.82	52 001	3.05	63 442	115.46	2 918	2 802
25 011	30	1.56	33 058	3.05	30 248	47.19	1 193	1 145
25 012	40	1.93	29 127	3.05	35 535	68.58	1 733	1 664
25A 013 & 24 013	40	2.35	51 938	3.05	63 364	148.90	3 763	3 613
24 012	40	2	21 444	3.05	26 161	52.32	1 322	1 270
24 013	40	2.2	13 770	3.05	16 799	36.96	934	897

Table A2: Total H-reef grade & resource estimation figures

Legend
- Green colour = more than 1.75 g/t and more than 40cm channel width
- Yellow colour = less than 1.75 g/t
- Blue colour = less than 40cm channel width

RSE line	Channel Width	Resource grade (6E) g/t	Area (m^2 85% extraction rate)	Density (t/m^3)	Tonnes (t)	6E (kg)	6E (Oz)	Refined ounces
23 011 & 23 012	40	2.22	57 526	3.05	70 181	155.80	3 938	3 780
22A 007, 22 008 & 22 007	40	3.62	41 874	3.05	51 086	184.93	4 674	4 487
21 008	40	2.25	45 858	3.05	55 946	125.88	3 181	3 054
21 012 & 22 012	40	2.11	58 280	3.05	71 102	150.03	3 792	3 640
22A 012 & 22A 013	50	2.83	39 194	3.05	59 770	169.15	4 275	4 104
23 014 & 23 015	20	0.97	31 330	3.05	19 111	18.54	469	450
22A 014	40	1.57	30 476	3.05	37 181	58.37	1 475	1 416
23 016	40	2.51	5 384	3.05	6 568	16.49	417	400
20 013	50	1.45	20 282	3.05	30 929	44.85	1 133	1 088
21 013	50	1.52	59 768	3.05	91 146	138.54	3 502	3 361
20 014	50	1.91	16 828	3.05	25 662	49.01	1 239	1 189
21 014	40	1.75	30 121	3.05	36 748	64.31	1 625	1 560
21 014A & 21 015	40	2.32	45 022	3.05	54 927	127.43	3 221	3 092
22A 015, 22A 016 & 22 015	40	1.88	32 680	3.05	39 869	74.95	1 894	1 819
22A 011	40	3.22	2 171	3.05	2 648	8.53	216	207
22 016	40	2.79	28 475	3.05	34 740	96.92	2 450	2 352
22 017	40	3.32	12 340	3.05	15 055	49.98	1 263	1 213
20 016	50	2.19	38 037	3.05	58 006	127.03	3 211	3 082
22 018	40	2.92	5 768	3.05	7 037	20.55	519	499
24 014	30	1.57	21 428	3.05	19 607	30.78	778	747
Total	41	2.5	1 130 793	3.05	1 095 560	2 696	68 147	65 421

Table A3: Total H-reef resource profitability

- Resource grade profitability

Revenue	Cost (Average actual R/T)	Profit/Loss
R2 360 202 273	R2 216 317 401	R143 884 872

- Refined grade profitability

Revenue	Cost (Average actual R/T)	Profit/Loss
R2 265 794 182	R2 216 317 401	R49 476 781

APPENDIX B. 20 21 014A RAISELINE PROJECT TRIAL SITE

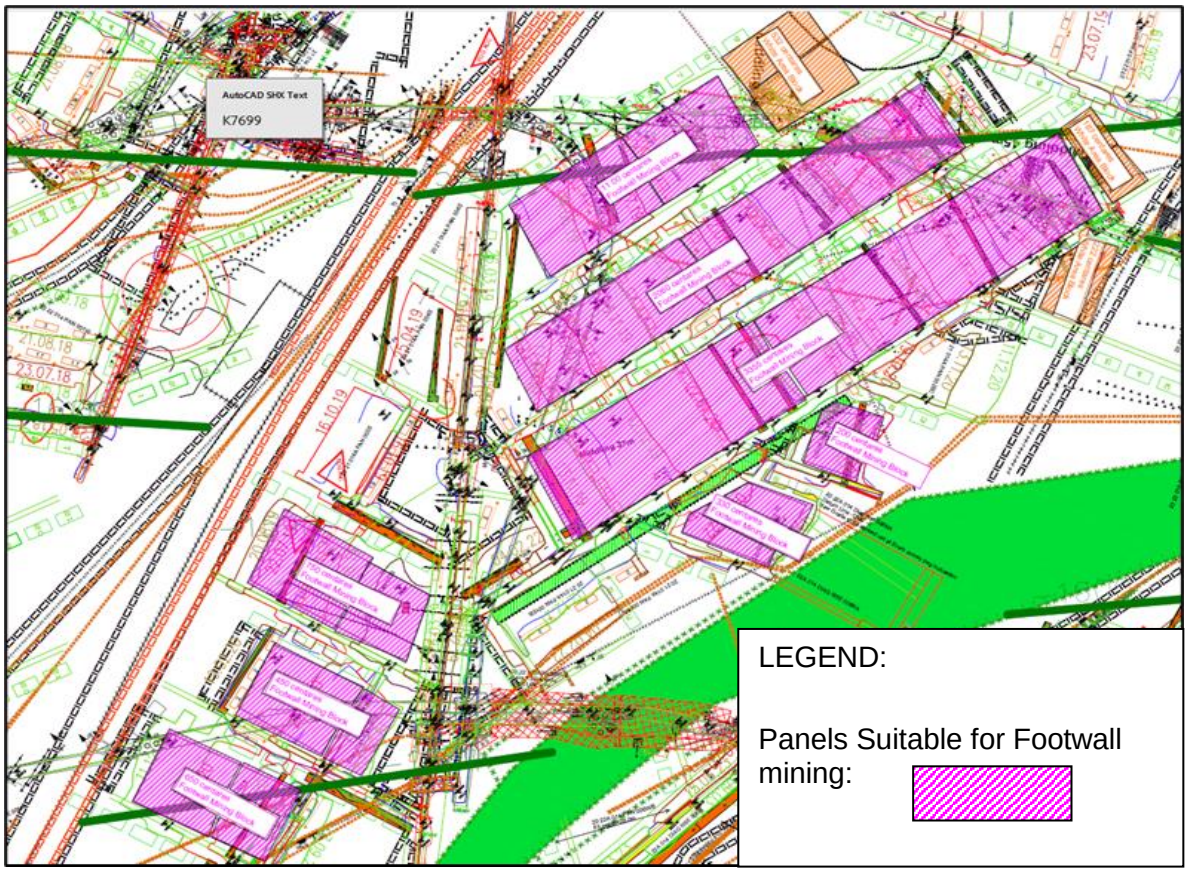


Figure B1: Plan showing panel blocks suitable for extraction in the 20 21 014A Project Trial Site

APPENDIX C: 2A SHAFT- INSTOPE BOLTING HIGH STOPING WIDTH SUPPORT STANDARD – VERSION 1

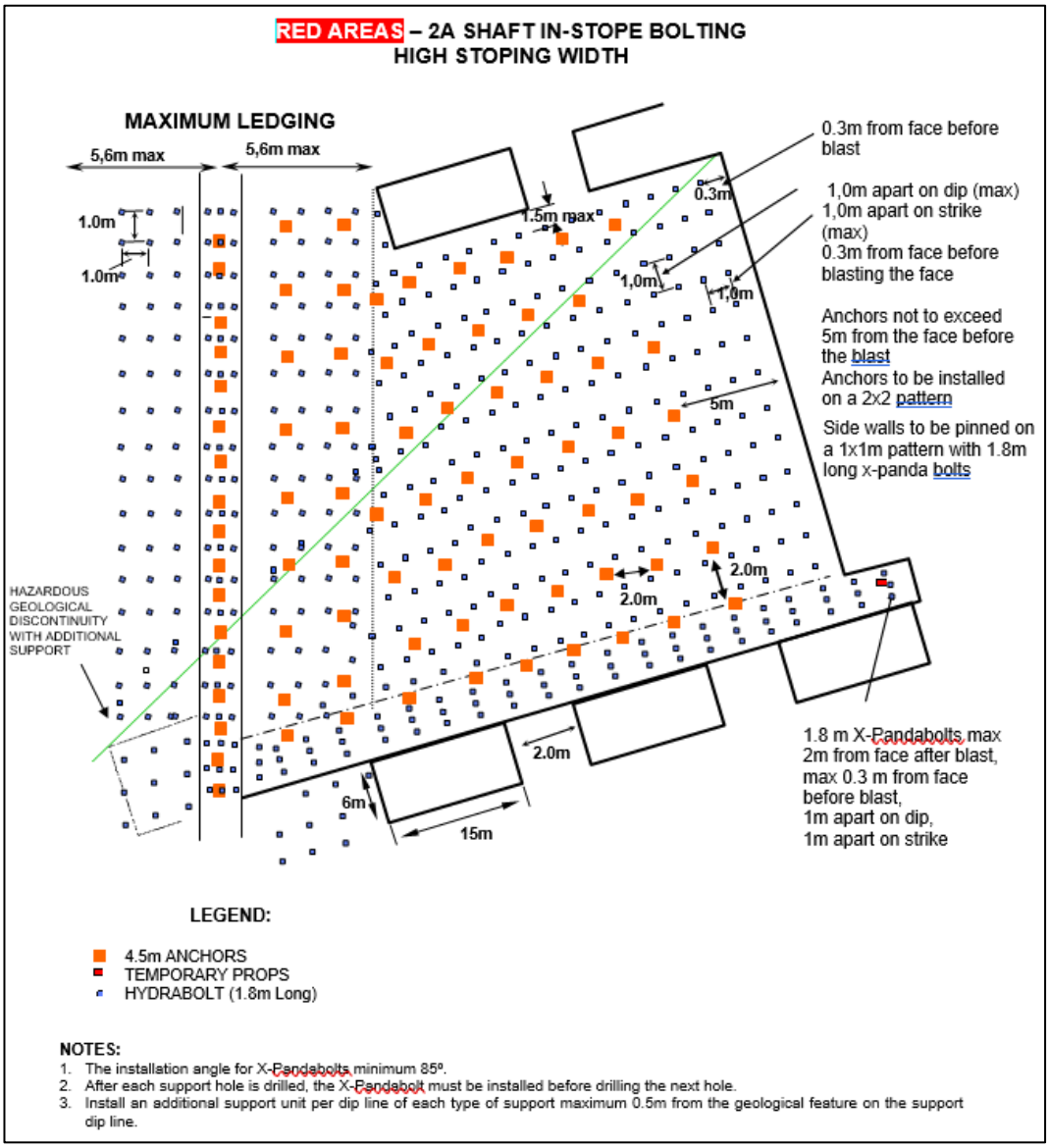


Figure C1: Support Standard for high stoping width panels at Impala 2A shaft – version 1

APPENDIX D: 2A SHAFT- INSTOPE BOLTING HIGH STOPING WIDTH SUPPORT STANDARD – VERSION 2

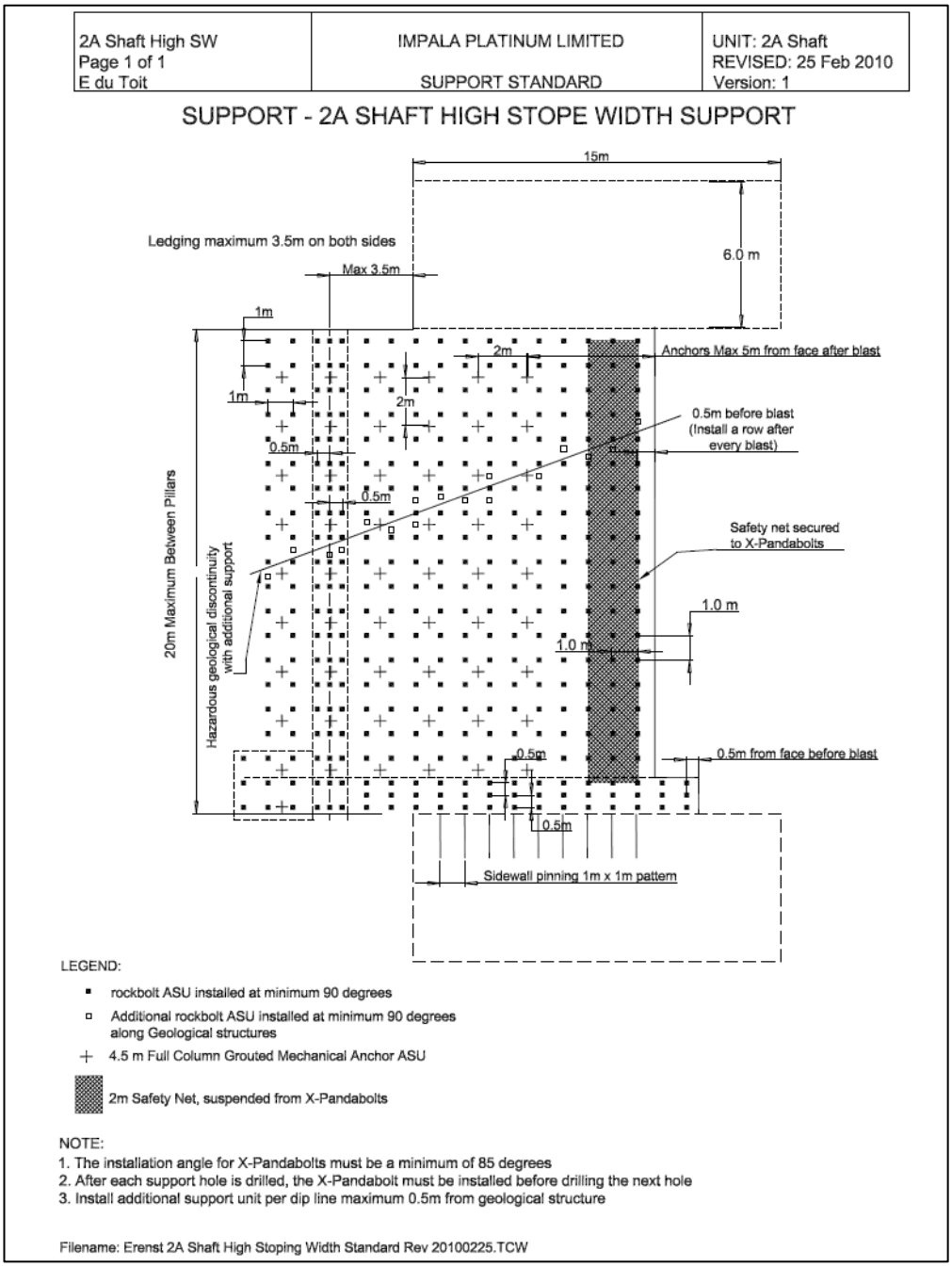


Figure C2: Support Standard for high stoping width panels at Impala 2A shaft – version 1

APPENDIX E: DMR INSTRUCTION



mineral resources

Department:
Mineral Resources
REPUBLIC OF SOUTH AFRICA

MINE HEALTH AND SAFETY INSPECTORATE – NORTH WEST REGION

Private Bag A1, Klerksdorp, 2570
Corner Voortrekker and Margaret-Prinsloo roads, Klerksdorp, 2570
Tel: (018) 487 9867 Fax: (018) 487 9838

Enquiries: E.T. Ngwenya
Ref number: 11/4/1 – Aquarius Platinum
Date: 15 July 2010

The Managing Director
Aquarius Platinum (SA) Pty Ltd
P O Box 624
Kroondal
0350

Attention: Mr. A. Lubbe

INSTRUCTION IN TERMS OF SECTION 9.(7) AND REGULATION 7.4.4 STILL IN FORCE IN TERMS OF SCHEDULE 6 OF THE MINE HEALTH AND SAFETY ACT (ACT 29 OF 1996) AS AMENDED – TO REVIEW THE CODE OF PRACTICE FOR THE PREVENTION OF ROCKFALLS AND ROCKBURSTS IN METALLIFEROUS MINES USING BORD AND PILLAR MINING METHOD

The above matter has reference.

It has been noted with grave concern that fall of ground accidents in this region continue to be a number one killer of mineworkers despite the awareness efforts from the department since the beginning of this year.

Exceptionally massive falls of ground have occurred in mines employing the bord and pillar mining method in this region in recent times. Unfortunately when these types of fall of ground accidents occur they result in mine disasters as it was seen at Impala Platinum Mine 14 shaft where nine (9) mineworkers were fatally injured on 20 July 2009 and at Aquarius Platinum (SA) Pty Ltd 4 shaft where an additional five (5) mineworkers were fatally injured on 06 July 2010.

The major similarities that have been noted during the in-loco inspections in the above-mentioned mine disasters is that these mine accidents occurred in a bord and pillar mining environment in which:

- The bord width was at least ten (10) metres;
- Extraction ratios were over 83 percent;
- Tendon/bolt support failed; and
- A combination of geological anomalies was intersected.

It is against this background that all mining companies in North West region employing the bord and pillar mining method are instructed in terms of Section 9.(7) read with Regulation 7.4.4 still in force in terms of Schedule 4 of the Mine Health and Safety Act (Act 29 of 1996) as amended, to immediately review the Code of Practice for the Prevention of rockfalls and rockbursts in metalliferous mines, related mine standards and procedures to cater for more effective safety measures including but not limited to:

- Maximum mining bord width of not more than 6 metres;
- Extraction ratios should not exceed 75 percent;
- Supporting of prominent geological features by pillars;
- Boxing of roadways must be towards one direction, and
- Orientation of leads and lags between headings must almost be aligned for the purposes of effective ventilation.

Until such time that the afore-said review is conducted, no headings/faces of more than six (6) metres bord widths should be advanced for the purposes of production. All mines employing the bord and pillar mining method where bord widths exceeds six (6) metres must notify the office of the Principal Inspector of Mines on their action plans to convert to more safer and conservative mining parameters.

Also, barrier pillars should be considered for the purposes of ventilation control, fire control and the prevention of domino effect in case of pillar failures.

Assuring you of our best intentions at all times.

Yours sincerely,

ET NGWENYA
PRINCIPAL INSPECTOR OF MINES
NORTH WEST REGION

APPENDIX F. GEOTECHNICAL LOGGING

Table F1: Joint data collected in 20 21 014A PAN 1ED face & ASG

Traverse ID	Tape Azimuth	Tape Plunge	Distance	Rock	Dip	Dip Direction	Persistence	Ends	JRC	Joint Alteration	Infill Type	Infill Thickness (mm)	Moisture	Wall Hardness	Separation	Joint Set	True Spacing
PAN 1EB Face	203	12	2.1	Pyroxenite	83	343	5	1	2.5	2	Serpentinite	1	1	51	1	0	
PAN 1EB Face	203	12	5.5	Pyroxenite	73	241	15.1	1	1.0	3	Serpentinite	1	1	84	1	0	2.5
PAN 1EB Face	203	12	6.4	Pyroxenite	83	252	2.3	0	1.0	2	Calcite (PV)	5	2	92	2	0	0.6
PAN 1EB Face	203	12	12.2	Pyroxenite	84	20	22.6	2	1.0	5	Serpentinite	1	1	54	1	0	5.6
PAN 1EB Face	203	12	16.8	Pyroxenite	74	239	32.6	0	1.0	4	Calcite (PV)	5	2	45	2	0	3.5
PAN 1EB Face	203	12	8.4	Pyroxenite	72	262	1.6	1	11.0	2	Serpentinite	1	1	62	1	1	
PAN 1EB Face	203	12	2.5	Pyroxenite	71	179	5	1	1.0	2	Serpentinite	1	1	64	1	2	
PAN 1EB Face	203	12	2.7	Pyroxenite	68	173	5	1	1.0	2	Serpentinite	1	1	93	1	2	0.2
PAN 1EB Face	203	12	3.1	Pyroxenite	78	181	5	1	1.0	2	Serpentinite	1	1	87	1	2	0.4
PAN 1EB Face	203	12	8.6	Pyroxenite	61	184	5.8	1	14.0	2	Serpentinite	1	1	95	1	2	4.4
PAN 1EB Face	203	12	9.2	Pyroxenite	80	189	4	1	1.0	2	Serpentinite	1	1	26	1	2	0.6
PAN 1EB Face	203	12	21.5	Pyroxenite	66	175	3.2	0	2.5	2	Serpentinite	1	1	8	1	2	9.7
PAN 1EB Face	203	12	1.2	Pyroxenite	81	156	5.8	1	2.5	2	Serpentinite	1	1	26	1	3	
PAN 1EB Face	203	12	2.4	Pyroxenite	71	161	5	1	1.0	2	Serpentinite	1	1	44	1	3	0.8
PAN 1EB Face	203	12	2.6	Pyroxenite	63	155	5	1	1.0	2	Serpentinite	1	1	64	1	3	0.1
PAN 1EB Face	203	12	4.9	Pyroxenite	87	151	4.5	2	14.0	2	Serpentinite	1	1	19	1	3	1.4
PAN 1EB Face	203	12	11.4	Pyroxenite	61	221	5.3	1	11.0	2	Serpentinite	1	1	96	1	4	
PAN 1EB Face	203	12	17.3	Pyroxenite	71	226	32.6	0	2.5	2	Calcite (PV)	4	2	84	2	4	5.0
PAN 1EB ASG	341	6	0.4	Pyroxenite	78	174	5.3	1	2.5	2	Serpentinite	1	1	56	1	2	
PAN 1EB ASG	341	6	0.5	Pyroxenite	82	181	5.3	1	2.5	2	Serpentinite	1	1	97	1	2	0.1
PAN 1EB ASG	341	6	1.8	Pyroxenite	76	175	4.3	2	2.5	2	Serpentinite	1	1	1	1	2	1.2
PAN 1EB ASG	341	6	10.9	Pyroxenite	74	192	3	2	1.0	2	Serpentinite	1	1	76	1	2	7.5
PAN 1EB ASG	341	6	2.9	Pyroxenite	81	135	19.6	0	14.0	4	Serpentinite	3	3	63	2	3	
PAN 1EB ASG	341	6	3.7	Pyroxenite	87	147	14.2	1	14.0	3	Serpentinite	1	1	29	1	3	0.8
PAN 1EB ASG	341	6	4.8	Pyroxenite	80	321	4.1	2	14.0	3	Serpentinite	1	1	96	1	3	1.0
PAN 1EB ASG	341	6	8.8	Pyroxenite	83	156	3.3	2	1.0	2	Serpentinite	1	1	81	1	3	3.9
PAN 1EB ASG	341	6	12.5	Pyroxenite	81	155	9.7	1	2.5	2	Calcite (PV)	5	1	43	1	3	3.6
PAN 1EB ASG	341	6	5.9	Pyroxenite	88	220	1.7	2	1.0	2	Serpentinite	1	1	25	1	4	
PAN 1EB ASG	341	6	9.3	Pyroxenite	84	209	21.8	0	1.0	2	Serpentinite	1	1	28	1	4	2.3
PAN 1EB ASG	341	6	12.3	Pyroxenite	79	215	3.2	0	1.0	2	Serpentinite	1	1	87	1	4	1.7

Table F2: Joint data collected in 20 21 014A PAN 1EC face

Traverse ID	Tape Azimuth	Tape Plunge	Distance	Rock	Dip	Dip Direction	Persistence	Ends	JRC	Joint Alteration	Infill Type	Infill Thickness (mm)	Moisture	Wall Hardness	Separation	Joint Set	True Spacing
PAN 1EC Face	42	15	2.6	Pyroxenite	79	309	1.3	2	1	1		1	1		2	0	
PAN 1EC Face	42	15	4.7	Pyroxenite	77	307	22.5	0	1	1		1	1		1	0	0.2
PAN 1EC Face	42	15	14.4	Pyroxenite	89	299	2.1	2	1	2	Serpentinite	2	1		1	0	2.1
PAN 1EC Face	42	15	17.65	Pyroxenite	67	10	5.5	1	0.5	1		1	1		1	0	2.5
PAN 1EC Face	42	15	17.65	Dome	33	128	1.4	1	0.5	1	Dome	1	1		1	0	0.0
PAN 1EC Face	42	15	19	Pyroxenite	87	115	11.4	2	1	1		1	1		1	0	0.4
PAN 1EC Face	42	15	0	Pyroxenite	68	290	0.8	1	2.5	1		1	1		1	1	
PAN 1EC Face	42	15	0.4	Pyroxenite	87	102	4.7	2	2.5	1		1	1		1	1	0.2
PAN 1EC Face	42	15	0.5	Pyroxenite	87	102	4.7	0	1	2	Serpentinite	2	1		1	1	0.0
PAN 1EC Face	42	15	1.5	Pyroxenite	86	292	1.5	2	2.5	1		1	1		1	1	0.3
PAN 1EC Face	42	15	2.2	Pyroxenite	78	97	1.1	2	1	1		1	1		2	1	0.4
PAN 1EC Face	42	15	4.3	Pyroxenite	86	99	4.8	2	1	1		1	1		1	1	1.1
PAN 1EC Face	42	15	14.9	Pyroxenite	53	283	1.4	1	0.5	1		1	1		1	1	4.0
PAN 1EC Face	42	15	15.1	Pyroxenite	89	285	1.4	1	0.5	1		1	1		1	1	0.1
PAN 1EC Face	42	15	15.3	Pyroxenite	85	95	1.4	1	0.5	1		1	1		1	1	0.1
PAN 1EC Face	42	15	18.2	Pyroxenite	89	268	4.3	0	0.5	1		1	1		1	1	1.9
PAN 1EC Face	42	15	19.1	Pyroxenite	86	277	21.7	0	1	3	Serpentinite	2	2		1	1	0.5
PAN 1EC Face	42	15	19.2	Pyroxenite	86	277	22.2	0	1	2	Serpentinite	2	2		1	1	0.1
PAN 1EC Face	42	15	19.5	Pyroxenite	69	270	6.6	0	2	1		4	1		1	1	0.2
PAN 1EC Face	42	15	19.7	Pyroxenite	69	270	23.6	0	1	1		1	1	8	1	1	0.1
PAN 1EC Face	42	15	6.5	Pyroxenite	79	195	16.1	1	2.5	1		1	1		1	2	
PAN 1EC Face	42	15	15.6	Pyroxenite	68	167	1.4	1	0.5	1		1	1		1	3	
PAN 1EC Face	42	15	18.9	Pyroxenite	72	149	6.6	2	11	2	Serpentinite	2	2		1	3	0.9

Table F3: Joint data collected in 20 21 014A PAN 1EC ASG

Traverse ID	Tape Azimuth	Tape Plunge	Distance	Rock	Dip	Dip Direction	Persistence	Ends	JRC	Joint Alteration	Infill Type	Infill Thickness (mm)	Moisture	Wall Hardness	Separation	Joint Set	True Spacing
PAN 1EC ASG	353	15	1.75	Pyroxenite	64	239	17.73	0	1.0	4	Lamprophyre dyke	5	2	76	4	0	
PAN 1EC ASG	353	15	2.8	Pyroxenite	85	72	5.1	0	1.0	4	Lamprophyre dyke	5	2	87	4	0	0.2
PAN 1EC ASG	353	15	9.8	Pyroxenite	80	170	3.5	0	0.5	1		1	1	29	1	0	6.6
PAN 1EC ASG	353	15	14.7	Pyroxenite	80	170	4.3	1	1	2	Serpentinite	2	2	11	2	0	4.7
PAN 1EC ASG	353	15	16.9	Pyroxenite	76	305	4.2	1	11	1		1	1	63	1	0	1.4
PAN 1EC ASG	353	15	19.6	Pyroxenite	58	310	3.1	0	1	1		1	1	14	1	0	1.6
PAN 1EC ASG	353	15	20.9	Pyroxenite	76	300	1.5	0	1.0	1		1	1	5	1	0	0.7
PAN 1EC ASG	353	15	21.7	Pyroxenite	83	306	1.5	0	1.0	3	Serpentinite	2	2	31	2	0	0.5
PAN 1EC ASG	353	15	25.4	Pyroxenite	60	300	2.5	0	1.0	1		1	1	12	1	0	1.9
PAN 1EC ASG	353	15	26.2	Pyroxenite	43	1	1.5	0	1.0	2	Serpentinite	2	1	50	1	0	0.5
PAN 1EC ASG	353	15	3.5	Pyroxenite	74	282	6.1	1	1.0	1		1	1	25	3	1	
PAN 1EC ASG	353	15	21.3	Pyroxenite	68	282	1.5	0	1.0	3	Serpentinite	2	2	68	1	1	5.2
PAN 1EC ASG	353	15	5	Pyroxenite	76	189	4.8	1	1.0	1		1	1	49	1	2	
PAN 1EC ASG	353	15	7.1	Pyroxenite	65	356	2.2	1	1.0	2	Serpentinite	1	1	85	1	2	1.8
PAN 1EC ASG	353	15	10.1	Pyroxenite	87	188	2.8	1	1.0	2	Serpentinite	2	1	8	1	2	2.8
PAN 1EC ASG	353	15	11.2	Pyroxenite	65	356	6.4	0	1	1		1	1	9	1	2	1.0
PAN 1EC ASG	353	15	16.1	Pyroxenite	87	188	4.7	2	1	2	Serpentinite	2	1	62	2	2	4.6
PAN 1EC ASG	353	15	17.9	Pyroxenite	81	2	3.5	1	11	2	Serpentinite	2	1	38	1	2	1.7
PAN 1EC ASG	353	15	19.1	Pyroxenite	67	355	2.3	1	11	1		1	1	62	1	2	1.1
PAN 1EC ASG	353	15	25.4	Pyroxenite	82	359	1.5	0	2.5	1		1	1	55	1	2	6.0
PAN 1EC ASG	353	15	25.7	Pyroxenite	75	354	1.5	0	2.5	1		1	1	10	1	2	0.3
PAN 1EC ASG	353	15	27.4	Pyroxenite	48	174	1.5	2	2.5	1		1	1	17	1	2	1.2
PAN 1EC ASG	353	15	27.7	Pyroxenite	56	177	1.5	2	2.5	1		1	1	12	1	2	0.2
PAN 1EC ASG	353	15	28.5	Pyroxenite	66	182	1	2	2.5	1		1	1	83	1	2	0.7
PAN 1EC ASG	353	15	28.7	Pyroxenite	51	197	1	2	2.5	1		1	1	43	1	2	0.1
PAN 1EC ASG	353	15	0.6	Pyroxenite	76	332	13.6	1	1.0	1		2	2	80	2	3	
PAN 1EC ASG	353	15	6.7	Pyroxenite	69	331	15.2	0	1.0	1		1	2	66	3	3	5.1
PAN 1EC ASG	353	15	9.3	Pyroxenite	74	143	5.7	0	2.5	2	Serpentinite	1	2	85	1	3	2.1
PAN 1EC ASG	353	15	10.8	Pyroxenite	69	331	7.9	0	2.5	2	Serpentinite	1	1	0	1	3	1.3
PAN 1EC ASG	353	15	13.1	Pyroxenite	74	145	5	1	1	2	Serpentinite	2	2	78	2	3	1.9
PAN 1EC ASG	353	15	18.6	Pyroxenite	64	318	3.3	2	11	1		1	1	14	1	3	3.9
PAN 1EC ASG	353	15	20.3	Pyroxenite	80	318	1.5	0	1	1		1	1	58	1	3	1.3
PAN 1EC ASG	353	15	22.3	Pyroxenite	77	329	1.5	0	0.5	3	Serpentinite	2	2	3	2	3	1.7
PAN 1EC ASG	353	15	22.6	Pyroxenite	88	145	1.5	0	0.5	3	Serpentinite	2	2	1	2	3	0.3
PAN 1EC ASG	353	15	0.6	Pyroxenite	55	220	4.6	1	1.0	1		2	1	82	1	4	
PAN 1EC ASG	353	15	2.3	Pyroxenite	76	43	3.5	0	2.5	2	Serpentinite	3	2	94	2	4	1.0
PAN 1EC ASG	353	15	3.5	Pyroxenite	66	28	4.5	1	1.0	1		1	1	81	3	4	0.9
PAN 1EC ASG	353	15	5.8	Pyroxenite	72	33	3.9	1	1.0	1		1	1	25	1	4	1.6
PAN 1EC ASG	353	15	6.7	Pyroxenite	64	216	2.1	1	1.0	1		1	1	59	1	4	0.6
PAN 1EC ASG	353	15	7.7	Pyroxenite	75	43	2	2	1.0	1		1	1	43	1	4	0.6
PAN 1EC ASG	353	15	8.4	Pyroxenite	68	49	5.1	1	11.0	1		1	1	62	1	4	0.4
PAN 1EC ASG	353	15	11.7	Pyroxenite	75	43	7.2	0	1	2	Serpentinite	2	2	48	1	4	2.0
PAN 1EC ASG	353	15	12.4	Pyroxenite	68	49	5.7	1	1	1		1	1	15	1	4	0.4
PAN 1EC ASG	353	15	24.5	Pyroxenite	79	209	5.2	0	0.5	4	Serpentinite	2	2	69	3	4	9.3

Table F4: Joint data collected in 20 21 014A PAN 2N face & ASG (zone 1 & zone 2)

Traverse ID	Tape Azimuth	Tape Plunge	Distance	Rock	Dip	Dip Direction	Persistence	Ends	JRC	Joint Alteration	Infill Type	Infill Thickness (mm)	Moisture	Wall Hardness	Separation	Joint Set	True Spacing
PAN 2N Face (1)	291	6	7.5	Pyroxenite	45	170	0.8	2	1.0	2	Serpentinite	1	1	17	1	0	1.6
PAN 2N Face (1)	291	6	8.4	Pyroxenite	45	117	1.8	2	1.0	2	Serpentinite	1	1	51	1	0	0.6
PAN 2N Face (1)	291	6	18.7	Pyroxenite	89	11	4.1	2	1.0	2	Serpentinite	1	1	40	1	0	1.8
PAN 2N Face (1)	291	6	21.1	Pyroxenite	56	22	2.6	2	1.0	2	Serpentinite	1	1	4	1	0	0.0
PAN 2N Face (1)	291	6	21.9	Pyroxenite	52	17	2.4	2	1.0	2	Serpentinite	1	1	76	1	0	0.0
PAN 2N Face (1)	291	6	23	Pyroxenite	45	276	1.5	2	1.0	3	Serpentinite	1	1	59	1	0	0.7
PAN 2N Face (1)	291	6	14.9	Pyroxenite	64	272	6	1	1.0	2	Serpentinite	1	1	87	1	1	
PAN 2N Face (1)	291	6	3.6	Pyroxenite	55	149	1.5	2	1.0	2	Serpentinite	1	1	88	1	3	
PAN 2N Face (1)	291	6	10.2	Pyroxenite	66	149	1.2	0	1.0	2	Serpentinite	1	1	77	1	3	4.7
PAN 2N Face (1)	291	6	11.8	Pyroxenite	61	155	24.5	0	1.0	2	Serpentinite	1	1	91	1	3	1.0
PAN 2N Face (1)	291	6	12.9	Pyroxenite	60	142	5.4	2	1.0	2	Serpentinite	1	1	22	1	3	0.8
PAN 2N Face (1)	291	6	14.4	Pyroxenite	67	148	3	2	1.0	2	Serpentinite	1	1	60	1	3	1.1
PAN 2N Face (1)	291	6	15.5	Pyroxenite	46	161	1.7	2	1.0	2	Serpentinite	2	1	96	2	3	0.5
PAN 2N Face (1)	291	6	16.3	Pyroxenite	63	164	8.5	2	1.0	2	Serpentinite	1	1	80	1	3	0.4
PAN 2N Face (1)	291	6	22.7	Pyroxenite	55	147	4.8	1	1.0	2	Serpentinite	1	1	30	1	3	4.2
PAN 2N Face (1)	291	6	19.7	Pyroxenite	87	33	23.6	0	1.0	3	Serpentinite	3	1	83	3	4	
PAN 2N ASG (Toe -1)	135	0	0.9	Pyroxenite	75	114	4.6	2	1.0	1		1	1	44	1	0	
PAN 2N ASG (Toe -1)	135	0	16	Pyroxenite	84	249	5.1	2	1.0	1		1	1	28	1	0	6.1
PAN 2N ASG (Toe -1)	135	0	13.3	Pyroxenite	65	350	2	2	1.0	1		1	1	55	1	2	
PAN 2N ASG (Toe -1)	135	0	1.5	Pyroxenite	72	148	11.4	1	2.5	1		2	1	99	1	3	
PAN 2N ASG (Toe -1)	135	0	2.4	Pyroxenite	74	140	7.1	2	1.0	1		1	1	29	1	3	0.9
PAN 2N ASG (Toe -1)	135	0	5.4	Pyroxenite	46	136	4.9	2	1.0	1		1	1	2	1	3	2.2
PAN 2N Face (2)	79	15	3.6	Pyroxenite	80	303	2.6	1	1	1		1	1		1	0	
PAN 2N Face (2)	79	15	4.1	Pyroxenite	85	103	4.3	1	1	1		1	1		1	1	
PAN 2N Face (2)	79	15	14.9	Pyroxenite	66	271	31.4	0	2.5	2	Calcite (PV)	2	1		1	1	9.3
PAN 2N Face (2)	79	15	15	Pyroxenite	68	287	8.5	1	1	1		1	1		1	1	0.1
PAN 2N Face (2)	79	15	15.5	Pyroxenite	68	287	27.3	1	1	1		1	1		1	1	0.4
PAN 2N Face (2)	79	15	10.2	Pyroxenite	87	178	28.2	0	2.5	3	Calcite (PV)	3	1		2	2	
PAN 2N Face (2)	79	15	19.8	Pyroxenite	75	187	1.8	2	1	1		1	1		1	2	2.8
PAN 2N Face (2)	79	15	20.3	Pyroxenite	68	183	1.5	2	1	1		1	1		1	2	0.1
PAN 2N Face (2)	79	15	9.2	Pyroxenite	84	138	26.2	0	1	5	Serpentinite	4	1		4	3	
PAN 2N Face (2)	79	15	10.3	Pyroxenite	77	155	11	2	1	1		1	1		1	3	0.3
PAN 2N Face (2)	79	15	19.2	Pyroxenite	50	166	2.1	2	1	1		1	1		1	3	0.3
PAN 2N Face (2)	79	15	4.4	Pyroxenite	70	207	4.6	1	2.5	2	Calcite (PV)	2	1		1	4	
PAN 2N Face (2)	79	15	10.8	Pyroxenite	85	206	7.6	2	1	1		1	1		2	4	3.7
PAN 2N Face (2)	79	15	3.6	Pyroxenite	80	303	2.6	1	1	1		1	1		1	0	
PAN 2N Face (2)	79	15	4.1	Pyroxenite	85	103	4.3	1	1	1		1	1		1	1	
PAN 2N Face (2)	79	15	14.9	Pyroxenite	66	271	31.4	0	2.5	2	Calcite (PV)	2	1		1	1	9.3
PAN 2N Face (2)	79	15	15	Pyroxenite	68	287	8.5	1	1	1		1	1		1	1	0.1
PAN 2N Face (2)	79	15	15.5	Pyroxenite	68	287	27.3	1	1	1		1	1		1	1	0.4
PAN 2N Face (2)	79	15	10.2	Pyroxenite	87	178	28.2	0	2.5	3	Calcite (PV)	3	1		2	2	
PAN 2N Face (2)	79	15	19.8	Pyroxenite	75	187	1.8	2	1	1		1	1		1	2	2.8
PAN 2N Face (2)	79	15	20.3	Pyroxenite	68	183	1.5	2	1	1		1	1		1	2	0.1
PAN 2N Face (2)	79	15	9.2	Pyroxenite	84	138	26.2	0	1	5	Serpentinite	4	1		4	3	
PAN 2N Face (2)	79	15	10.3	Pyroxenite	77	155	11	2	1	1		1	1		1	3	0.3
PAN 2N Face (2)	79	15	19.2	Pyroxenite	50	166	2.1	2	1	1		1	1		1	3	0.3
PAN 2N Face (2)	79	15	4.4	Pyroxenite	70	207	4.6	1	2.5	2	Calcite (PV)	2	1		1	4	
PAN 2N Face (2)	79	15	10.8	Pyroxenite	85	206	7.6	2	1	1		1	1		2	4	3.7
PAN 2N ASG (Toe -2)	95	3	0.2	Pyroxenite	76	309	3.4	2	1	1		1	1		1	0	
PAN 2N ASG (Toe -2)	95	3	5.7	Pyroxenite	7	7	7.4	1	1	2	Dome	2	1		1	0	0.0
PAN 2N ASG (Toe -2)	95	3	7.9	Pyroxenite	86	254	1.2	1	1	2	Serpentinite	2	1		1	0	2.0
PAN 2N ASG (Toe -2)	95	3	10.4	Pyroxenite	7	207	26.3	0	1	2	Calcite (PV)	3	2		2	0	0.1
PAN 2N ASG (Toe -2)	95	3	3.2	Pyroxenite	85	268	3.3	1	1	2	Serpentinite	2	2		2	1	
PAN 2N ASG (Toe -2)	95	3	3.8	Pyroxenite	79	285	1.8	1	1	2	Serpentinite	1	2		1	1	0.6
PAN 2N ASG (Toe -2)	95	3	4.6	Pyroxenite	87	265	5.5	1	1	1		1	1		1	1	0.8
PAN 2N ASG (Toe -2)	95	3	8.9	Pyroxenite	65	278	27.3	0	1	2	Serpentinite	2	1		2	1	3.9
PAN 2N ASG (Toe -2)	95	3	9.4	Pyroxenite	88	276	5.8	1	1	2	Serpentinite	1	1		2	1	0.5
PAN 2N ASG (Toe -2)	95	3	1.1	Pyroxenite	72	182	7.6	1	2.5	3	Serpentinite	2	2		2	2	
PAN 2N ASG (Toe -2)	95	3	1.2	Pyroxenite	88	349	4.9	1	2.5	2	Serpentinite	2	1		2	2	0.0
PAN 2N ASG (Toe -3)	54	5	12.2	Pyroxenite	75	240	9	2	1	3	Serpentinite	2	2		2	0	
PAN 2N ASG (Toe -3)	54	5	15.1	Pyroxenite	85	123	1.8	2	1	1		1	1		1	0	1.0
PAN 2N ASG (Toe -3)	54	5	19.4	Pyroxenite	88	200	1.8	2	1	1		1	1		1	0	3.5
PAN 2N ASG (Toe -3)	54	5	20	Pyroxenite	84	81	2.5	1	1	2	Serpentinite	2	1		1	0	0.5
PAN 2N ASG (Toe -3)	54	5	22.3	Pyroxenite	78	236	5.2	2	1	2	Serpentinite	2	2		1	0	2.2
PAN 2N ASG (Toe -3)	54	5	14	Pyroxenite	84	282	1.5	2	2.5	1		1	1		1	1	
PAN 2N ASG (Toe -3)	54	5	14.7	Pyroxenite	80	290	1.2	2	2.5	1		1	1		1	1	0.4
PAN 2N ASG (Toe -3)	54	5	15.6	Pyroxenite	81	282	1.8	2	2.5	1		1	1		1	1	0.6
PAN 2N ASG (Toe -3)	54	5	17.7	Pyroxenite	77	268	4.3	1	1	1		1	1		2	1	1.7
PAN 2N ASG (Toe -3)	54	5	18.9	Pyroxenite	57	277	1.8	1	1	1		1	1		1	1	0.7
PAN 2N ASG (Toe -3)	54	5	20.8	Pyroxenite	54	146	11	1	1	1		1	1		3	3	

APPENDIX G. FALL OF GROUND DATABASE

Table G1: FOG database for all 20# FOG accidents in Merensky stope panels, face area, back area and ASGs

DATE	SHAFT	SECTION	HALF LEVEL	WOKPLACE NAME	REEF TYPE	EXCAVATION TYPE	ZONE AREA	DISTANCE FROM FACE	MEASURED FALL OUT HEIGHT	MEASURED STRIKE LENGTH	MEASURED DIP LENGTH	FOG AREA (m2)	FOG REPORT REFERENCE
2016/02/05	20#	2010	22MN	20 22 012 PAN 005N	MR	CG / ASG	ZONE 3	3.00	0.50	0.80	0.80	0.64	S20_118_20160205_20 22 012 PAN 5N
2016/04/08	20#	206	21MN	20 21 013 PAN 007S	MR	STOPE - CONV	ZONE 3	2.00	0.10	0.35	0.25	0.09	S20_402_20160408_20 21 013 PAN 007S
2016/04/25	20#	2010	22MN	20 22 013 PAN 001W	MR	STOPE - CONV	ZONE 1	0.50	0.01	0.74	0.34	0.25	S20_468_20160425_FOG_GIK
2016/06/22	20#	2011	23MN	20 23 011 PAN 001N	MR	STOPE - CONV	ZONE 1	0.50	0.02	0.17	0.15	0.02	S20_727_20160622_20 23 011 PAN 001N
2016/07/23	20#	2020	20MS	20 20 008 PAN 002S	MR	STOPE - CONV	ZONE 1	0.50	0.02	0.15	0.20	0.03	S20_904_20160723_FOG_AR
2016/08/13	20#	2020	22MS	2022 013 PAN 4W	MR	STOPE - CONV	ZONE 5	20.00	0.15	1.00	0.50	0.50	S20-1091-216-08-23-FOG AR
2016/12/02	20#	2011	23MN	20 23 012 PAN 002N	MR	STOPE - CONV	ZONE 1	7.00	2.50	2.10	12.00	25.20	S20_2033_20161202_20 23 012_002N_GM
2017/05/11	20#	2011	23MN	20 23 012 PAN 002N	MR	STOPE - CONV	ZONE 1	0.00	2.00	11.50	22.50	258.75	S20_657_20170511_20 23 012 PAN 2N_GM
2017/06/06	20#	206	23MN	20 23 013 PAN 003S	MR	STOPE - CONV	ZONE 1	0.00	1.40	1.60	4.00	6.40	S20_826_20170605_20 23 013 PAN 003S_GM
2017/07/26	20#	2020	21MN	2021 012 PAN 1N	MR	STOPE - CONV	ZONE 3	3.10	0.90	1.30	1.00	1.30	S20-1194-2017-0731- FOG-AR
2017/08/06	20#	2011	25MN	20 25 009 PAN 2S	MR	STOPE - CONV	ZONE 1	0.00	0.40	2.50	1.70	4.25	S20_1236_2017-08-07_FOG_GIK
2017/08/24	20#	2010	22MS	2022A 007 PAN 4W	MR	STOPE - CONV	ZONE 5	16.00	0.06	0.27	0.11	0.03	S20-1338-2017-08-24-FOG-AR
2017/08/29	20#	2012	19MN	2019 012 1WC	MR	STOPE - CONV	ZONE 3	0.00	0.03	0.26	0.17	0.04	S20-1389-20170829-FOG ACC-PT
2017/11/23	20#	2012	19MN	20 19 012 PAN 1WB	MR	STOPE - CONV	ZONE 1	0.00	0.10	0.43	0.21	0.09	S20-1943-20171123-20 19 012 1WB FOG-AR
2017/10/25	20#	2020	21MN	20 21 014 PAN Centre gully	MR	CG / ASG	ZONE 5	25.00	0.04	0.50	0.30	0.15	S20-1717-20171025-20 21 014 Cenre gully
2017/11/24	20#	2011	24MS	20 24 009 PAN 004S	MR	STOPE - CONV	ZONE 5	0.00	0.19	0.32	19.00	6.08	S20_1973_20171130_20 24 009 PAN 004S_GM
2017/12/15	20#	2010	23MN	20 23 013 PAN 001S	MR	STOPE - CONV	ZONE 1	0.00	0.03	0.31	0.12	0.04	S20_2095_20171215_20 23 013 PAN 001S_GM
2017/12/15	20#	2010	23MN	20 23013 PAN 001S	MR	STOPE - CONV	ZONE 1	1.00	0.03	0.31	0.12	0.04	S20_2095_20171215_20 23 013 PAN 001S_GM
2018/04/16	20#	2010	23MN	2023 011 PAN 5N	MR	STOPE - CONV	ZONE 5	3.90	0.05	0.30	0.25	0.08	S20-697-20180416-FOG ACCIDENT-BBT
2018/05/30	20#	2020	21MN	2021 013 PAN 1N	MR	STOPE - CONV	ZONE 1	28.10	0.23	0.27	0.23	0.06	S20-20180605-FOG ACC-AR
2018/05/13	20#	2020	21MN	2021014 PAN 2N	MR	STOPE - CONV	ZONE 5	0.50	0.70	1.30	0.65	0.85	S20-1020-20180530-FOG ACC -AR
2018/07/23	20#	2010	24MN	2024 011 PAN 03S	MR	STOPE - CONV	ZONE 4	1.30	0.17	1.30	0.60	0.78	S20-1304-20180723-FOG ACC-PT
2018/08/23	20#	2010	24MN	2024 011 PAN 03S	MR	STOPE - CONV	ZONE 4	0.50	0.25	3.60	21.30	76.68	S20-1554-20180823-FOG INC-PT
2018/11/28	20#	2012	20MS	20 20 006 PAN 2N	MR	STOPE - CONV	ZONE 1	0.50	1.10	2.20	2.70	1.21	S20-3023-20181130-FOG INC/AR
2018/12/01	20#	2012	21MN	2021 014 PAN 002S	MR	STOPE - CONV	ZONE 4	1.20	0.02	0.08	0.07	0.01	S20-3075-2018101-FOG ACC-PT
2018/12/10	20	2012	20MN	20 20 014 PAN 2S RE-DEV	MR	STOPE - CONV	ZONE 5	14.00	3.50	23.00	28.00	587.00	S20-3087-20181210_FOG_INC_AR
2019/01/08	20#	2010	23MS	20 24 007 PAN 11S	MR	STOPE - CONV	ZONE 4	0.00	0.60	3.50	1.40	4.90	S20-034-20190108-FOG INC-GIK
2019/06/11	20#	2011	25MN	20 25 011 PAN 4N	MR	STOPE - CONV	ZONE 1	0.00	1.30	10.60	9.30	98.58	S20-858-19-2025 011 PAN 004N-FOG ACC
2019/06/15	20#	2012	20 MN	20 19 013 PAN 2N	MR	STOPE - CONV	ZONE 1	0.50	0.12	0.18	0.18	0.03	S20-880-20190616-FOG ACC/AR
2019/07/28	20#	2012	21MN	20 21 014A PAN 2S	MR	STOPE - CONV	ZONE 1	0.50	0.60	3.00	1.50	4.50	S20-1038-20190713-FOG INC/A
2019/10/12	20#	2012	21MN	20 21 014A PAN3S	MR	STOPE - CONV	ZONE 1	0.50	1.00	1.00	2.50	2.50	S20-1630-20191015-FOG INC/AR
2019/10/12	20#	2012	21MN	20 21 014A PAN 3S	MR	STOPE - CONV	ZONE 1	1.00	1.10	2.50	1.10	2.75	S20-1630-20191015-FOG INC/AR
2019/11/11	20#	2010	24MS	2024 007 PAN 009N	MR	STOPE - CONV	ZONE 1	0.80	0.14	0.37	0.29	0.11	S20-1866-19-24 007 PAN 009N-FOG ACC
2019/11/15	20#	2011	25MN	20 25 012 PAN 1S	MR	STOPE - CONV	ZONE 1	0.30	0.30	0.30	0.08	0.02	S20-1875.20191116-FOG/GIK
2020/02/06	20#	2011	24MS	2024 007 PAN 004S	MR	STOPE - CONV	ZONE 1	0.00	0.15	0.30	0.07	0.02	S20-291-20-24 007 PAN 004S-FOG ACC
2020/05/07	20#	2012	19MS	20 19 007 PAN 4S	MR	STOPE - CONV	ZONE 1	1.20	0.30	1.70	0.70	1.19	S20-795-20200508-FOG INC-AR
2020/05/08	20#	2012	19MS	20 19 007 PAN 4S	MR	STOPE - CONV	ZONE 1	3.50	1.20	2.50	3.20		S20-796-20200508-FOG Incident –AR
2020/05/27	20#	2020	20MS	20 22 005 PAN 14E	MR	STOPE - CONV	ZONE 1	2.50	1.30	0.90	3.20	2.88	S20-84-20200121-FOG ACC-AR
2020/09/11	20#	2011	24MN	20 24 014 PAN 4S	MR	STOPE - CONV	ZONE 1	0.25	0.03	0.13	0.12	0.02	S20-1842-20200912 FOG ACC/AR
2020/09/20	20#	2020	20MS	20 20 004 PAN 3S	MR	STOPE - CONV	ZONE 1	0.00	0.05	0.21	0.21	0.04	S20-1802-20200908 FOG ACC/AR
2020/12/22	20#	2011	24MS	2025 007 PAN 007N	MR	STOPE - CONV	ZONE 4	0.00	0.16	0.69	0.56	0.39	S20-2562-20-25 007 PAN 007N-FOG ACC
2021/01/16	20#	2020	20MS	20 22 006 PAN 8E1	MR	STOPE - CONV	ZONE 5	1.70	0.10	0.23	0.20	0.05	S20-110-20210119-FOG ACC-AR
2021/02/09	20#	2012	19MS	20 19 008 PAN 1WB	MR	STOPE - CONV	ZONE 1	0.00	0.25	1.00	0.40	0.40	S20-271-20210209 -FOG ACC/AR
2021/02/13	20#	206	18MN	20 18 014 Diagonal Raise Ledge 001	MR	LEDGE	ZONE 5	0.00	0.20	0.60	0.30	0.18	S20-311-20210215-FOGACC-JM
2021/03/08	20#	2011	20MS	2024 005 PAN 001S	MR	STOPE - CONV	ZONE 1	1.20	0.02	0.16	0.08	0.01	S20-594-20-24 005 PAN 001S-FOG ACC
2021/03/23	20#	2017	24MS	2024A 005 Ledge	MR	LEDGE	ZONE 5	0.00	0.03	0.08	0.06	0.00	S20-667-20210323-24 005 Ledge -FOG ACC
2021/04/07	20#	2011	25MN	2025 011 PAN 4S	MR	STOPE - CONV	ZONE 1	0.00	0.04	0.08	0.06	0.005	
2021/04/12	20#	2020	20MS	20 20 004 PAN 12S	MR	STOPE - CONV	ZONE 1	10.20	0.04	0.06	0.08	0.005	
2021/11/24	20#	2015	24MN	2024 014 PAN 010N	MR	STOPE - CONV	ZONE 1	2.10	0.08	0.27	0.60	0.162	S20-2682-20211125-2024 014 PAN 010N-FOG ACC
2022/01/13	20#	2017	24MS	20 24 003 PAN 1WB	MR	LEDGE	ZONE 5	3.5m	0.29	0.42	0.27	0.113	S20-102-20220114-FOG-OS
2022/02/05	20#	2012	18MS	20 18 004 PAN 4S	MR	STOPE - CONV	ZONE 1	0.10	0.15	0.50	0.48	0.240	S20-483-20220302-FOG ACC-AR
2022/07/05	20#	206	21MN	20 21 014A PAN 2N	MR	STOPE - CONV	ZONE 1	8.30	0.10	0.34	0.20	0.068	S20-1511-20220706-FOG ACC
2022/10/04	20#	2027	19MN	20 19 015 PAN 004N	MR	STOPE - CONV	ZONE 1	0.00	0.63	0.62	0.10	0.062	S20-2348-20221005-FOG-KM
2023/02/22	20#	2010	22 MN	20 23 016 PAN 2N	MR	STOPE - CONV	ZONE 1	6.00	1.00	4.00	1.80	7.20	S20-673-23-02-2023- AR
2023/02/27	20#	2026	24MN	20 25 007 PAN 5S	MR	STOPE - CONV	ZONE 1	0.50	0.19	1.55	0.31	0.48	S20-639-27-02-2023-PT
2023/03/06	20#	2012	18MN	20 18 014 PAN 3N	MR	STOPE - CONV	ZONE 1	5.00	1.30	3.00	4.00	12.00	S20-712-2023_03_07-AR
2023/03/13	20#	2011	25MN	20 25 017 PAN 2S LEDGE	MR	LEDGE	ZONE 5	1.20	0.31	0.53		0.71	S20_815_31-03-2023-FOG-BBT
2023/05/18	20#	2012	18MN	20 19 013 PAN 011S	MR	STOPE - CONV	ZONE 5	3.50	1.50	3.50	11.00	38.50	S20-1470-202306-20-FOG INC-AR
2023/06/10	20#	2027	19MN	20 19 015A LEDGE	MR	LEDGE	ZONE 5	0.50	0.70	3.50	1.20	4.20	S20_1390_10-06-2023-FOG INC-AR
2023/07/12	20#	2010	23MN	2023 016 PAN 003S	MR	STOPE - CONV	ZONE 1	0.00	1.10	1.50	2.00	3.00	S20-1744-2023 016 PAN 003S-FOG Inc

APPENDIX H. J-BLOCK RUN HAZARD RESULTS

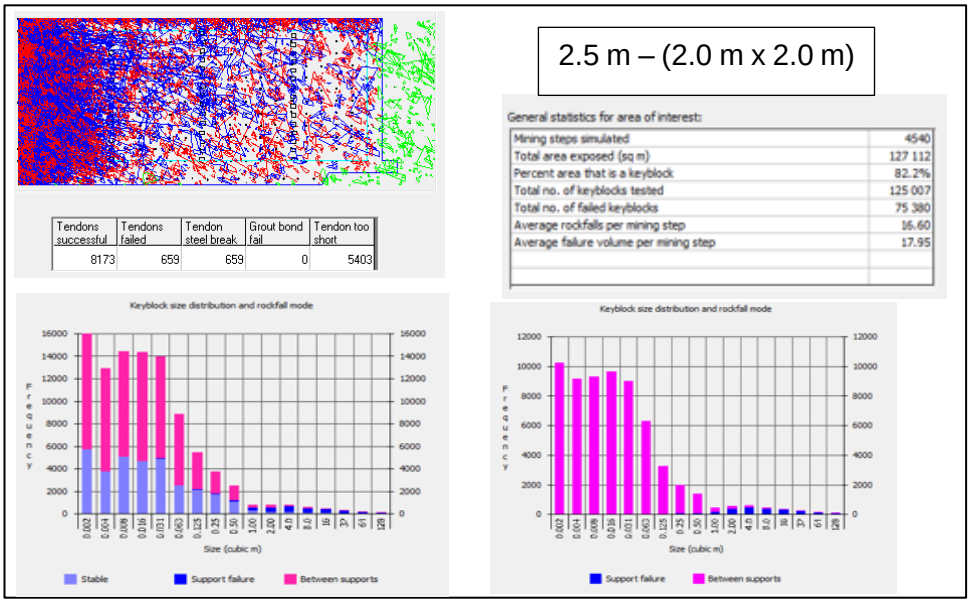


Figure H1: J-Block Output Results for 2.5m CA at a 2.0 m x 2.0 m spacing

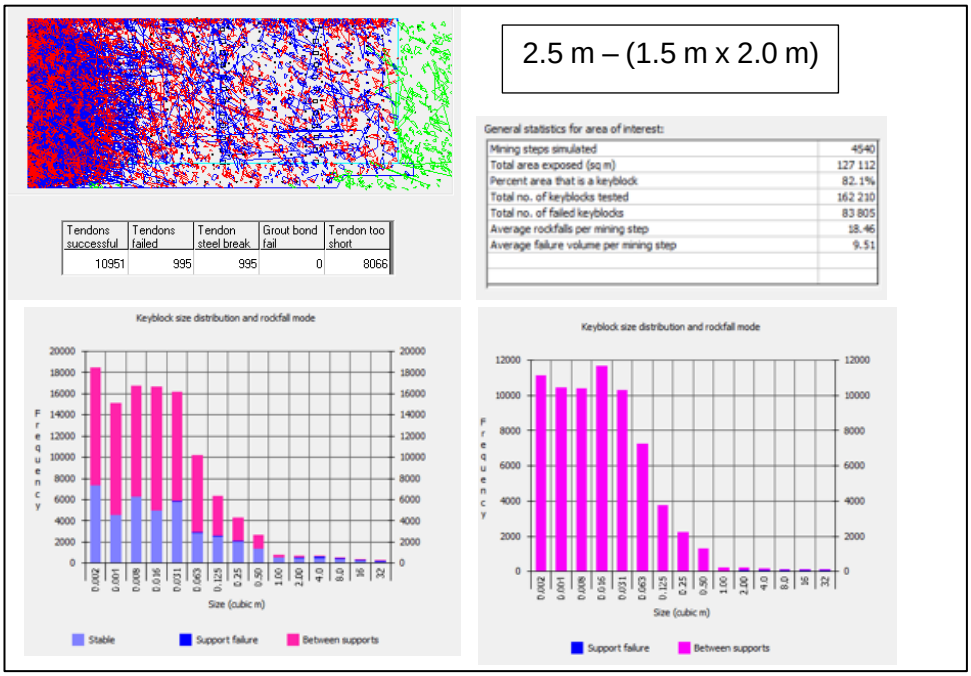


Figure H2: J-Block Output Results for 2.5 m CA at a1.5m x 2.0 m spacing

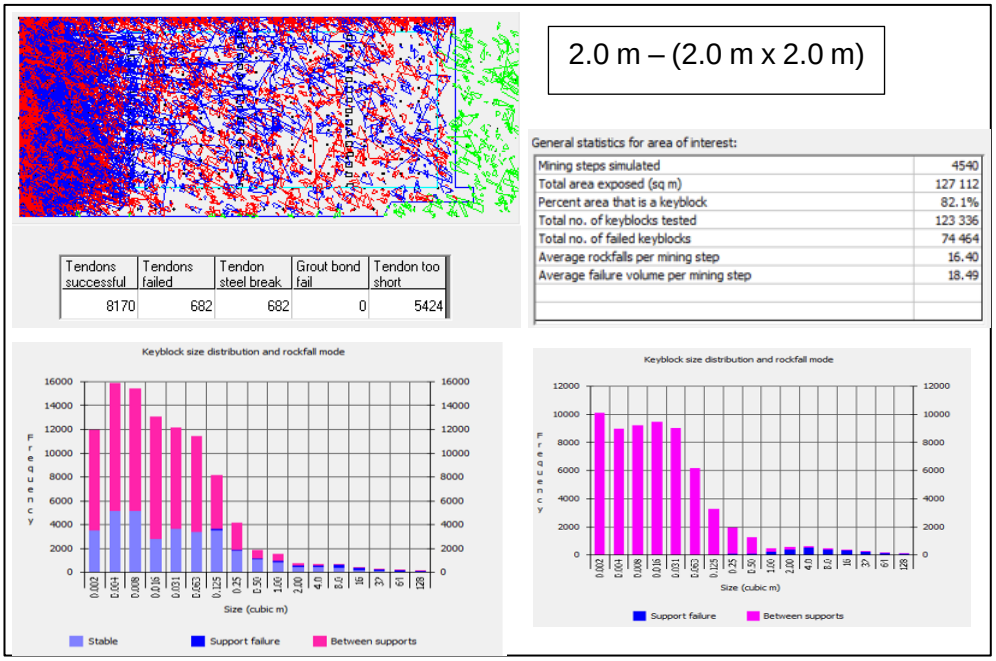


Figure H3: J-Block Output Results for 2.0 m CA at a 2.0 m x 2.0 m spacing

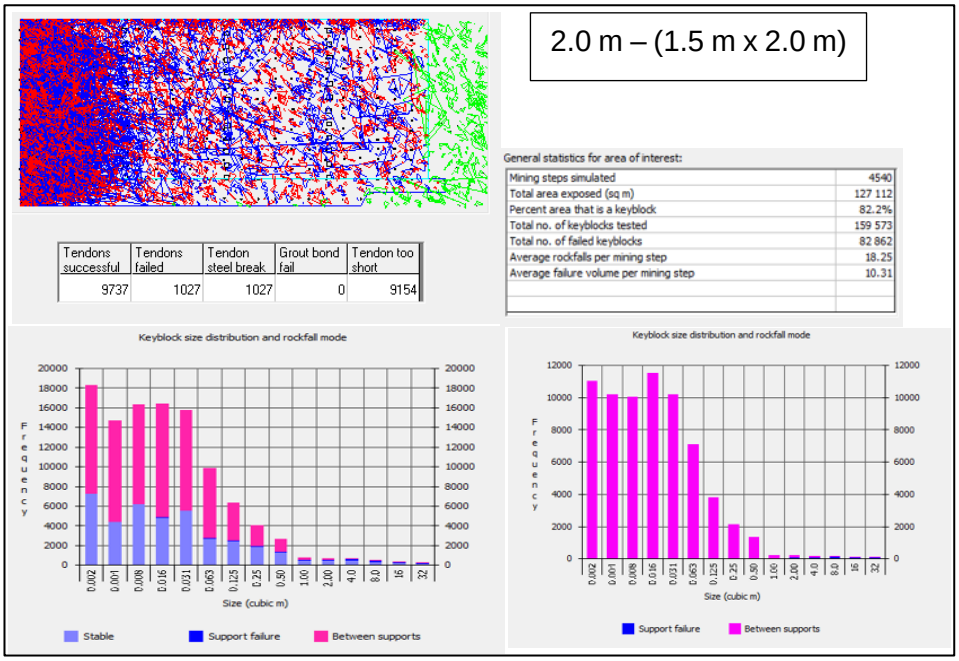


Figure H4: J-Block Output Results for 2.0 m CA at a 1.5 m x 2.0 m spacing

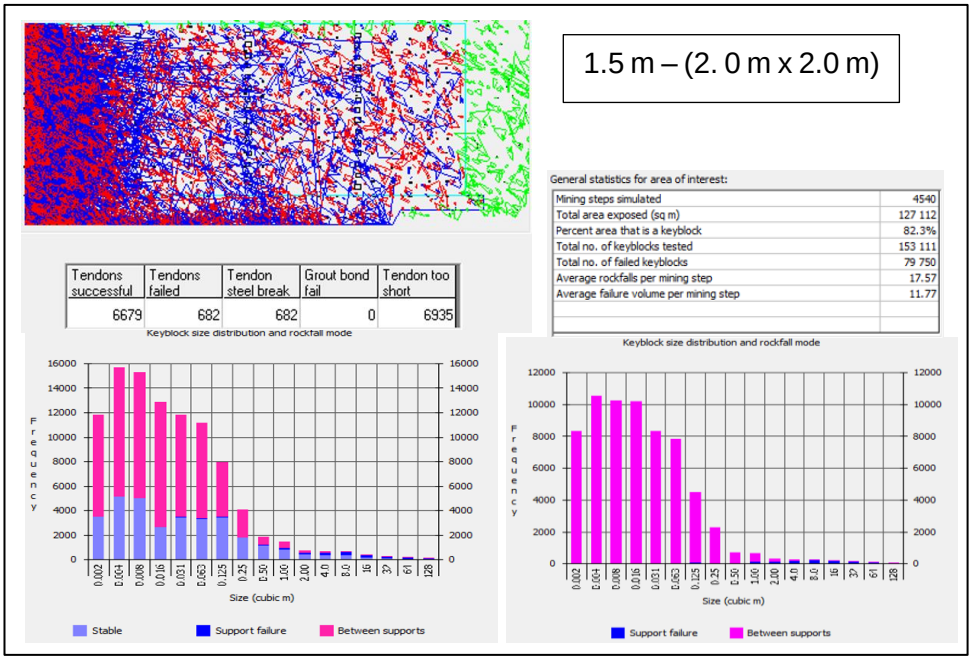


Figure H5: J-Block Output Results for 1.5 m CA at a 2.0 m x 2.0 m spacing

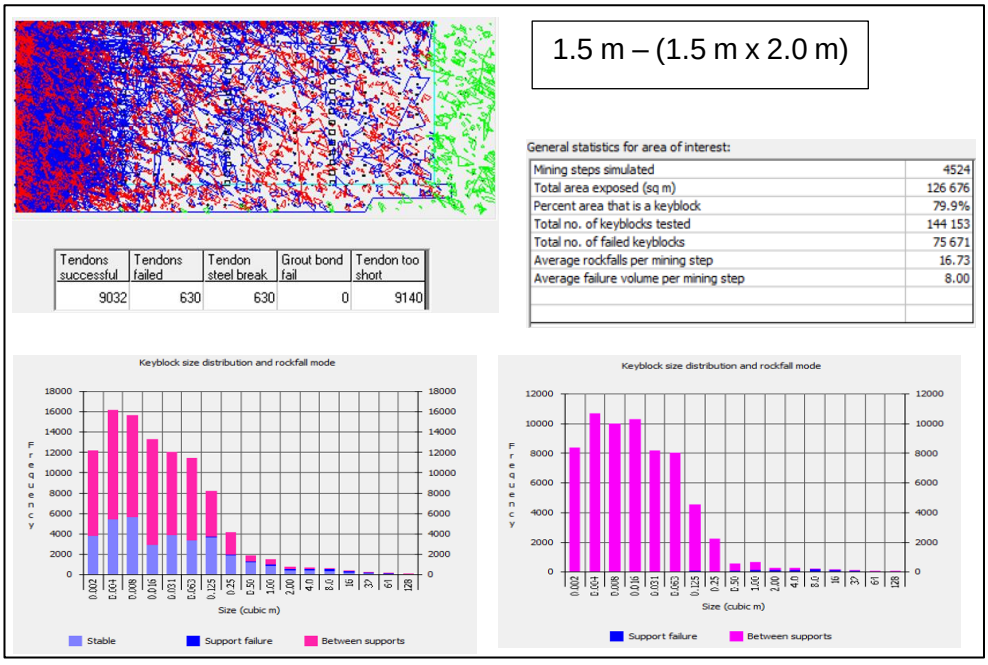


Figure H6: J-Block Output Results for 1.5 m CA at a 1.5 m x 2.0 m spacing

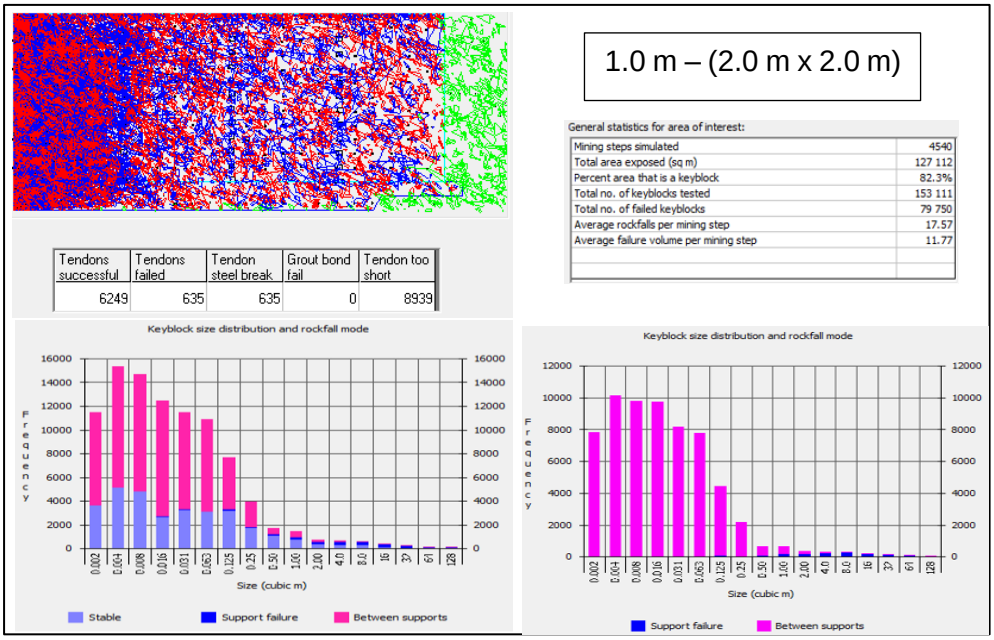


Figure H7: J-Block Output Results for 1.0 m CA at a 2.0 m x 2.0 m spacing

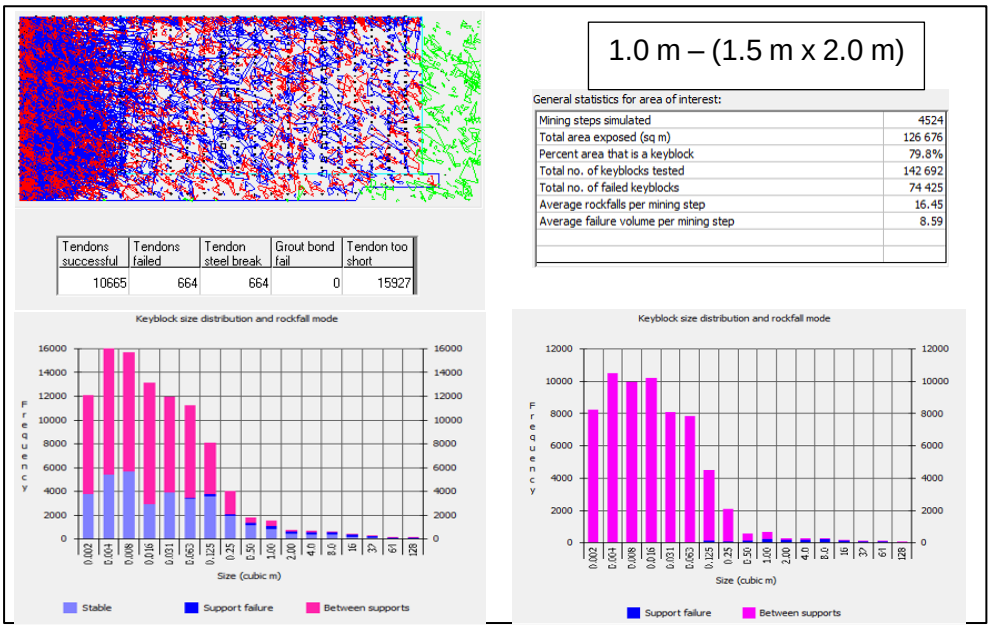


Figure H8: J-Block Output Results for 1.0 m CA at a 1.5 m x 2.0 m spacing